

1-1-2008

Nanostructured polymer electrolyte membranes for fuel cell applications : structure vs properties.

Akinbode I. Isaacs-Sodeye
University of Massachusetts Amherst

Follow this and additional works at: https://scholarworks.umass.edu/dissertations_1

Recommended Citation

Isaacs-Sodeye, Akinbode I., "Nanostructured polymer electrolyte membranes for fuel cell applications : structure vs properties." (2008). *Doctoral Dissertations 1896 - February 2014*. 1118.
<https://doi.org/10.7275/cr00-b331> https://scholarworks.umass.edu/dissertations_1/1118

This Open Access Dissertation is brought to you for free and open access by ScholarWorks@UMass Amherst. It has been accepted for inclusion in Doctoral Dissertations 1896 - February 2014 by an authorized administrator of ScholarWorks@UMass Amherst. For more information, please contact scholarworks@library.umass.edu.

* UMASS/AMHERST *



312066 0336 5477 8



University of
Massachusetts
Amherst

L I B R A R Y





Digitized by the Internet Archive
in 2015

<https://archive.org/details/nanostructuredpo00isaa>

This is an authorized facsimile, made from the microfilm master copy of the original dissertation or master thesis published by UMI.

The bibliographic information for this thesis is contained in UMI's Dissertation Abstracts database, the only central source for accessing almost every doctoral dissertation accepted in North America since 1861.

UMI ^{INC.} Dissertation
Services

From: ProQuest
COMPANY

300 North Zeeb Road
P.O. Box 1346
Ann Arbor, Michigan 48106-1346 USA
800.521.0600 734.761.4700
web www.il.proquest.com

**NANOSTRUCTURED POLYMER ELECTROLYTE MEMBRANES FOR FUEL
CELL APPLICATIONS: STRUCTURE vs PROPERTIES**

A Dissertation Presented

by

AKINBODE I. ISAACS-SODEYE

Submitted to the Graduate School of the
University of Massachusetts Amherst in partial fulfillment
of the requirements for the degree of

DOCTOR OF PHILOSOPHY

May 2008

Polymer Science and Engineering

UMI Number: 3325115

Copyright 2008 by
Isaacs-Sodeye, Akinbode I.

All rights reserved

INFORMATION TO USERS

The quality of this reproduction is dependent upon the quality of the copy submitted. Broken or indistinct print, colored or poor quality illustrations and photographs, print bleed-through, substandard margins, and improper alignment can adversely affect reproduction.

In the unlikely event that the author did not send a complete manuscript and there are missing pages, these will be noted. Also, if unauthorized copyright material had to be removed, a note will indicate the deletion.

UMI[®]

UMI Microform 3325115

Copyright 2008 by ProQuest LLC

All rights reserved. This microform edition is protected against
unauthorized copying under Title 17, United States Code.

ProQuest LLC
789 East Eisenhower Parkway
P.O. Box 1346
Ann Arbor, MI 48106-1346

© Copyright by Akinbode I. Isaacs-Sodeye 2008

All Rights Reserved

**NANOSTRUCTURED POLYMER ELECTROLYTE MEMBRANES FOR FUEL
CELL APPLICATIONS: STRUCTURE vs PROPERTIES**

A Dissertation Presented

by

AKINBODE I. ISAACS-SODEYE

Approved as to style and content by:

Samuel P. Gido, Chair

Richard J. Farris, Member

Thomas P. Russell, Member

Mark T. Tuominen, Member

Shaw Ling Hsu, Department Head
Polymer Science and Engineering

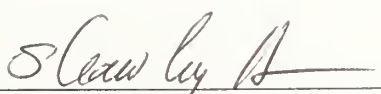
**NANOSTRUCTURED POLYMER ELECTROLYTE MEMBRANES FOR
FUEL CELL APPLICATIONS: STRUCTURE vs PROPERTIES**

A Dissertation Presented

by

AKINBODE I. ISAACS-SODEYE

Approved as to style and content by:


Samuel P. Gido, Chair
Richard J. Farris, Member
Thomas P. Russell, Member
Mark T. Tuominen, Member
Shaw Ling Hsu, Department Head
Polymer Science and Engineering

DEDICATION

To my wife Omotowunmi and daughter Layo for their love and patience

To my sisters Toyin and Ayo for their financial support and goading

To my father Prof. W.A. Isaacs-Sodeye for initiating us into the world of learning

ACKNOWLEDGMENTS

I thank my Lord and savior Jesus Christ , who is my wisdom , righteousness , sanctification, redemption, and Ebenezer. By His grace I have reached this position, and by his grace I will reach my high places.

Here on earth, I count myself fortunate to have been advised by professor Gido. I appreciate the freedom he granted me to follow diverse research interests, take initiative, and most of all build my confidence as a scientist/engineer through challenging projects. His pieces of advice on financial matters have also been eye opening, though still being assimilated. In the same vein I must also thank professor Farris for allowing my to “play around” in his lab, and for life lessons in timeliness. I also immensely appreciate the constructive criticism by Professor Russell , and access to his electric field alignment apparatus. Lastly but not the least , I am grateful to Professor Tuominen , my committee member from the physics department, for his patience with my URGENT emails and for access to his Electrochemical Impedance equipment, without which this work could not have been concluded.

I would also like to thank my research collaborators for supplying polymer samples vital to this dissertation work: Professor Jimmy Mays and Dr. Tianzi Huang at the University of Tennessee in Knoxville; Professor Robert Weiss and Shurui Shang at University of Connecticut Storrs. I am also grateful to the various funding sources throughout my PhD work : US Army Research Office, Boston Scientific Corporation and the NSF supported Materials Research Science and Engineering Center(MRSEC).

I have received a lot of technical help, training and advice from a lot of people to whom I am very grateful. These include Lou(TEM,SEM), Sekar, Evgenia, Jack (XPS), Ozgur (EIS), Andre(computers), Russell group members for Electric Field alignment (Ting, Suresh, Jiayu, Joonwon, Tomomi). I also owe a debt of gratitude to Jyotsana Lal, Ed Lang and Jan Ilavsky at Argonne National Laboratory for their help with Neutron and X-ray scattering experiments and helpful discussions thereafter. I am much indebted to Dr. Sergio Granados-Focil for his mentoring role in my research and his friendship. I do appreciate the excellent administrative assistance provided by the PSE office staff: Vivien, Eileen, Sophie, Ann, Moreen, Anne(Gaddy), Linda. I also thank Barry and the rest of the custodial staff.

I have had many fun memories with different groups of people through my five odd years in UMass. First of all I appreciate my class of 2002: Jay, Roberto, Joanna, Jess, Peter, Brad, Ryan, Chris, Qingling....We made it! Do also appreciate the past Gido group members (am the last of an era): Yuqing, Xiaochuan, Engin, Sungkyun, Ashoutosh, Tomo, Xiaodong, Manoj, and Roland Horst. I did enjoy the “ Intellectual Gentleman’s Club”. To the Farris group members who taught me along the way: Tao, Angelo, Sian,I say thank you.

Most of my friendship and support came from my church family in RCCG (Pastors Tola and Bola Adelani, The Uwaias, The Mcfinis, The Benns, The Adedirans, The Fagades....); in Mercy House(The Evans, The Krumreys, The Speights, Matt Burgoon, Chris Metera, Lios, Cindy, Jo...); in Maple Ridge (Sanjoy and Erin, John and

Rachel, Jarret, Armando, the Tans, Mark and Julia...) and all their music teams. The Love we shared, may we share with our world more and more.

Finally, I would like to express my deepest appreciation to my extended and nuclear family. To my dad , for taking the first PhD in our family and blazing the trail. To my elder sisters (Toyin, Ayo ,Ibukun, Bukky) for the love and pampering. Bros Tunde you just dey chill wid yor new ododo. BIMBO OSE TO WAPELUMI. A YE E KALE. LAYOMI IWO NO A SI BAWA JERE RE.

ABSTRACT

NANOSTRUCTURED POLYMER ELECTROLYTE MEMBRANES FOR FUEL CELL APPLICATIONS: STRUCTURE vs PROPERTIES

MAY 2008

AKINBODE I. ISAACS-SODEYE, B.Sc., OBAFEMI AWOLOWO UNIVERSITY

M.S., UNIVERSITY COLLEGE LONDON

M.S., UNIVERSITY OF MASSACHUSETTS AMHERST

Ph.D., UNIVERSITY OF MASSACHUSETTS AMHERST

Directed by: Professor Samuel P. Gido

This dissertation explores various topics within the theme of nanostructured polymer electrolyte membranes having controlled morphology, and their resulting properties. Chapter 1 gives an introduction to the field of Polymer electrolyte membranes (PEM) in its current state, and an overview of the work done. In chapter 2, relatively inexpensive block copolymer ionomers of fluorinated poly(Isoprene)-*block*-sulfonated poly(Styrene) (FISS) with various sulfonation levels, in both the acid form and the cesium neutralized form, have been cast into membranes of desired random phase separated morphology. The morphology of these membranes were characterized by TEM and SAXS, as well as water uptake, proton conductivity and methanol permeability from 20 to 60°C. The transport properties increased with increasing sulfonation and temperature for all samples. The acid form samples absorbed more water than the cesium samples with a maximum swelling recorded at 60°C for the acid sample with 50mol% sulfonation. Methanol permeability for the latter sample was more than an order of magnitude less than Nafion 112 but so was the proton conductivity at 20°C within the

plane of the membrane. Across the plane of the membrane this sample had half the conductivity of Nafion 112 at 60°C.

In chapter 3, neutron and x-ray scattering techniques have been used to study the structural evolution of FISS materials as they have evolved from the dry state to the water soluble state. A dilation of the nanometer-scale hydrophilic domains have been observed as hydration has been increased, with higher swelling for the higher sulfonated sample or upon hydrating at higher temperatures. Furthermore a decrease in the order in these phase separated structures is reduced upon swelling. The glass transition temperature of the fluorinated blocks decreased upon hydration, and at the highest hydration levels loosely bound water was evident. Thermal and dynamic mechanical characterization of these materials have shown there is a high degree of softening beyond the 45°C glass transition temperature. Finally highly sulfonated samples have shown the formation of spherical micelles, even at concentrations as low as 0.05 mg/ml. The sizes of these micelles range from 13-13.5 nm, with the higher concentration solutions having smaller radius of gyration, possibly due to crowding effects.

In chapter 4, Ionomers from the cesium salt (20 mol %) of fluorinated Poly(Isoprene)-block-sulfonated Poly(Styrene) have been spun cast into membranes and annealed under an electric field of ~40 V/μm at 130°C for 24 hours. This resulted in the transformation of the morphology from a random phase separated state to one preferentially oriented in the direction of the electric field but with smaller domain sizes. The effect of this change in morphology was a 2.5 times increase in the ionic

conductivity, as measured by electrochemical impedance spectroscopy, at all humidity conditions measured. This can be attributed to the increased connectivity of the ionic domains.

In chapter 5, The applicability of electropun nanostructure with high surface to volume ratios for PEM application is presented. To this end, sulfonated poly(ether ether ketone) has been electrospun and electrosprayed by varying concentration in DMF, yielding isotropic fibrous mats and beads. The glass transition temperatures of these materials have been shown to be higher those of the unsulfonated precursors and they increase with increasing sulfonation, due to hydrogen bonding induced rigidity. The presence of sulfonic acid groups on the surface has been confirmed by means of x-ray photoelectron spectroscopy, with sulfur representing 3% of the surface elemental composition. These acid groups on the surface of internal fibers, help to form a 3 dimensional network of conducting channels in the voids of the fibrous mats upon hydration. This in turn has led to an improvement of conductivity from 0.033 S/cm for void-less solution cast membranes to 0.040 S/cm for the electrospun fibrous mats.

TABLE OF CONTENTS

	Page
ACKNOWLEDGMENTS	v
ABSTRACT.....	viii
LIST OF TABLES.....	xiv
LIST OF FIGURES	xv
 CHAPTER	
1. POLYMER ELECTROLYTE MEMBRANES FOR FUEL CELLS	1
1.1 Background.....	1
1.2 Operating Principles.....	2
1.3 Types of Fuel Cells	3
1.4 PEM Materials	5
1.5 PEM Morphology And Its Control	9
1.6 Materials for this work.....	13
1.7 Work Done.....	14
1.7.1 Membrane Structure and Transport Properties	14
1.7.2 Membrane Structural evolution with hydration and heating	16
1.7.3 Membrane Microdomain Orientation by external field	17
1.7.4 PEMs from Electrospun Poly(Aryl ether ketone)s	18
1.8 References	20
2. POLYMER ELECTROLYTE MEMBRANES FROM FLUORINATED POLY(ISOPRENE)-BLOCK-SULFONATED POLY(STYRENE): MEMBRANE STRUCTURE AND TRANSPORT PROPERTIES.....	30
2.1 Abstract	30
2.2 Introduction.....	31
2.3 Experimental Section.....	33
2.3.1 Materials	33
2.3.2 Preparation of Membranes	34
2.3.3 Structural Characterization	34
2.3.4 Transport Properties	36
2.4 Results and Discussions.....	38

2.5 Conclusions.....	49
2.6 References.....	50
3. POLYMER ELECTROLYTE MEMBRANES FROM FLUORINATED POLY(ISOPRENE)-BLOCK-SULFONATED POLY(STYRENE): STRUCTURAL EVOLUTION WITH HYDRATION AND HEATING.....	63
3.1 Abstract.....	63
3.2 Introduction.....	63
3.3 Experimental Section.....	65
3.3.1 Materials	65
3.3.2 Preparation of Membranes	66
3.3.3 Structural Characterization	67
3.3.4 Thermal characterization	69
3.4 Results and Discussions.....	69
3.4.1 Structural evolution with hydration	69
3.4.2 Thermal and Mechanical Transitions	74
3.4.3 Micelle Formation	76
3.5 Conclusions.....	78
3.6 References.....	80
4. POLYMER ELECTROLYTE MEMBRANES FROM FLUORINATED POLY(ISOPRENE)-BLOCK-SULFONATED POLY(STYRENE): MICRODOMAIN ORIENTATION BY EXTERNAL FIELD.....	94
4.1 Abstract.....	94
4.2 Introduction.....	94
4.3 Experimental Section.....	97
4.3.1 Materials	97
4.3.2 Preparation of Membranes	97
4.3.3 E-Field Alignment Experiments	97
4.3.4 Transmission Electron Microscopy(TEM)	98
4.3.5 Ionic conductivity	98
4.4 Results and Discussions.....	99
4.5 Conclusions.....	102
4.6 References.....	103

5.	POLYMER ELECTROLYTE MEMBRANES FROM ELECTROSPUN SULFONATED POLY(ARYL ETHER KETONE) NANOFIBER MATS.....	111
5.1	Abstract	111
5.2	Introduction.....	111
5.3	Experimental Section	115
5.3.1	Materials	115
5.3.2	Preparation of Membranes	115
5.3.3	Thermal characterization	116
5.3.4	Scanning Electron Microscopy(SEM)	117
5.3.5	X-Ray Photoelectron Spectroscopy(XPS)	117
5.3.6	Ionic conductivity	117
5.4	Results and Discussions.....	118
5.5	Conclusions.....	121
5.6	References.....	123
6.	SUMMARY AND POSSIBLE FUTURE DIRECTIONS	132
	BIBLIOGRAPHY	135

LIST OF TABLES

Table	Page
1.1: The different Fuel Cells that have been realized and are in current use and development	23
2.1: Thickness, Water uptake, methanol permeability and ionic conductivity of materials investigated in this work	58
3.1: Dry sample center-to-center distances for fluorinated poly(Isoprene)- <i>block</i> -sulfonated poly(Styrene) (FISS) obtained by USAXS	82
3.2: Neutron Scattering length densities calculated for different parts of fluorinated poly(Isoprene)- <i>block</i> -sulfonated poly(Styrene) and D ₂ O	84
3.3: Thermal properties of fluorinated poly(Isoprene)- <i>block</i> -sulfonated poly(Styrene) and Nafion TM	91
5.1: Conductivity, and membrane thickness for sulfonated poly(ether ether ketone) (1.97 meq/g) obtained by EIS, and micrometer	131

LIST OF FIGURES

Figure	Page
1.1. Membrane Electrode Assembly (MEA)	22
1.2. Chemical structures for (a) Nafion TM (b) BAM TM (c) sSEBS (d) sPEEK (e) sulfonated Poly(Arylene ether Sulfone) (f) Sulfonated Poly(Imide) (g) Sulfonated PBI (h) sulfonated Poly[(3-methylphenoxy)(phenoxy)phosphazene (i) poly(arylene ether)s bearing phosphonic acid groups (j) Nafion like bis(perfluoroalkyl) sulfonamide (k) Free and tethered polymer backbones	24
1.3. TEM micrographs of a) SPSF (IEC 1.55); b)SPSF1-b-PVDF(IEC=1.62); c) SPSF (IEC=0.83); d) SPSF1-b-PVDF(IEC=0.78).....	27
1.4. Synthetic Scheme for Fluorinated PI- <i>b</i> -Sulfonated PS.....	28
1.5. Electro-spinning experimental setup.....	29
2.1. Flow diagram and pictures of Methanol Permeability measurement Experimental Setup.....	53
2.2. Experimental Setup for a) Two Probe , b) four Probe EIS measurements	54
2.3. Transmission electron Microscopy images for the FISS samples	55
2.4. Ultra Small Angle Scattering Profiles for the FISS samples.	57
2.5. Specific concentration of permeated methanol versus Time measured at 20°C.....	59
2.6. Ionic Conductivity of measurable samples.	60
2.7. AFM images of membrane surface adjacent to casting glass plane.	61
3.1. SANS profiles from fluorinated poly(Isoprene)- <i>block</i> -sulfonated poly(Styrene) dry at 23°C	83
3.2. SANS profiles from fluorinated poly(Isoprene)- <i>block</i> -sulfonated poly(Styrene) soaked for 16 hours in D ₂ O at (a) 23°C and (b) 60°C	85

3.3.	SANS profiles from fluorinated poly(Isoprene)- <i>block</i> -sulfonated poly(Styrene) soaked for 16 hours in D ₂ O and its vapor for (a) AC28 and (b) AC50.....	86
3.4.	Schematic of structural evolution with increased hydration.....	87
3.5.	DSC thermogram from fluorinated poly(Isoprene)- <i>block</i> -sulfonated poly(Styrene) as received samples dried under nitrogen flow overnight at 105°C.....	88
3.6.	DMTA curves for fluorinated poly(Isoprene)- <i>block</i> -sulfonated poly(Styrene) and Nafion TM samples pre-dried under nitrogen flow overnight at 105°C. Tension Mode	89
3.7.	DSC thermograms from fluorinated poly(Isoprene)- <i>block</i> -sulfonated poly(Styrene) soaked for 16 hours in H ₂ O at (a) 23°C and (b) 60°C	90
3.8.	8 SANS profiles from fluorinated poly(Isoprene)- <i>block</i> -sulfonated poly(Styrene) micelles formed in D ₂ O (a) profiles with Power law fits (b) Kratky plots (c)Guinier plots and analysis.....	92
4.1.	TEM micrographs showing sSEBS samples (a) As-Cast , (b) After Electric field of ~ 45V/um applied at 208°C, for 24 hours	105
4.2.	Schematic of spin casting operation	106
4.3.	Schematic of Electric Field Alignment Experimental Setup	107
4.4.	TEM micrographs showing FISS-CS20 samples (a) As-Cast , (b) After annealing under Electric field of ~ 40V/um applied at 130oC, for 24 hours.....	108
4.5.	Ionic (cesium) conductivity results for As-Cast and Efield annealed FISS-CS20 samples.....	110
5.1.	Schematic of Electrospinning Experimental Setup.....	125
5.2.	Thermograms for PEEK, sPEEK0.66, sPEEK1.97 from (a) TGA (b) DSC measurements.....	126
5.3.	SEM images for sPEEK1.97 from (a),(b) electrospun from 20wt% solution in DMF (c),(d) electrosprayed from 10wt% solution in DMF, at 18kV, 100ul/min and 13cm distance from target.....	127
5.4.	SEM images for sPEEK1.97 from electrospun from 22wt% solution in DMF at 12kV, 12.5 ul/min and 7 cm distance from target.....	129

5.5.	XPS images for sPEEK1.97 from electrospun from 22wt% solution in DMF at 12kV, 10 - 12.5 ul/min and 5-7 cm distance from target	130
------	--	-----

CHAPTER 1

POLYMER ELECTROLYTE MEMBRANES FOR FUEL CELLS

1.1 Background

Alternative sources of energy, besides fossil fuels, are a pressing need in the world we live in today. One such promising alternative is a fuel cell. In the broadest sense a fuel cell is an electrochemical device which converts chemical energy to electrical energy while giving off heat. Such devices can be contrasted with the internal combustion engine, in that they convert directly to electrical energy and not indirectly through a mechanical system and dynamos, and are generally more efficient¹.

Fuel Cells were first developed as early as 1839, by Sir William Grove, based on his idea of producing electricity by reversing the electrolysis of water. However, he called it a "Gaseous voltaic Battery" and the name fuel cells was only coined later by two engineers Charles Langer and Ludwig Mond in their efforts to build a practical Fuel Cell using air and coal gas². Subsequent progress on fuel cell development was impeded by the advent of cheap fossil fuels and the steam engine.

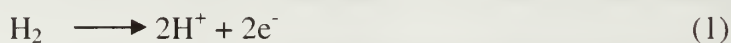
The NASA space program, as well as a few persistent researchers such as Francis Bacon, led to the use of Fuel cells to produce electricity and water for the space missions from the late 1950s. In more recent times, the drive to reduce dependence on foreign oil, cut emissions and their related environmental impact, as well as the global population increase has greatly increased the interest in fuel cell research and development in industry, government and academia alike. This is particularly true in the Automobile

industry, where most major car manufacturers have some form of fuel cell Vehicle (FCV) development ongoing.

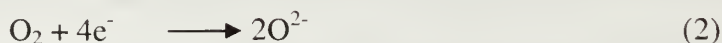
1.2 Operating Principles

Fuel cells basically consist of two electrodes, separated by and in contact with an electrolyte, and connected to each other by an electrical circuit (conductor). This basic unit is known as a Membrane electrode Assemblies (MEA), many of which are clamped together to form a stack of many units. As can be seen in Figure 1.1 below the MEA typically has a porous electrode which also acts as a gas diffusion layer, a catalyst layer which includes a binder to adhere it to the membrane, a membrane, the former two layers repeated on the other side. The catalyst is usually supported on finely divided carbon to increase surface area.

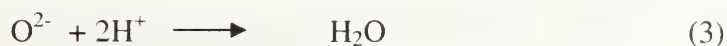
In a Hydrogen-oxygen fuel Cell, hydrogen enters through the pores of the anode and is oxidized at the catalyst layer according to the equation for this half reaction³:



This results in protons being released into the electrolyte, and electrons being conducted away through the external circuit and load (if any) around to the cathode. At the cathode, the oxygen entering through the gas diffusion layer is reduced by the electrons in the circuit according to the equation:



These oxygen ions eventually react with the protons that conduct through the membrane thus closing the second half reaction and producing water as follows:



Through this process bonds are broken and new ones form requiring less energy and thus the net energy is released in the form of heat. Through this whole process the membrane plays the crucial role of a cell separator, forcing electrons to flow through the external circuit thus ensuring half reactions happen separately.

1.3 Types Of Fuel Cells

Fuel Cells are typically classified according to their type of membrane they possess and are named accordingly. In a broad sense membranes can be classified as being solid or liquid electrolytes. Typically the liquid is immobilized to reduce or prevent leakage. The five major fuel cell types are as follows:

1. Alkaline Fuel Cell (AFC)
2. Polymer Electrolyte Membrane Fuel cell (PEMFC)
3. Phosphoric Acid Fuel Cell (PAFC)
4. Molten Carbonate Fuel Cell (MCFC)
5. Solid Oxide Fuel Cell (SOFC)

Other types of fuel cells do exist; the most important of these with regard to this work is the Direct Methanol Fuel Cell (DMFC). The Table 1.1 below summarizes the main features of the above listed Fuel Cell types.

Fuel Cells can also be classified according to their operating temperature. Thus there are low temperature fuel cells, which include the Alkaline, Polymer electrolyte membrane, Direct Methanol and Phosphoric acid types. The Molten Carbonate and the solid Oxide types are meant for high operating temperatures between 600-1000°C where catalysts function more efficiently. The Phosphoric Acid type of fuel cell can be said to operate at a relatively intermediate temperature between 160-220°C, which has increasingly become the target temperature range for new polymeric membrane development.

Fuel cells are made for various market niches, according to their power output, temperature ranges, and feed requirement. Typically the low temperature fuel cells put out less power and lend themselves to portable applications, whereas the high temperature ones are more feed tolerant, put out more power and can serve as stationary combined heat and electricity generation plants.

The PEMFC is the type of fuel cell of interest to this study, of course, having at their core a polymer electrolyte membrane. These fuel cells typically possess a polymeric acid bearing membrane such as NafionTM sandwiched between catalyst layers. The most common catalyst used is Platinum dispersed onto carbon supports, held together by PTFE based binders. These catalysts are typically sensitive to feed impurities, such as carbon monoxide so pre-cleaning is often required for reformed hydrogen. Other options include the use of CO- tolerant Pt-Ru catalyst.

The DMFC can be seen as a variant of the PEMFC. The membranes are typically the same; however, the feed is methanol in an aqueous 1-2M solution or vaporized. This fuel cell type has the most promise for portable applications as system complexities are reduced since there is no need to reform or store hydrogen, and the existing liquid fuels infrastructure can be used for methanol. Catalysts as well as operating temperature ranges are very similar to the PEMFC. The main technical challenge for the DMFC is the cross-over of methanol from anode to cathode, reducing cell efficiencies.

1.4 PEM Materials

Due to the reasonable commercial success of PEMFC membrane materials such as NafionTM and their technical limitations, a plethora of Polymer electrolyte materials have been and are being developed till date. These materials range from fluoropolymer to aromatic to hydrocarbon backboned materials, bearing pendant acid groups in one configuration or another. Except for some new materials, they typically require water to serve as a vehicle to facilitate proton conductivity via a “hopping” mechanism. Though some polymer electrolytes are better in some aspects than others, the crucial factors for a good polymer electrolyte membrane are as listed⁴

1. High Proton Conductivity
2. Low electronic conductivity.
3. Low Permeability of fuel and oxidant
4. Low water transport through diffusion and electro-osmosis.
5. Oxidative and hydrolytic stability.
6. Good mechanical properties in dry and hydrated states.

7. Low cost.
8. Capability for fabrication to a MEA.

A summary of such materials reported in literature is given below.

Poly(Perfluorosulfonic Acid) Membranes:

The most common PEM is NafionTM, having PTFE based backbone and perfluorosulfonic acid pendant chains as shown in figure 1.2. This chemical structure derives good thermal and chemical stability from the fluoropolymer backbone and strong acidity from the fluorosulfonic acid side chains where the fluorine atoms are electron withdrawing.

NafionTM was developed by Dupont, and is the most researched and developed PEM. Dow has made a variant of this with shorter side chains, as have Asahi chemical, and Asahi Glass of Japan with carboxylic acid. Composites of Teflon and Nafion have been made into PEMs by W.L Gore, as have organic-inorganic composites.

Styrenesulfonic Acid Membranes:

Sulfonating styrene has been found as a facile route to adding acidic functionality to back bone chains that contain them. Two companies have commercialized product based on this approach. Ballard's BAM PEMs are based on trifluorostyrene, and Dais analytical has sulfonated poly(Styrene)-block- (Ethylene-co-Butylene)-block-sulfonated poly(Styrene) (sSEBS) block copolymers as shown in figure 1.2 below.

The BAM membranes have similar conductivity and chemical stability as Nafion, while the SEBS ones have less due to their aliphatic nature. However they have only been reportedly applied to portable applications that require temperatures less than 60°C⁵. Other PEM materials have been made from styrenesulfonic acid macromonomers grafted to polystyrene backbones and Poly(Acrylonitrile)⁶. Radiation grafting techniques have also been used in the attachment of Poly(styrene sulfonic acid) to Poly (Ethylene-co-tetrafluoroethylene), Poly(vinylidene fluoride), and tetrafluoroethylene-co-hexafluoropropylene.

Poly(Arylene Ether) Membranes:

Aromatic polymers used in high performance polymer applications, are expected to be good materials for PEM membranes. Their high chemical and oxidative stability have made them attractive for use as fuel cell membranes. Their chemical modification has proven to be very flexible and so they can be easily sulfonated or even fluorinated.

Some early work on the sulfonation of poly (ether ether ketone) (PEEK) was done here at PSE in the Karasz group in order to reduce its crystallinity and dissolve and characterize the polymer⁷. Other promising candidates in this category are Poly(Arylene ether Sulfone)s. Though they maintain good mechanical properties and thermal stability even after sulfonation, their adhesive compatibility with the fluorinated catalyst layer is generally poor. To eliminate this effect copolymers based on hexafluoroisopropylidene bisphenol have been made with some success. Their chemical structures⁴ after modification are shown in figure 1.2 below:

Poly(Imide) and other high performance membrane materials:

Five and six membered ring polyimides being stiff, tough polymers have been thought to be good candidates for fuel cell membranes. It has been found that the naphthalenic polyimides are more stable in these applications. Six membered ring polyimides as the one shown below have shown promise, however their low solubility remains a technical challenge.

Other ductile polymers and copolymer that have been sulfonated for use as PEM materials include Poly(phenylquinonexaline), Poly(2,6 dimethyl- 1,4 phenylene oxide)(PPO), Poly(4-phenoxybenzoyl-1,4-phenylene) (PPBP), and Polybenzimidazole (PBI). The PBI though good in its unmodified state as a host for phosphoric acid electrolyte, in high temperature FC applications, becomes insoluble and brittle upon sulfonation⁸.

Polyphosphazene Membranes:

These polymers are attractive for PEM use because of their chemical and thermal stability as well as their ease and flexibility of side chain addition. They exhibit suitable proton conductivity but are reported to have low T_g and poor mechanical properties.

Other Proton Conducting Membrane Materials:

All the above mentioned PEM materials derive their conductivity from sulfonic acid groups attached in some way to a backbone. Another rare approach is to put a phosphonic acid functionality into the backbone to facilitate conductivity. This has

resulted in lower conductivity values than their sulfonic acid analogues, due to the greater acidity of the later, but they prove to have better chemical and thermal properties than them⁹. Another substitute acidic moiety that has been investigated is the sulfonamide, which is strongly acidic. However these have not shown increased conductivity when substituted for Sulfonic acid in the NafionTM structure¹⁰.

The U.S Department of energy's guidelines for PEM to be applied for automotive Fuel Cells aims at operating at 120°C and 50% relative humidity , with 0.1 S/cm for its proton conductivity. This benchmark cannot be reached by the previously cited PEM materials as they depend heavily on water for their proton transport mechanism. In view of this some new approaches that have been tried include using organic-inorganic composite membranes¹¹ or using imidazole proton conductors tethered to a polymer backbone as water substitutes¹² as shown in figure 1.2 below.

A similar approach is actively being pursued by the Coughlin group here at PSE, as well as the Kerr group at Lawrence Berkeley National lab. In their approach they have utilized both perfluorosulfonic groups and imidazole solvation groups so as to operate over a wide temperature range with little to no water.

1.5 PEM Morphology And Its Control

PEM performance is limited by factors such as thermal, Mechanical, and selectivity of the membranes. Selectivity issues arise from methanol permeation which closely tracks water based proton conductivity. Water facilitated conductivity depends on

the shape and size of the water domains and state of the water in these domains, which both largely depend on the morphology of the membrane¹³.

A largely synthetic approach has been taken to the manipulation of PEM morphology as reported in literature. Generally the molecular architecture of the polymer electrolyte has been designed to give a certain expected morphology, which is then characterized. Copolymers containing hydrophilic and hydrophobic components in some form or the other have been used typically, given the rich morphologically diverse structures these can produce even without ions.

Copolymers can be made with random (Statistical), block, graft, or star architectures, which will phase separate(de-mix) depending on the enthalpic-entropic balance between their different components. The extent of separation depends on the degree of mismatch, the molecular weight of the components and crystallinity. Block copolymers microphase separate on the nanometer length scales to form spherical, cylindrical, lamellar and bicontinuous morphologies¹⁴. When ionic groups are added to one component of the copolymer, the resulting morphology is a compromise between the above mentioned driving force and the electrostatic interactions amongst the ionic groups.

NafionTM for instance which is a random copolymer of a hydrophobic backbone and grafts of ionic side chains, forms membranes with a phase separated structure, which is more pronounced upon hydration. Gebel and others have done extensive scattering

(SAXS,SANS) studies on these materials and have come up with a dry membrane structure having isolated spherical ionic clusters 15 Angstroms in diameter and 27 Angstroms apart in the midst of the hydrophobic domain. Upon addition of water SANS data has eventually indicated ribbon-like aggregates with characteristic thickness, width and length of 20, 80 and 1,000 Angstroms respectively¹⁵.

An example of diblock copolymer PEM materials was synthesized by Holdcroft et al. and consists of a polysulfone and poly(vinylidene fluoride), SPSF-*b*-PVDF. This was done in order to study the effect of the fluoropolymer block on conductivity and morphology. The TEM micrographs obtained are as in figure 1.3 below.

Ionic aggregates are seen in both the homo and block sulfonated polysulfones, however an increased conductivity is noticed for the block copolymers when there is lower sulfonation (or Ion Exchange Capacity IEC). This is attributed to enhanced ionic aggregate and network formation from the fluorinated block. The size of the aggregates are smaller in the block copolymers (7 nm vs. 11nm)¹⁶.

Morphological work has also been done on A-B-A triblock copolymers of Polystyrene-*b*-Poly(ethylene-*r*-butylene)-*b*-Polystyrene, with the styrene block partially sulfonated (sSEBS). In this work the membrane morphology was tuned using different solvent combinations to shield or enhance the electrostatic interactions.

The effect of increasing the MEOH co-solvent on the morphology was the frustration of the normal block copolymer lamellae structure. This may be due to the distortion of the volume fractions due to swelling. The disordered structure had a higher proton conductivity and methanol permeability as it is more difficult to have transport through domains lying parallel to the membrane surface¹⁷. Another study used crosslinking to fix proton conducting channels in similar materials and in effect increased conductivity and lowered methanol permeability¹⁸.

Other morphological studies have been done on the PS-g-macPSSA graft copolymers mentioned previously⁶. These membranes show connected ionic domains 5-10 nm wide which yield a continuous network. The graft copolymers show no significant phase separation and the phase separated network of nanochannels is developed as the sulfonation increases. This seems to explain the fact that conductivity in the graft copolymers is much higher than the random ones and increases with increasing sulfonation. This trend is consistent for most studies reported for low IEC. However as IEC (sulfonation) increases the percolation limit is reached and phase separation does not prove to make that much of a difference in conductivity. However it may also enhance mechanical properties and reduce gross macroscopic swelling⁶.

Finally the backbone flexibility determines the extent of phase separation and the sharpness of the interface, which will ultimately dictate the conformation of water in the nano-channels. Generally, a less stiff backbone allow more phase separation and more loosely bound water which facilitates conductivity.

1.6 Materials For This Work

Two sets of materials have been used in this work. However both types will fall under the theme of creating and characterizing nanostructured PEMs.

The first group of materials are fluorinated Poly(isoprene)-*b*- sulfonated Poly (Styrene) (fPI-*b*-sPS) polymers which have been used to form PEMs (Films) , and the resulting structure and properties investigated. These materials have been synthesized using facile post-polymerization modification methods to Fluorinate and sulfonate well defined Poly(Styrene)-*b*- Poly(Isoprene) (PSPI) diblock copolymers.

In the light of mounting energy costs and environmental concerns, there has been a renewed thrust to develop and commercialize fuel cell systems as alternative sources of energy. Full commercialization has been impeded by factor such as cost , feed storage and deployment to mention a few. On the other hand , inadequate understanding of the relationship between structure/morphology and fuel cell relevant properties have slowed the development of suitable alternative PEM materials to replace the expensive and structurally ill-defined Nafion.

To this end, our sample produced by fluorinating the Poly(diene) block and partially sulfonating the poly(Styrene) block of anionically polymerized PS-PI, is seen as a possible less expensive PEM candidate material, and a model compound for accurate study of the relationship between polymer architecture, morphology ,and ultimately, properties of block copolymer based PEMs.

The synthetic route employed is as follows : The Polydiene block of the PS-PI was fluorinated via the addition of *in situ* generated difluorocarbene to the double bond of poly(Isoprene). The sulfonation of the polystyrene block with controlled degree of sulfonation was performed by using a mixture of acetyl sulfonate and sulfuric acid. Further synthetic details are available elsewhere¹⁹ and briefly described in the scheme shown in figure 1.4 below.

The other type of materials used are a family of Sulfonated Poly(Aryl ether Ketone)s which are electrospun to make PEMs based on nanofibrous mats of said polymers. As discussed earlier aromatic polymers are seen as good candidate precursors for PEMs because of their good chemical, oxidative, thermal and mechanical stability which carry over to some extent when they are sulfonated. .

The most common of these is poly(ether ether ketone) (PEEK) which is commercially available under the trade name Victrex. The other two are also available commercially. Lower cost, higher use temperatures and easy processing and sulfonation have made these polymers attractive substitute PEM materials. Sulfonation is achieved by use of sulfuric acid²⁰

1.7 Work Done

1.7.1 Membrane Structure and Transport properties

Polymer electrolyte membranes have been fabricated from the above described materials, synthesized by Prof. Jimmy Mays group in University of Tennessee Knoxville.

Solvents or solvent mixtures with varying dielectric constants have been used to cast films from these materials in order to produce different membranes with controlled morphologies.

The fuel cell relevant transport properties have been measured namely, Proton conductivity and Methanol permeability. Our potential target application for such materials are powering portable devices. Such applications are best served by Direct Methanol Fuel Cells as explained in the introduction section.

Electrochemical Impedance Spectroscopy (EIS) has been employed to measure the proton conductivity of these membranes. As is the case with NafionTM and other PEM materials, conductivity in a material varies with water content, operating temperature, and counterion quantity and type. All these variables have been explored. EIS involves applying a small AC current to an Electrochemical Cell, comprising of the PEM and electrodes in some configuration or the other. The voltage response of this cell is measured and analyzed, giving a resistance or better put impedance of the membrane, which is used to calculate ionic conductivity through the membrane.

Methanol permeability have been measured using a horizontal diffusion Cell that comprises of two side-by-side jacketed liquid chambers with holes facing each other. 1-2 M aqueous Methanol solution was put in one chamber while water was put in the other chamber. The membrane was sandwiched in between and the change in methanol concentration on the water only chamber is to be measured by pumping this liquid in a

cycle through and RI detector and the signal monitored via a LabVIEW PC based data acquisition system.. This has been done at different possible operating temperatures.

1.7.2 Membrane Structural evolution with hydration and heating.

According to the foregoing discussion on PEM morphology, it is clear that the structural/morphological characteristics of a PEM affect its fuel cell relevant properties, especially proton conductivity. It is also well established that these properties evolve with varying hydration and operating temperature, which implies that the structure also changes.

Extensive Small angle scattering work has been done by a couple of researchers on NafionTM by Gebel et al and show that PEM morphology changes with heating and hydration , however the NafionTM microstructure is still under debate. This area of research for PEMs is important because it can elucidate the structure and water management of these membranes, especially under conditions mimicking operations. This will facilitate the development of appropriate models to estimate and eventually predict properties.

Small angle scattering and microscopy have been the main tools for investigating PEM structure. DSC has been used to determine the structure of water within the conducting hydrophilic domain. In this work, scattering and microscopy facilities (SAXS, TEM, DSC) have been used to study the structure of dry fPI-*b*-sPS membranes.

Hydrated membranes have been studied at the Argonne National Laboratory using SANS and Ultra SAXS over extended angular ranges. These all have been carried out at different temperature and hydration levels, over as wide an angular range as possible, so as to map the complex structures formed in our fPI-*b*-sPS samples at different length scales.

1.7.3 Membrane microdomain orientation by external fields.

All the PEM materials discussed so far have hydrophilic acid bearing side chains or pendant groups and some relatively less hydrophilic (or distinctly hydrophobic) components. The proton conductivity takes place in the hydrophilic domains as this is where the water resides. This means that for the protons to conduct from one surface of the membrane to the other side there must be a continuous hydrophilic pathway from one end to the other. If this pathway is straight it would take a proton less time to get to the other side than if the path had all sorts of twists and turns (tortuosity).

Different external fields have been used to orient or order block copolymer morphologies successfully and they include: shear forces, Solvent, rate of solvent evaporation and film thickness⁶. One report has been published of electric field orientation of the conducting phase of PEM blends, and another of magnetic field alignment of nanoparticle conducting phase in LiI:PEO polymer electrolytes for Lithium ion batteries. Significant enhancements of conductivity were noticed in both cases, with the Li ion battery gaining up to an order of magnitude increase^{21,22}.

To orient microdomains of our fPI-*b*-sPS perpendicular to membrane plane electric fields have been applied, in order to reduce tortuosity and thus enhance conductivity. The problem is however not a straightforward as for normal block copolymers because the sulfonate groups in our block copolymer ionomers frustrate the normal self assembly due to strong electrostatic interactions. These interactions favor disordered morphology. These membranes and their control have been characterized by TEM and EIS.

1.7.4 PEMs from electrospun poly (Aryl ether ketone)s

Electro-spinning is a process whereby fibers of polymeric materials can be spun from solution or melt by means of an electrostatic field induced drawing and is schematically shown in figure 1.5. The polymer solution is typically forced out of a needle by a syringe pump, and when the surface charges on the polymer droplet at the tip of the needle overcomes its surface tension, the drop is elongated and a jet of fluid is accelerated towards a grounded target. By the times this jet reaches the target it would be evaporated to a web of fibers of size ranging from tens of nanometers to microns.

This process depends on certain parameters such as;

- Polymer Properties: Type, and architecture of polymer.
- Solution Properties: viscosity, elasticity, conductivity, and surface tension.
- Process Parameters: Electric potential, gap distance, and flow rate.
- Ambient Conditions: Temperature, humidity and Air velocity in chamber.

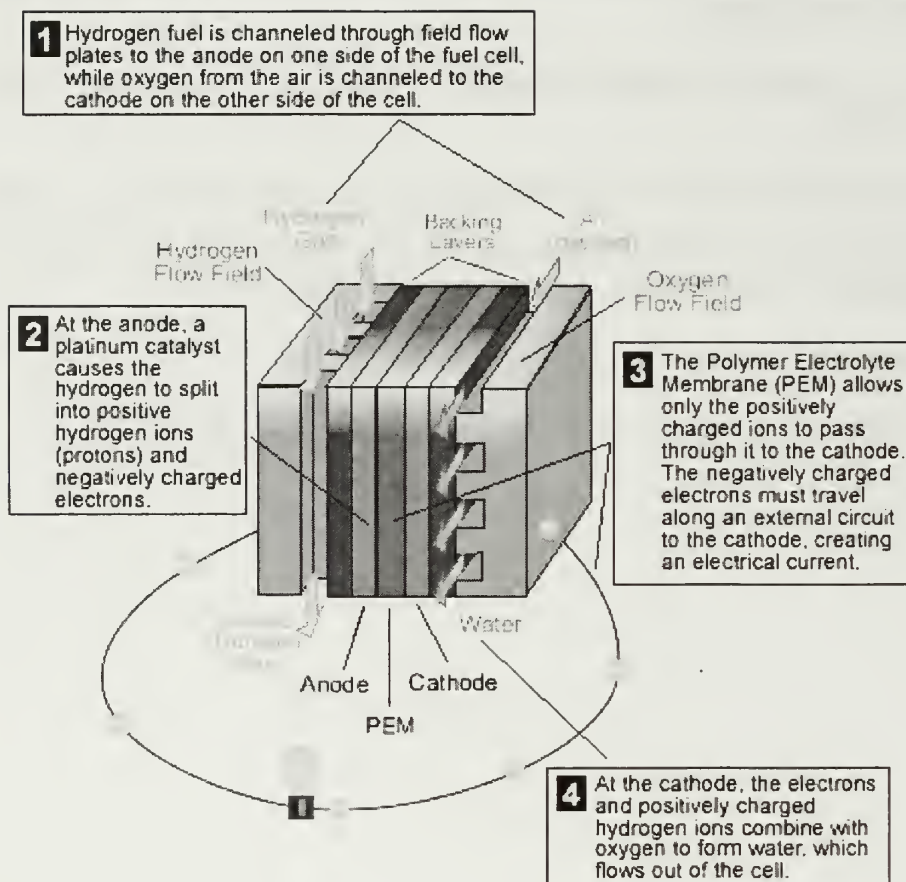
The technique has been applied to end uses such as nanofiber based membranes and smart cloth using nanofiber mats; biomedical usage like porous mats for wound dressing, gene encapsulation; Supports for enzymes and catalysts, PEO encapsulated enzymes; Sensors, Electrodes and Electro-optical devices; Sacrificial templates.

Little work has been done on electro-spinning of nanofibrous mats from polymer electrolytes for membrane applications. This part of the work comprised of the investigation of the electro-spinning characteristics, and the potential for use of electrospun sulfonated PEEK or PEKK as nanoporous PEMs. It is known that the presence of unbound water or electrolyte in a membrane's pores or channels enhance conductivity. This will be measure using Electrochemical Impedance Spectroscopy.

1.8 References

- (1) O'Hayre, R.P.; Cha, S.; Cololla, W.; Prinz, F.B. *Fuel Cell Fundamentals*; 1 ed.; John Wiley & Sons, Inc. NY, **2006**.
- (2) <http://www.sae.org/technology/fuelcells-history.htm>.
- (3) Carrette, L.; Friedrich, K.A.; Stimming, U. *Fuel Cells* **2001**, 1, 5.
- (4) Hickner, M.A.; Ghassemi, H.; Kim, Y.S.; Einsla, B.R.; McGrath, J.E. *Chemical Reviews* ,**2004**, 104, 4587.
- (5) Arico, A.S.; Srinivasan, S.; Antonucci, V. *Fuel Cells* **2001**, 1, 133.
- (6) Yang, Y.; Holdcroft, S. *Fuel Cells* **2005**, 5, 171.
- (7) Bishop, M.T.; Karasz, F.E.; Russo, P.S.; Langley, K.H. *Macromolecules* **1985**, 18, 86.
- (8) Wainright, J.S.; Wang, J.T.; Weng, D.; Savinell, R.F.; Litt, M.J. *J. Electrochem. Soc.* **1995**, 142, L121.
- (9) Miyatake, K.; Hay, A.S.; *J. Polym. Sci., Part A: Polym. Chem* **2001**, 39, 3770.
- (10) Savett, S.C.; Atkins, J.R.; Sides, C.R.; Harris, J.L.; Thomas, B.H.; Creager, S.E.; Pennington, W.T.; DesMarteau, D.D. *J. Electrochem. Soc.* **2002**, 149, A 1527.
- (11) Kim, Y.S.; Wang, F.; Hickner, M.; Zawodzinski, T.A.; McGrath, J.E. *J. Membr. Sci.*, **2003**, 212, 263.
- (12) Herz, H.G.; Kreuer, K.D.; Maier, J.; Scharfenberger, G.; Schuster, M.F.; Meyer, W.H. *Electrochim. Acta* **2003**, 48, 2165.
- (13) Hickner, M.A.; Pivovar, B.S. *Fuel Cells* **2005**, 5, 213.
- (14) Khandpur, A.K.; forster, S.; Bates, F.S.; Hamley, I.M.; Ryan, A.J.; Bras, W.; Almdal, K.; Mortensen, K. *Macromolecules* **1995**, 28, 8796.
- (15) Rubatat, L.; Rollet, A.L.; Gebel, G.; Diat, O. *Macromolecules* **2002**, 35, 4050.
- (16) Yang, Y.; Shi, Z.; Holdcroft, S. *Macromolecules* **2004**, 37, 1678.

- (17) Kim, J.; Kim, B.; Jung, B.; Kang, Y.S.; Ha, H.Y.; Oh, I.H.; Ihn, K.J. *Macromol. Rapid. Commun.* **2002**, 23, 753.
- (18) Won, J.; Park, H.H.; Kim, Y.J.; Choi, S.W.; Ha, H.Y.; Oh, I.H.; Kim, H.S.; Kang, Y.S.; Ihn, K.J. *Macromolecules* **2003**, 36, 3226.
- (19) Huang, T.; Gido, S.P.; Mays, J.W. in *Synthesis and characterization of Fluorinated and sulfonated Block copolymers for Fuel Cell Proton Exchange Membranes*. Unpublished Manual.
- (20) Swier, S.; Chun, Y.S.; Gasa, J.; Shaw, M.T.; Weiss, R.A. *Polymer Eng. & Sci.* **2005**, 1081.
- (21) Weiss, R.A.; Shaw, M.T. *DOE Hydrogen Program FY 2004 Progress Report*.
- (22) Golodnitsky, D.; Livshits, E.; Kovarsky, R.; Peled, E.; Chung, S.H.; Suarez, S.; Greenbaum, S. *Electrochem. & Solid State Lett.* **2004**, 7, A412.
- (23) Huang et al. *Composites Sci. and Tech.* **2003**, 63, 2223.
- (24) Choi, S.W.; Jo, S. M.; Lee, W.S.; Kim, Y. *Adv. Mater.* **2003**, 15, 2027.

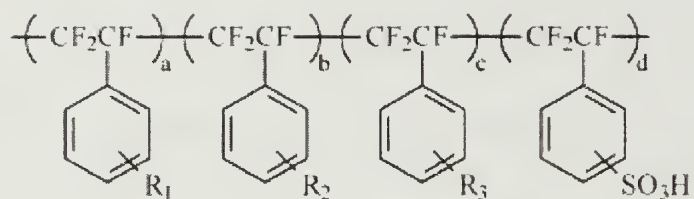
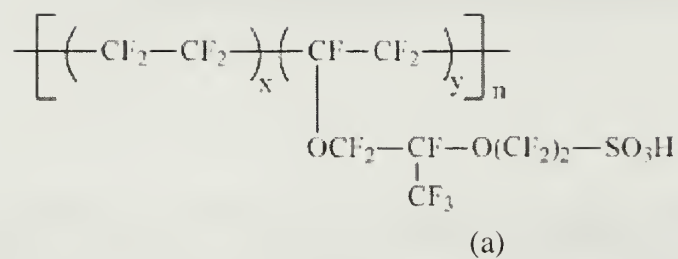


www.fueleconomy.gov/.../fuel_cell_still.gif

Figure 1.1 Membrane Electrode Assembly (MEA)

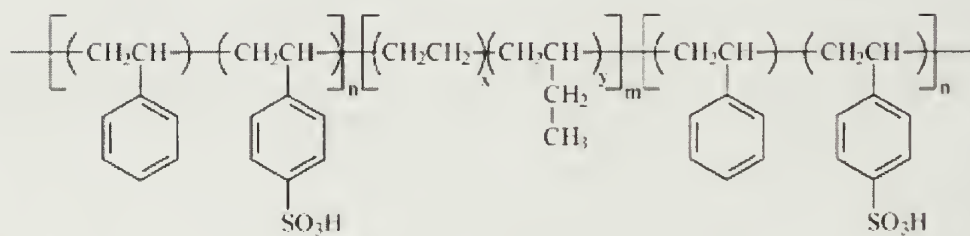
Table 1.1 The different Fuel Cells that have been realized and are in current use and development.³

	AFC (Alkaline)	PEMFC (Polymer Electrolyte Membrane)	DMFC (Direct Methanol)	PAFC (Phosphoric Acid)	MCFC (Molten Carbonate)	SOFC (Solid Oxide)
<i>Operating temp. (°C)</i>	<100	60–120	60–120	160–220	600–800	800–1000 low temperature (500–600) possible
<i>Anode reaction</i>	$\text{H}_2 + 2\text{OH}^- \rightarrow 2\text{H}_2\text{O} + 2\text{e}^-$	$\text{H}_2 \rightarrow 2\text{H}^+ + 2\text{e}^-$	$\text{CH}_3\text{OH} + \text{H}_2\text{O} \rightarrow \text{CO}_2 + 6\text{H}^+ + 6\text{e}^-$	$\text{H}_2 \rightarrow 2\text{H}^+ + 2\text{e}^-$	$\text{H}_2 + \text{CO}_3^{2-} \rightarrow \text{H}_2\text{O} + \text{CO}_2 + 2\text{e}^-$	$\text{H}_2 + \text{O}^{2-} \rightarrow \text{H}_2\text{O} + 2\text{e}^-$
<i>Cathode reaction</i>	$\frac{1}{2} \text{O}_2 + \text{H}_2\text{O} + 2\text{e}^- \rightarrow 2\text{OH}^-$	$\frac{1}{2} \text{O}_2 + 2\text{H}^+ + 2\text{e}^- \rightarrow \text{H}_2\text{O}$	$\frac{3}{2} \text{O}_2 + 6\text{H}^+ + 6\text{e}^- \rightarrow 3\text{H}_2\text{O}$	$\frac{1}{2} \text{O}_2 + 2\text{H}^+ + 2\text{e}^- \rightarrow \text{H}_2\text{O}$	$\frac{1}{2} \text{O}_2 + \text{CO}_2 + 2\text{e}^- \rightarrow \text{CO}_3^{2-}$	$\frac{1}{2} \text{O}_2 + 2\text{e}^- \rightarrow \text{O}^{2-}$
<i>Applications</i>	Transportation Space Military Energy storage systems			Combined heat and power for decentralised stationary power systems	Combined heat and power for stationary decentralised systems and for transportation (trains, boats, ...)	
<i>Realised Power</i>	Small plants 5–150 kW modular	Small plants 5–250 kW modular	Small plants 5 kW	Small – medium sized plants 50 kW – 11 MW	Small power plants 100 kW– 2 MW	Small power plants 100–250 kW
<i>Charge Carrier in the Electrolyte</i>	OH^-	H^+	H^+	H^+	CO_3^{2-}	O^{2-}

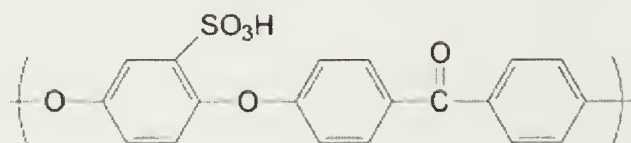


R_1, R_2, R_3 = alkyls, halogens, OR, $\text{CF}=\text{CF}_2$, CN, NO_2 , OH

(b)

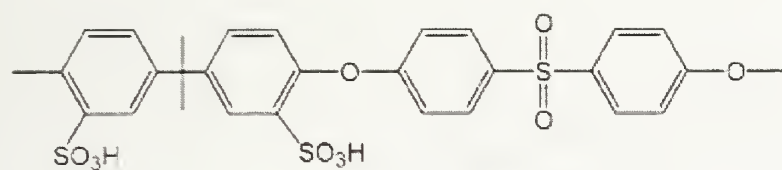


(c)

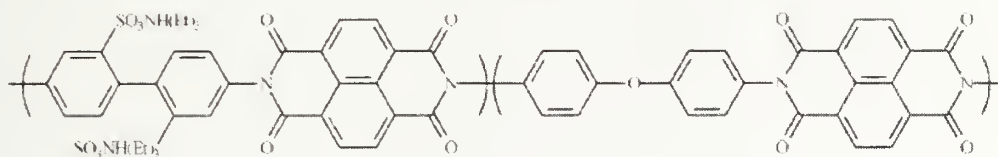


(d)

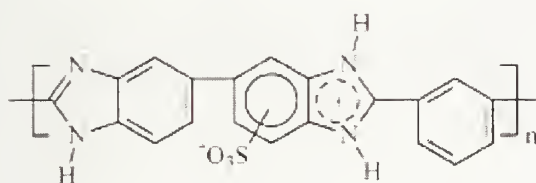
Figure 1.2: Chemical structures⁴ for (a) NafionTM (b) BAMTM (c) sSEBS (d) sPEEK
(Continued)



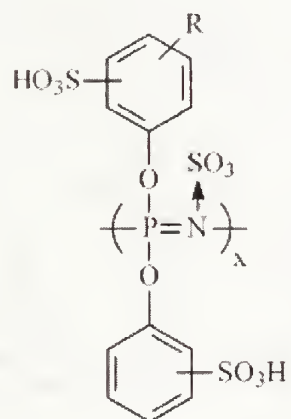
(e)



(f)

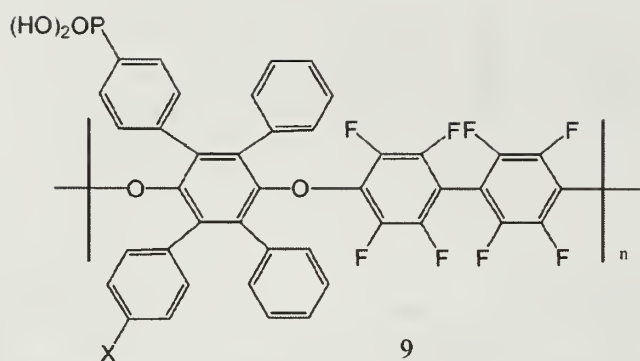


(g)



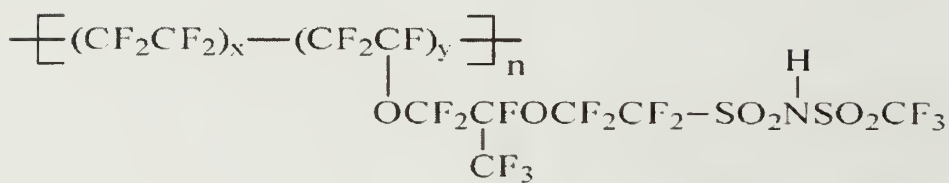
(h)

Figure 1.2: Chemical structures⁴ for (e) sulfonated Poly(Arylene ether Sulfone) (f) Sulfonated Poly(Imide) (g) Sulfonated PBI (h) sulfonated Poly[(3-methylphenyloxy)(phenoxy)phosphazene (Continued)

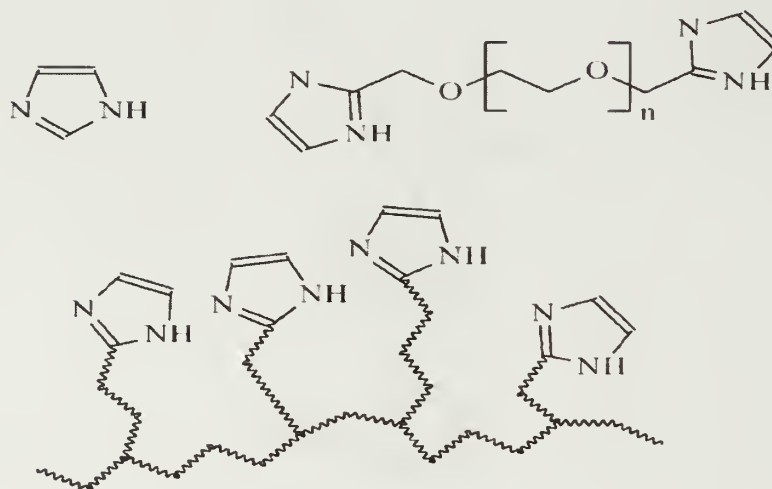


X: H(a), PO(OH)₂(b)

(i)



(j)



(k)

Figure 1.2: Chemical structures⁴ for (i) poly(arylene ether)s bearing phosphonic acid groups (j) Nafion like bis(perfluoroalkyl) sulfonamide (k) Free and tethered polymer backbones .

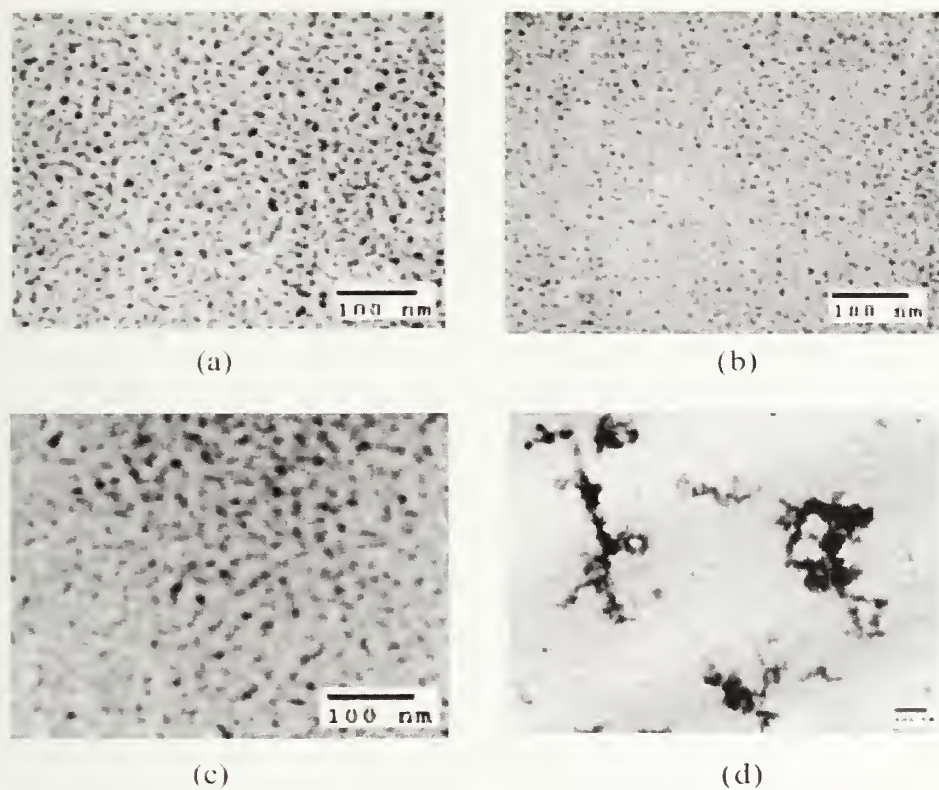


Figure 1.3 TEM micrographs⁶ of a) SPSF (IEC 1.55); b) SPSF1-b-PVDF (IEC=1.62); c) SPSF (IEC=0.83); d) SPSF1-b-PVDF (IEC=0.78).

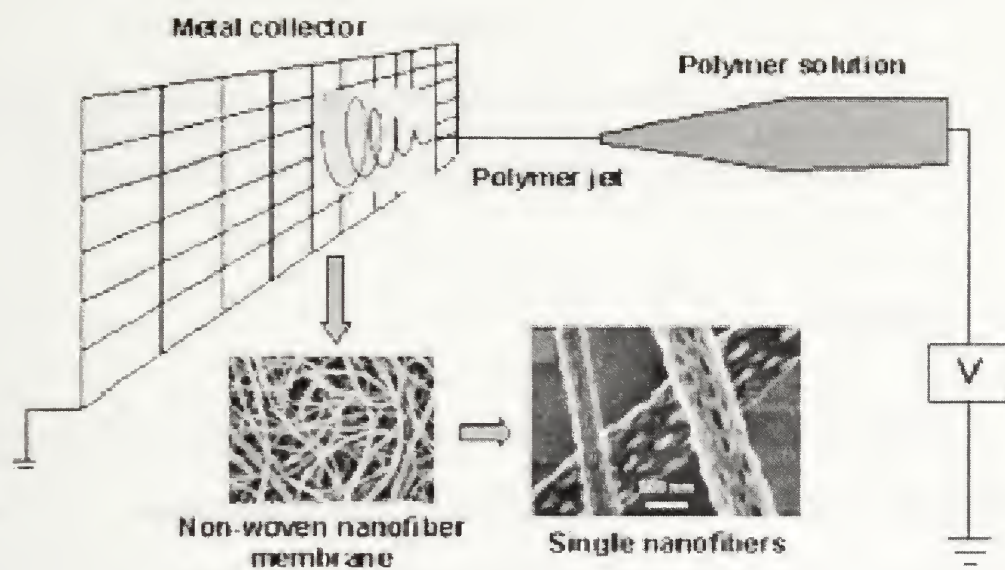


Figure 1.5 Electro-spinning experimental setup²³.

CHAPTER 2

POLYMER ELECTROLYTE MEMBRANES FROM FLUORINATED POLY(ISOPRENE)-BLOCK-SULFONATED POLY(STYRENE): MEMBRANE STRUCTURE AND TRANSPORT PROPERTIES

2.1 Abstract

With a view to optimizing morphology and ultimately properties, membranes have been cast from relatively inexpensive block-copolymer ionomers of fluorinated poly(Isoprene)-*block*-sulfonated poly(Styrene) (FISS) with various sulfonation levels, in both the acid form and the cesium neutralized form. The morphology of these membranes were characterized by TEM and USAXS, as well as water uptake, proton conductivity and methanol permeability within the temperature range from 20 to 60°C. Random phase separated morphologies were obtained for all samples except the cesium sample with 50mol% sulfonation. The transport properties increased with increasing degree of sulfonation and temperature for all samples. The acid form samples absorbed more water than the cesium samples with a maximum swelling of 595% recorded at 60°C for the acid sample with 50mol% sulfonation. Methanol permeability for the latter sample was more than an order of magnitude less than for Nafion 112 but so was the proton conductivity at 20°C within the plane of the membrane. Across the plane of the membrane this sample had half the conductivity of Nafion 112 at 60°C.

2.2 Introduction

Alternative sources of energy, besides fossil fuels, are a pressing need in the world we live in today. One such promising alternative is a fuel cell. Fuel Cells are typically classified according to their type of membrane, which serve both as a cell separator and a proton conductor¹. Two of the existing types of fuel cell membranes use polymers namely, Polymer Electrolyte Membrane Fuel Cells (PEMFC) and Direct Methanol Fuel Cells (DMFC)

The DMFC can be seen as a variant of the PEMFC. The membranes are typically the same; however, the feed for DMFC is methanol in an aqueous 1-2 M solution or in its vapor form. This fuel cell type has the most promise for portable applications as system complexities are reduced since there is no need to reform or store hydrogen, and the existing liquid fuels infrastructure can be used for methanol. Catalysts, as well as operating temperature ranges, are very similar to the PEMFC. Widespread commercialization of such devices has been impeded by factors including catalyst cost, mechanical or chemical instability and poor selectivity of the Polymer Electrolyte Membranes (PEM)². Selectivity issues arise from the cross-over of methanol from the anode to the cathode, which closely tracks water based proton conductivity, ultimately reducing cell efficiencies.

NafionTM, which is the prototypical PEM material, has a hydrophobic fluoropolymer backbone and hydrophilic fluorosulfonic acid bearing side chains^{3,4}. At present it is costly and still exhibits poor selectivity in DMFC applications. This has led

to a concerted effort to develop alternatives⁵⁻¹¹. These materials range from fluoropolymer to aromatic to hydrocarbon backboned materials, bearing pendant acid groups in one configuration or another.

Block copolymer ionomers are one such category gaining interest. As in normal block copolymers, nanometer scale microphase separation occurs, creating separate hydrophobic and ion-cluster containing hydrophilic domains with similar morphological diversity to neutral block copolymers. These phase separated systems have been shown to yield greater conductivity than the more homogeneous structures from random copolymers⁵. Also having random phase separated domains in these systems has been shown to give better transport properties than in systems where well ordered domains do not line up with direction of transport^{12,13}. Furthermore block copolymer ionomers with one block being a fluoropolymer have been shown to exhibit enhanced network formation and mechanical integrity especially when hydrated⁵.

Swelling or dilation of ionomers upon increasing water or methanol content and at service temperatures is also an important factor affecting conductivity and mechanical integrity. Backbone stiffness and counterions attached to the acid sites are known to affect the degree of water uptake and, hence swelling³. Upon neutralizing NafionTM from its acid form to its Cesium form, one study has shown decreased water uptake and methanol permeability, due to its lower hydration energy and hence water uptake¹⁴.

With a view to developing inexpensive phase separated PEMs we have synthesized, block copolymer ionomers comprising of a fluorinated hydrophobic block and a partially sulfonated hydrophilic block by means of post polymerization modification of the common poly(Styrene)-*block*-poly(Isoprene). The structures of membranes fabricated from these material as well as their transport properties (i.e proton conductivity and methanol permeability) have been investigated under conditions mimicking fuel cell usage, to assess their viability for low temperature DMFC applications. Also being synthesized from anionically polymerized precursors these materials will serve as suitable model molecules with precise architectures, to study the relationships between chemical structure and morphology.

2.3 Experimental Section

2.3.1 Materials

The synthetic procedure and characterization for fluorinated poly(Isoprene)-block- sulfonated poly(Styrene) (FISS) materials have been described in detail elsewhere¹⁵. The precursor poly(Styrene)-block- poly(Isoprene) (PS-PI) diblock copolymer used in this work was anionically polymerized, having reported properties: $M_w = 31,000$, $PDI = 1.05$, 27mol% PS. Fluorinated samples were sulfonated to 23,28 and 50 mol%, as determined by 1H NMR. Some samples were neutralized to the cesium salt form, and the balance left in the acid form. The cesium form facilitates contrast in the x-ray scattering experiments, besides exhibiting different transport properties. A sample coded FISS-AC50 would refer to the acid form of the material, sulfonated to 50mol% of the styrene units in the PS block. NafionTM 112 was generously donated by Atofina

Chemicals Inc., and was pretreated to the acid form according to the procedure reported elsewhere¹⁶.

2.3.2 Preparation of Membranes

Freeze dried FISS samples were dissolved in a mixture of Toluene/N-methylformamide(TOL/NMF:85/15 (w/w)) with a concentration ranging from 12-15 wt%. The NMF was used as a polar cosolvent. These solutions were then cast unto glass plates for a day in the fume hood at room temperature for rapid casting of kinetically trapped disordered morphology. Subsequently they were placed in an oven for 1 day at 60°C, and finally in the oven at 60°C plus vacuum for a day to remove most residual solvent. The acid form samples were further reactivated by soaking overnight in a 2M aqueous HCL solution containing methanol (20v/v) to enhance swelling and acid permeation. They were thereafter rinsed repeatedly in deionized water until PH was neutralized and then dried at 60°C in a vacuum oven for a day, and again in vacuum plus 60°C for one day. Cast membranes were subsequently removed and stored in airtight bags for further usage. Dry membrane thicknesses were measured using a digital micrometer and range from 60-90 um. The Nafion 112 samples were also rinsed until PH was neutralized and then dried at 60°C in a vacuum oven for a day and stored in the same way.

2.3 .3 Structural Characterization

The morphology of the dry membranes were determined by transmission electron microscopy (TEM). The membranes were first coated with gold and carbon on both sides, to serve as marker and epoxy diffusion barrier respectively. They were

subsequently embedded in epoxy(Araldite 516) and 50 nm thin sections of samples were cut across the thickness of the membrane using a Leica Ultracut UCT cryomicrotome at -120°C. These were then collected on copper grids and stained with RuO₄ vapor for 1 hour. It is assumed that only the unsulfonated Polystyrene domains were stained. TEM images were obtained using a JEOL-2010 microscope operating at an accelerating voltage of 200Kv. In the bright field mode.

Small angle x-ray scattering(SAXS) was performed at the Advanced Photon Source(APS) in Argonne National Laboratory on beamline 32-ID, fitted with a Bonse-Hart camera typically used for ultra small angle x-ray scattering (USAXS), which has been described elsewhere¹⁷. The x-ray energies range from 7 to 18 keV, yielding a q range from 0.0001 to 1.0 Å⁻¹ (where q , the scattering vector is equal to $4\pi \sin(\theta) / \lambda$, where 2θ is the scattering angle and λ is the wavelength of the incident radiation). The beam size was 1 mm x 2mm, and a 1-dimensional photodiode detector was used. Air-blanks were subtracted and slit desmearing of the resulting data was carried out using the lake method. All SAXS data were collected with the samples in the transmission position, with membrane normal in the direction of the beam.

In order to determine the surface morphology of the membranes, which significantly affects the interfacial properties in both Proton and methanol transport measurements, scanning probe microscopy (SPM) technique was used. SPM images of both sides of each membrane were collected using a Digital Instruments DimensionTM 3100 Atomic Force Microscope (a type of SPM) in the tapping mode.

2.3.4 Transport Properties

The water uptake behavior of the membranes were determined by soaking the samples in deionized water for at least 16 hours each at both room temperature(20°C) and 60°C. The difference in weight from dry to wet state was measured using a weighing scale accurate to 0.01 mg. The amount of water uptake was then calculated according to the expression:

$$WaterUptake(\%) = \frac{W_{Wet} - W_{Dry}}{W_{Dry}} \times 100 \quad (1)$$

Where W_{Wet} and W_{Dry} are the weights of wet and dry samples respectively. The permeation of methanol was measured using a horizontal diffusion cell, procured from PermeGear Inc. the whole experimental setup is shown in the Schematic in figure 2.1 below.

The cell was customized to have two 5ml jacketed chambers side by side, between which a membrane was clamped after being soaked in deionized water for at least a week. Holes in between the chambers allowed for 0.502 cm² of active membrane area exposed to 2M aqueous methanol solution on the feed side and HPLC grade water on the receiving side. Two ports in the receiving side allowed for continuous recirculation of content at a rate of 100ul/min, through a Waters 410 differential refractometer with voltage signal output to a National Instruments data acquisition interface sampling at a rate of 20,000 Hz. The voltage signal was calibrated to reflect changes in methanol concentration on the receiving side. Contents of both chambers were stirred continuously and water from a bath recirculation through the thermal jackets surrounding the chambers

was used to control the temperature. The procedure was according to the technique reported by Elabd et al. with the difference being the detection method¹⁸.

Upon solving the equation for one-dimensional diffusion through a plane sheet and rearranging, the expression below can be used to determine the permeability of methanol through membranes of different thicknesses at early times.

$$\frac{C_B(t)V_B L}{C_A A} = P \left(t - \frac{L^2}{6D} \right) \quad (2)$$

Where C_A and C_B are the methanol concentrations in the feed and receiving chambers and the condition $C_A \gg C_B$ is satisfied. A and L represent the membrane area exposed to fluid and its thickness, while V_B is the volume of the receiving chamber. P represents the permeability of methanol through the membrane and is calculated as the slope of $[(C_B(t) V_B L) / (C_A A)]$ versus time. P is equivalent to the product of the membrane diffusion and partition coefficients, D and K respectively^{18,19}.

Proton (and cesium) conductivity of the membranes were measured by means of four and two probe complex impedance spectroscopy techniques, which measure conductivity within and normal to the plane of the membrane respectively. A solartron 1252A frequency response analyzer linked to a an SI 1287 electrochemical interface was used within a frequency range of 0.1 and 300KHz. The 4 probe used was similar to that described in literature²⁰, however graphite paper strips were used as the blocking electrode. The 0.5 x 3cm membrane samples were initially soaked in deionized water for 16 hours at desired temperatures, and then removed and sealed in plastic container with

some water added to maintain 100% relative humidity and left to equilibrate for a day at relevant temperature (20 °C or 60°C), before measurements were made at room temperature. The two and four probe setups are as illustrated in the schematic Figure 2.2 below.

A similar procedure has been used for preparing sample for the two probe method as for the four probe method; however samples larger than the 1.18 cm² probe surface were sandwiched between the graphite paper to allow for good equilibration. The value of the real intercept in the Imaginary vs. real impedance plot (Bode plot) in the high frequency range is taken as the bulk resistance of the membrane. This is used in the expression below to calculate ion conductivity.

$$\sigma = \frac{l}{RA} \quad (3)$$

Where σ is the conductivity in (Siemens, S/cm), l is the distance between electrodes in cm (counter and working electrodes in the 4-probe method), R is the bulk resistance (Ω), and A is the membrane area normal to ion flux (cm²).

2.4 Results and Discussion

Membranes were cast in this study with the intent of kinetically trapping a random but phase separated morphology. This has been shown in previous block copolymer studies to decrease the effective tortuosity, and hence shorten the diffusion path length of the domain through which the species being transported permeates the membrane, resulting in improve transport properties²¹. In block copolymer ionomer

systems the use of a mixture of polar and nonpolar solvents have been shown to produce a more random phase separated microstructure which also had the effect of increasing permeability across the membrane^{13,22}, due to an enhanced connectivity of domains which provide more favorable diffusion of penetrant across the membrane¹². With the careful choice of the other block(s) to disallow diffusion of fluid, this can serve the purpose of maintaining mechanical integrity of the material especially in cases where transport of fluid is dependent on water content.

To this end a mixed solvent pair was chosen comprising toluene, which is a good solvent for FISS neutral copolymer, and NMF a highly polar cosolvent which will solvate the ionic domains in all the samples, especially the cesium neutralized samples. Also to varying degrees, this solvation is accomplished by dissociation of the counterions, which upon drying are available to frustrate the formation of regular equilibrium block copolymer morphologies due to presence of strong columbic interactions which lead to aggregation in the ionic domains.

Block copolymer systems have been well studied and exhibit a rich diversity of morphologies which include the classical spherical, cylindrical and lamellar morphologies, as well as the gyroid²³. These morphological forms are brought about by the process of self assembly into separated phases, which is governed by the degree of dissimilarity in the adjacent blocks, as well as the volume fraction of each block. It is usually observed by means of small angle x-ray scattering (SAXS) or TEM, with feature

sizes ranging from 5 to 50nm²⁴. The figures 2.3 below shows TEM images of the membrane samples prepared.

The dark parts of all images represent the partially sulfonated domains. Solid thick dark lines in the images represent gold used as a marker at the surface of the membrane, so a normal to this gold line in the direction of the film represents its depth. As was desired we observe a disordered morphology having sulfonated PS domains interconnected to essentially the same degree in the AC50, AC28 and CS23 samples. These grainy structures represent cylinders of partially sulfonated PS domains in a fluorinated PI matrix. A hexagonally packed cylindrical morphology is typically observed in unsulfonated PS-PI diblock copolymer with same volume fraction of PS as the precursor material (27mol% of PS). However as reported in other block copolymer ionomer studies there is a reduction in long range order upon addition of ionic groups^{22,25}. These disordered cylindrical domains can be seen to impinge on one another in the images, this will lead to a degree of interconnectivity in the transporting phase. Upon swelling in water and/or methanol this is expected to be further enhanced under fuel cell operating conditions, leading to a network proton conducting channels across the thickness of the membrane. This structural evolution has been shown in other copolymer ionomer studies^{4,26}, and is the subject of a subsequent publication²⁷.

The CS50 sample however, shows a lamella morphology with domains aligned parallel to the film surface. The reason for the formation of this classical neutral block copolymer morphology is not fully understood, however when the choice of the polar cosolvent was being made, it was observed that this sample was the most difficult to

dissolve, n-butanol and DMSO were tried but could not dissolve this sample, necessitating the use of NMF in this and all other samples for consistency. The cosolvents listed above are in order of increasing dielectric constant , which is an indirect measure of their ability to dissociated the counterion from the sulfonic acid group and hence dissolve the ionomer. With the foregoing it is safe to assume that this sample had the least amount of counterion dissociation (due to the larger quantity of Cs ions in the ionic domain), and hence there was minimal interference to the normal block copolymer self assembly process by free counter ions. This may also have to do with the low affinity of Cesium for polar solvents.

Self-assembly in block copolymer ionomers have consistently shown ordering at two length scales, due to the neutral block copolymer phase separation and ionic cluster formation^{28,29}. To capture the sizes of the different structural features (domains or ionic clusters) in this hierarchical microstructure, different configurations of SAXS cameras are typically used for the different q ranges; however we have been able to use a USAXS camera to capture several decades at one shot.

The characteristic dimension of the scattering objects can be obtained by substituting the value q^* of the first-order peak from the scattering intensity versus scattering vector plot $I(q)$ versus q), into the Bragg law given by the expression:

$$d = \frac{2\pi}{q^*} \quad (4)$$

This bragg spacing represents the average center-to-center distance between scatterers. In scattering profiles of samples with more regular spatial arrangement , the higher order

peaks are visible, and the type of structures packed on the lattice can be determined using the ratio of higher-order peaks to the first-order peak (q^i/q^*). A profile with hexagonally packed cylinders would therefore have a relative peak ratio of $1, \sqrt{3}, 2, \sqrt{7} \dots$, while a lamellar morphology, would have a ratio of $1, 2, 3, 4 \dots$ ³⁰. The inter-aggregate distance in the ionic domains can also be calculated by using the ionomer peak position in the Bragg equation. These will be found in a separate phase embedded in the PS domains which are in turn phase separated from the fluorinated PI domains³¹. The slit desmeared USAXS profiles from the membrane samples studied are shown in figure 2.4 below

We observed a prominent peak in both the AC28 and the CS23 samples at a position $q = 0.030861 \text{ \AA}^{-1}$. This corresponds to a characteristic dimension of 20.3 nm for both samples. A faint peak at $q = 0.052879 \text{ \AA}^{-1}$ can be seen in the profile for the CS23, and this would have a q^i/q^* ratio of 1:1.71, which is approximately representative of hexagonally packed cylinders (q^i/q^* ratio of 1:1.73). Combining this information with the TEM images obtained we can deduce that these two samples have a morphology composed of cylinders arranged imperfectly on a hexagonal lattice. Since the SAXS beam went into the membrane normal to the surface and there is a slight secondary peak in the CS23 sample, there is evidence of some cylinders oriented perpendicular to the film surface. It is worthwhile noting that there is no difference in the peak position for both samples. This is due to the fact the molecular weights of both samples are similar and so are their styrene weight fractions.

We also observe at a smaller length scale a broad peak in both samples with peak position centered around $q = 0.13264 \text{ \AA}^{-1}$ which corresponds to a bragg spacing of 4.7 nm. This is known as the ionomer peak, which represents the ionic clusters or aggregates. The intensity of this peak is greater in the cesium sample, as expected, due to the higher X-ray contrast relative to the acid samples.

In the CS50 sample we observed a similar hierarchical structure with the first order peak position at $q = 0.026455 \text{ \AA}^{-1}$, corresponding to a bragg spacing of 23.7nm. Two other peaks were visible at $q = 0.052876 \text{ \AA}^{-1}$ and $q = 0.077556 \text{ \AA}^{-1}$, which yield a q^i/q^* ratio of 1:1.99:2.93. This confirms the lamellar morphology observed in the TEM image and suggests that the lamellae sheets lie predominantly in a direction normal to the membrane surface. For both this sample and the AC28/CS23 samples, there is evidence of mixed or random orientation of the domains as the orientation evident in the TEM images are opposite to that in the SAXS. However SAXS information gives a better average of the existing morphology.

We also observe an ionomer peak for this sample within approximately the same q range as seen for the other samples however, the peak is centered at a position yielding a bragg spacing of 3.2nm. It is not clear as to why this sample has a smaller ionic characteristic dimension, however it is safe to assume that with an increased sulfonation there will be a greater crowding of aggregates in a similarly sized block domain, leading to shorter center-to-center distances. We collected USAXS data down to $q = 0.0001 \text{ \AA}^{-1}$ for all samples. The general trend shows an $I \sim q^{-d}$ dependence, where $2 < d < 3$ for AC28,

CS23 and CS50 samples, suggesting a self-similar mass fractal structure³². However the AC50 sample has a power law slope of -3.5 suggesting a rough surface fractal structure. This sample also shows a weak peak at a bragg spacing around $q = 0.027679 \text{ \AA}^{-1}$, yielding a bragg spacing around 22.7 nm. This peak represents the block copolymer characteristic dimensions. The ionomer peak was however indistinguishable.

The transport properties of the investigated membranes are summarized in table 2.1 below. Data from NafionTM 112 of similar thickness are also included for comparison. All experiments have been done under the same conditions.

The water uptake data show an increase in uptake both for increasing level of sulfonation as well as for increasing temperature. For the samples with the cesium counterion the water uptake measured is relatively lower than their acid counterpart. This is similar to results for Cs⁺ ion doped NafionTM reported by Tricoli¹⁴. Cesium ions are known to have less affinity for water, due to their lower hydration energy³³. This may however be dependent on other factors such as membrane morphology, and glass transition of the material. The CS50 sample disintegrate upon soaking in water at 60°C, whereas the AC50 sample does not. With lamellae layers lying perpendicular to the membrane surface the CS50 samples can be more easily pried apart upon swelling. The AC50 samples also swell markedly by 595% upon soaking in water at 60°C and are softened significantly. The results shown are an average of two samples per polymer.

Methanol permeation through our FISS and NafionTM membrane samples were measured by the method earlier described, and the specific concentration of permeated methanol in the receiving chamber has been plotted as a function of time in Figure 2.5. The slope of these graphs in the linear regions, yield the permeability of methanol through the membrane and have also been summarized in table 2.1. For samples prepared at 20°C we observe an order of magnitude less methanol permeability for the AC50 sample compared to NafionTM 112, however the result for the CS50 sample is just a little less. This may reflect the difference in morphologies of these two FISS samples. These values measured are similar to those reported for other styrene based ionomers^{13,18,34}.

No methanol cross-over could be detected for the AC28 and CS23 samples. However at 60°C these samples showed 27 times less permeability than NafionTM 112. The higher sulfonation membranes could not be measured at this temperature as they had swollen excessively and suffered mechanical failure under the osmotic pressure exerted by the 2M methanol solution.

Proton conductivity has been measured both in the plane and normal to the plane of our membrane samples, using the four-probe and two-probe methods respectively. The two methods should ideally give the same result, since the ions are moving through the same membrane, however there is a significant impedance contribution by the interface at low frequencies²⁰. For the application of block copolymer ionomers to DMFC technology, the more relevant measurement is that taken normal (across) the plane of the membrane as the methanol flux in a functioning fuel cell is in that direction. Also block copolymer domains

may possess some orientation which will impact the transport of ions the conducting phase. For these and other reasons the conductivity values measured using the two probe method are typically less than for the Four point probe³⁵. The conductivity values obtained have also been summarized in table 2.1 and are represented in figure 2.6 below.

The conductivity values for Nafion 112TM were measured for comparison with the FISS samples and published work in literature. Though most of the literature reports for Nafion conductivity measurements have been made using thicker Nafion 117TM, however one study using the 50 micron thick Nafion 112TM has reported an in-plane conductivity of 0.06 S/cm³⁶ at 80°C, whereas this study reports 0.065 S/cm at 60°C. The conductivity values measured with this geometry at room temperature for our AC50 and CS50 materials are about the same at 0.0011 S/cm and 0.0013 S/cm respectively. The CS50 samples has a higher conductivity under these conditions possibly due to the lamellar morphology lying perpendicular to the film surface. The conductivity value measure at 60°C are higher for both Nafion 112TM and AC50 due to greater chain mobility at higher temperature, and higher water uptake which facilitates proton transport.

The ionic conductivity measured in this geometry for both the AC50 and CS 50 samples are less than that for Nafion 112TM by more than an order of magnitude. In like manner, the conductivity of other styrenic copolymer ionomers have been reported to be less than Nafion,^{18,26} depending on the degree of sulfonation, as well as the morphology of the copolymer. This can also be attributed to the fact that the

fluorosulfonic acid found in nafion is a stronger acid than the styrene sulfonic acid in the styrenic systems. This deficit in conductivity can usually be made up for by increased sulfonation, but usually at the cost of softening due to increased swelling. Some sulfonated aromatic polymers having significantly more chain stiffness have however been able to bear more sulfonic acid groups with minimal swelling³.

For the two probe conductivity measurement which measures ionic conductivity across(through) the plane of the membrane, we see more than an order of magnitude less conductivity for all the samples with respect to the four probe method. This is mainly due to the difference in the experimental setup as this configuration has a much higher electrode surface area than the four probe configuration, and also there is charge buildup at the membrane-electrode interface leading to increased effective resistance^{37,38}. This typically leads to lower conductivity values³⁵. For the samples soaked at 60°C AC50, the in-plane conductivity is 48 times less than nafion112 whereas the, through plane conductivity of AC50 is only 2 times less than Nafion112. Since the through plane measurements are more relevant to a functional fuel cell, and both materials were measured in the same way these values are more descriptive of the actual membrane conductivity in a fuel cell.

The AC28 and CS23 samples did not show any measurable conductivity values. This is possibly due to the sulfonic acid concentration being less than the percolation threshold for these materials, or their low water uptake. Also for these samples with low sulfonation the fluorinated phase will tend to have less competition in migrating to the

surface layer as they have a lower surface energy than the sulfonated phase, leading to interfaces with reduced surface tension which is preferred. In order to test this hypothesis, an atomic force microscopy (AFM) study of the membrane surfaces was carried out. The scan from the smoother surface of each membrane adjoining the neutralized glass plate are shown in the figure 2.7 below.

The darker domains in the contrast image on the right represent the fluorinated phase which is softer. In the AC28 and CS23 images there is an almost uniform dark phase, which signifies the presence of a surface layer of mainly the fluorinated phase. This can explain the non-detectable ionic conductivity or methanol permeability of these samples, since the phase that allows permeation would have to be present on each surface and be connected from one surface of the membrane to the other.

However in the images for the AC50 and CS50 samples with higher sulfonation levels there is evidence of both a lighter and a darker phase at the surface. As seen in the TEM images for these samples the AC50 sample has a speckled morphology with spots of the lighter domain (sulfonated PS, and PS) will dispersed in the darker domain, where as the CS50 sample shows stripes of both light and dark domains running diagonally across the surface resembling a lamellar morphology. These surface morphologies with the hydrophilic phase present in greater amount, would favor higher ionic conductivity to the surface as is the case from our conductivity results.

2.5 Conclusions

New proton conducting membranes have been developed based on partially sulfonated poly(Styrene)-block- fluorinated poly(Isoprene). A randomly microphase separated morphology has been achieved using mixed polar and non-polar solvents, and USAXS has been used to elucidate the hierarchical structure and fractal dimensions which are favorable for enhanced transport properties. Low methanol permeability has been recorded relative to Nafion 112TM, however modest proton conductivity values were obtained. We believe that with further crosslinking of the residual polystyrene units to reduce swelling and optimization of the casting process, promising inexpensive candidates for low temperature direct methanol fuel cells will emerge.

2.6 References

- (1) O'Hayre, R. P.; Cha, S.; Cololla, W.; Prinz, F.B. In *Fuel Cell Fundamentals*; 1 ed.; John Wiley & Sons, Inc: New York, **2006**; p 12.
- (2) Arico, A.S.; Srinivasan, S.; Antonucci, V. *Fuel Cells* **2001**, 1, 133.
- (3) Hickner, M. A.; Ghassemi, H.; Kim, Y. S.; Einsla, B.R.; McGrath, J. E. *Chemical Reviews* **2004**, 104, 4587.
- (4) Gierke, T.D.; Munn, G.E.; Wilson, F.C. *J. Polymer Sci: Polym. Phys. Ed.* **1981**, 19, 1687.
- (5) Yang, Y.; Holdcroft, S. *Fuel Cells* **2005**, 5, 171.
- (6) Bishop, M.T.; Karasz, F.E.; Russo, P.S.; Langley, K.H. *Macromolecules* **1985**, 18, 86.
- (7) Wainright, J. S.; Wang, J.T.; Weng, D.; Savinell, R.F.; Litt, M.J. *J. Electrochem. Soc.* **1995**, 142, L121.
- (8) Miyatake, K.; Hay, A. S. *J. Polym. Sci., Part A: Polym. Chem* **2001**, 39, 3770.
- (9) Savett, S.C.; Atkins, J.R.; Sides, C.R.; Harris, J.L.; Thomas, B.H.; Creager, S.E.; Pennington, W.T.; DesMarteau, D.D. *J. Electrochem. Soc.* **2002**, 149, A 1527.
- (10) Kim, Y.S.; Wang, F.; Hickner, M.; Zawodzinski, T. A.; McGrath, J.E. *J. Membr. Sci.*, **2003**, 212, 263.
- (11) Herz, H.G.; Kreuer, K.D.; Maier, J.; Scharfenberger, G.; Schuster, M.F.; Meyer, W.H. *Electrochim. Acta* **2003**, 48, 2165.
- (12) Gido, S.P. In *ACS Symposium series: New Polymeric Materials* **2005**, 916, 309.
- (13) Kim, B.; Kim, J.; Jung, B. *J. of Membrane Science* **2005**, 250, 175.
- (14) Tricoli, V. *J. Electrochem. Soc.* **1998**, 145, 3798.
- (15) Huang, T.; Gido, S.P.; Mays, J.W. *Synthesis and Characterization of Fluorinated and Sulfonated Block Copolymers for Fuel Cell Proton Exchange Membrane*, Unpublished manuscript.
- (16) Miyake, N.; Wainright, J.S.; Savinell, R.F. *J. Electrochem. Soc.* **2001**, 148, A898.

- (17) Long, G.G.; Allen, A.J.; Ilavsky, J.; Jemian, P.R.; Zschack, P. In *Synchrotron Radiation Instrumentation: Eleventh US National Conference*, CP521, Pianetta, P.; Winick, H. Eds.; , American Institute of Physics, College Park, 2000, pp. 183–187.
- (18) Elabd, Y. A.; Napadensky, E.; Sloan, J. M.; Crawford, D.M.; Walker, C.W. *J. Membr. Sci.* **2003**, 217, 227.
- (19) Crank, J. *The Mathematics of Diffusion*; Oxford University Press: Oxford, 1975.
- (20) Cahan, B.D.; Wainright, J.S. *J. Electrochem. Soc.* **1993**, 140, L185.
- (21) Drzal, P.L.; Halasa, A.F.; Kofinas, P. *Polymer* **2000**, 41, 4671.
- (22) Elabd, Y. A.; Napadensky, E.; Walker, C. W.; Winey, K. I. *Macromolecules* **2006**, 39, 399.
- (23) Bates, F. S. *Science* **1991**, 251, 898.
- (24) Bucknall, D.G.; Anderson, H.L. *Science* **2003**, 302,1904.
- (25) Storey, R.F.; Baugh III, D.W. *Polymer* **2000**, 41, 3205.
- (26) Serpico, J.M; Ehrenberg, S.G; Fontanella, J.J.; Jiao, X. Perahia, D.; McGrady, K.A.; Sanders, E.H.; Kellogg, G. E.; Wnek, G. E. *Macromolecules* **2002**, 35,5916.
- (27) Isaacs-Sodeye A. I.; Huang T.; Mays J.; Gido S. P. “Block copolymer ionomers from Fluorinated Poly(Isoprene)-*block*-Sulfonated Poly(Styrene) 2: Structural evolution with swelling and in solution” *Manuscript in Preparation*.
- (28) Williams, C.E.; Russell, T.P.; Jerome, R.; Horrion, J. *Macromolecules* **1986**, 18, 2877.
- (29) Lu, X.; Steckle, W.P. Weiss, R.A. *Macromolecnles* **1993** 26, 5876.
- (30) Sakurai, S.; Momii, T; Taie, K.; Shibayama, M.; Nomura, S.; Hashimoto, T. *Macromolecules* **1993**, 26, 485.
- (31) Yarusso, D.J.; Cooper, S. L. *Macromolecules* **1983**,16,1871.
- (32) Roe, R. *Methods of X-Ray and Neutron Scattering in Polymer Science*; Oxford University Press: New York, 2000; p189.
- (33) Cotton, F.A.; Wilkinson, G. *Advanced Inorganic Chemistry*, John Wiley: New York, 1972, p 645.

- (34) Carretta, N.; Tricoli, V.; Picchioni, F. J. *J. Membr. Sci.* **2000**, 166, 189.
- (35) Deluca, N. W.; Elabd, Y. A. J. *Polym. Sci., Part B: Polym. Phys.* **2006**, 44, 2201.
- (36) Swier, S.; Chun, Y.S.; Gasa, J.; Shaw, M.T.; Weiss, R.A. *Polymer Eng. Sci.* **2005**, 45,1081.
- (37) Pivovar, B.S.; Wang, Y.; cussler, E.L. *J. Membr. Sci.* **1999**, 154, 155.
- (38) Alberti. G.; Constantino, U.; Casciola, M.; Ferroni, S.; Massinelli, L.; Staiti, P. *Solid State Ionics* **2001**,145, 249.

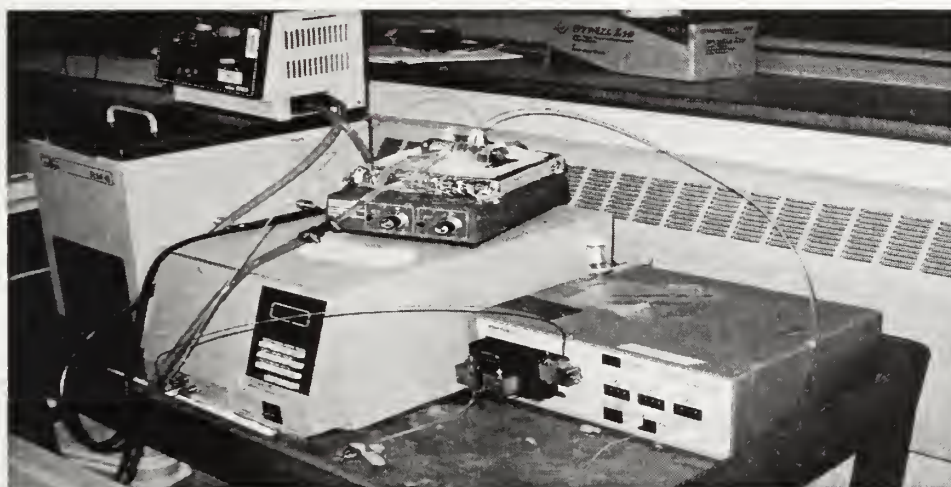
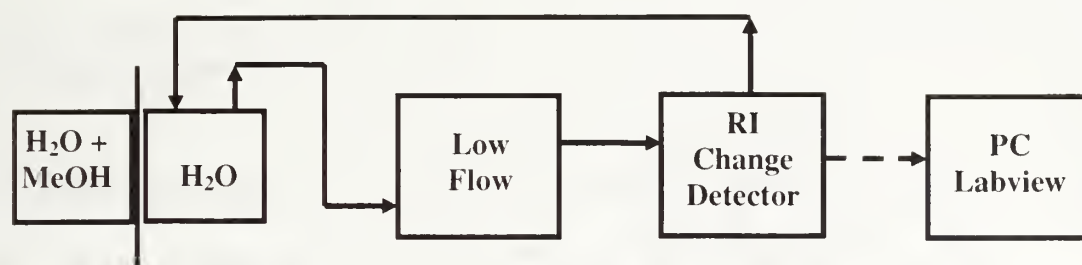
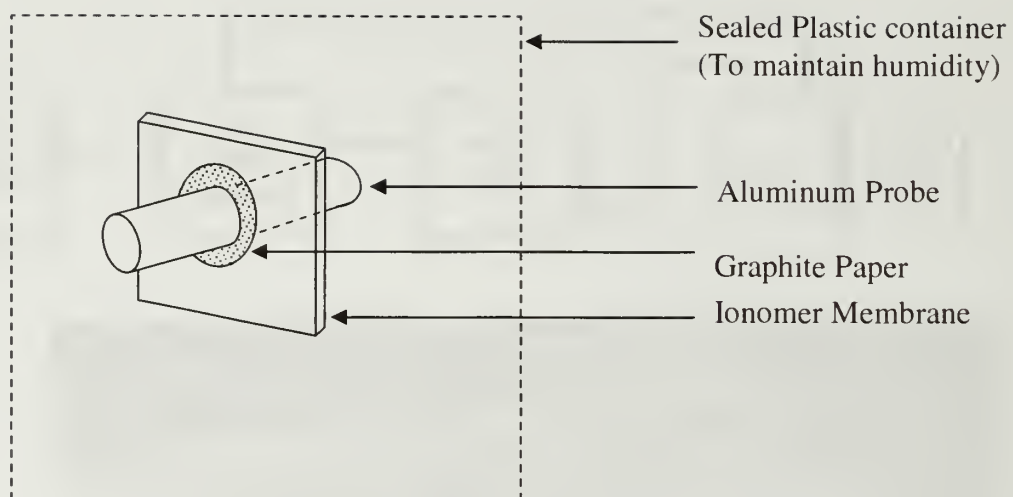
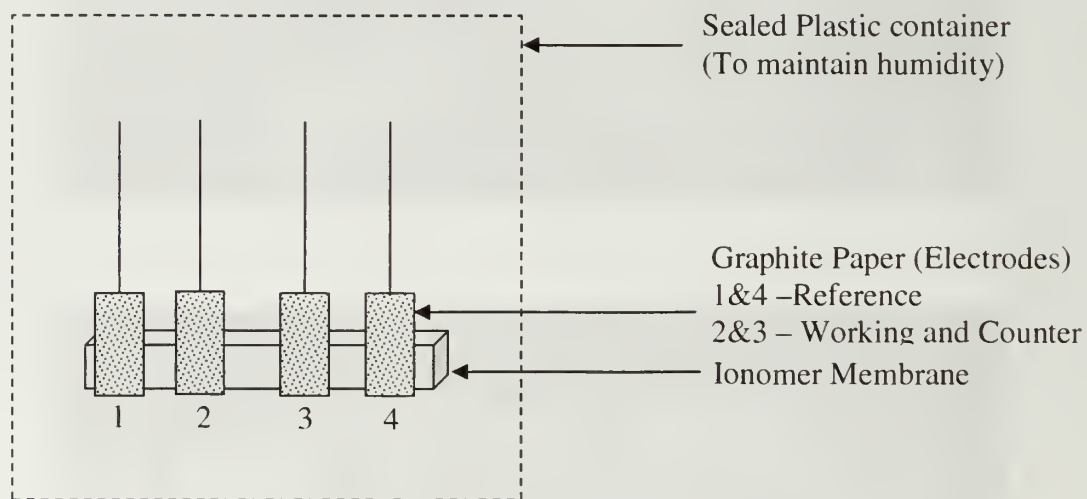


Figure 2.1 Flow diagram and pictures of Methanol Permeability measurement Experimental Setup.

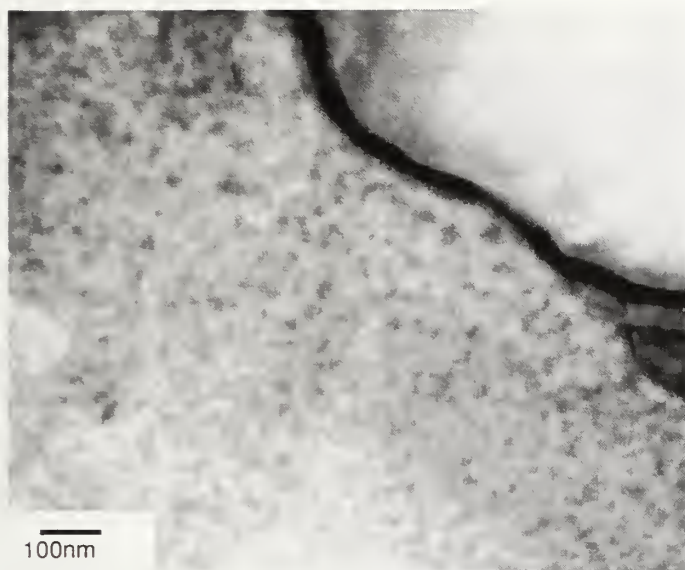


(a)

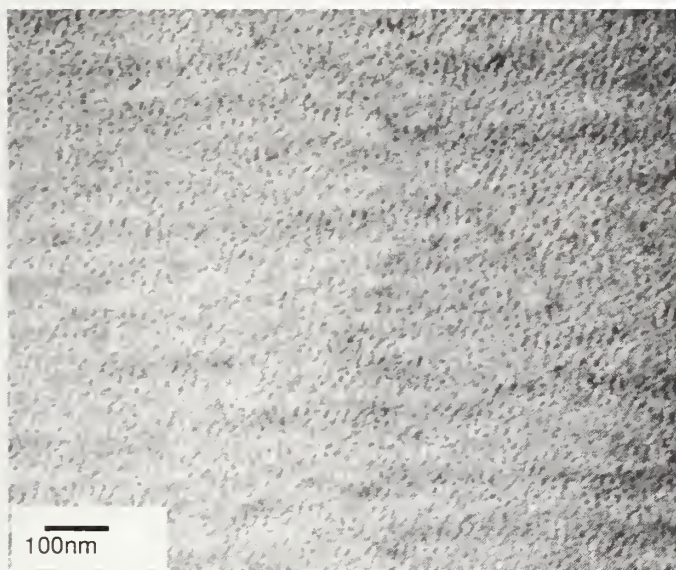


(b)

Figure 2.2 Experimental Setup for a) Two Probe , b) Four Probe EIS measurements.

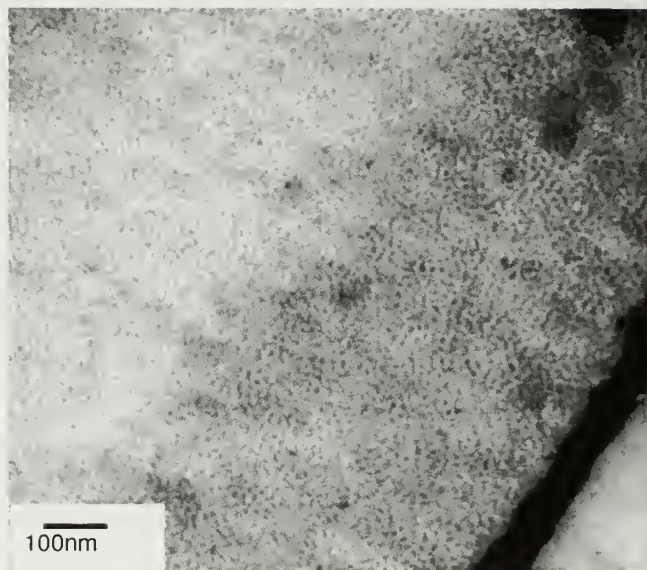


AC28

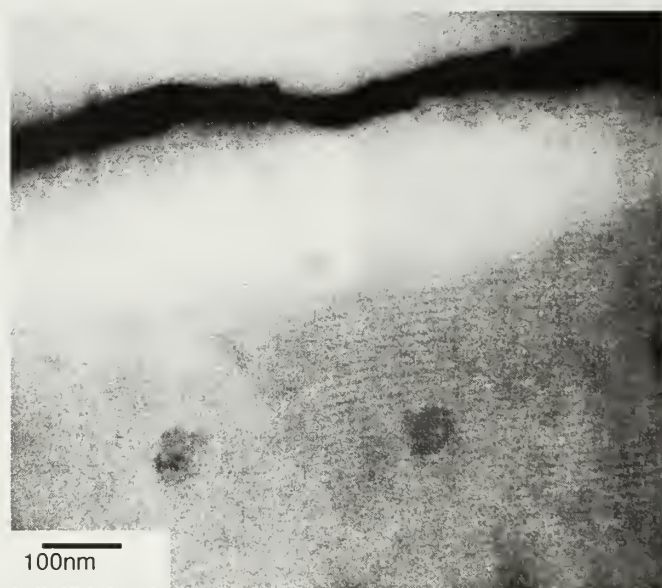


AC50

Figure 2.3 Transmission electron Microscopy images for the FISS samples.
(Continued)



CS23



CS50

Figure 2.3 (Continued)

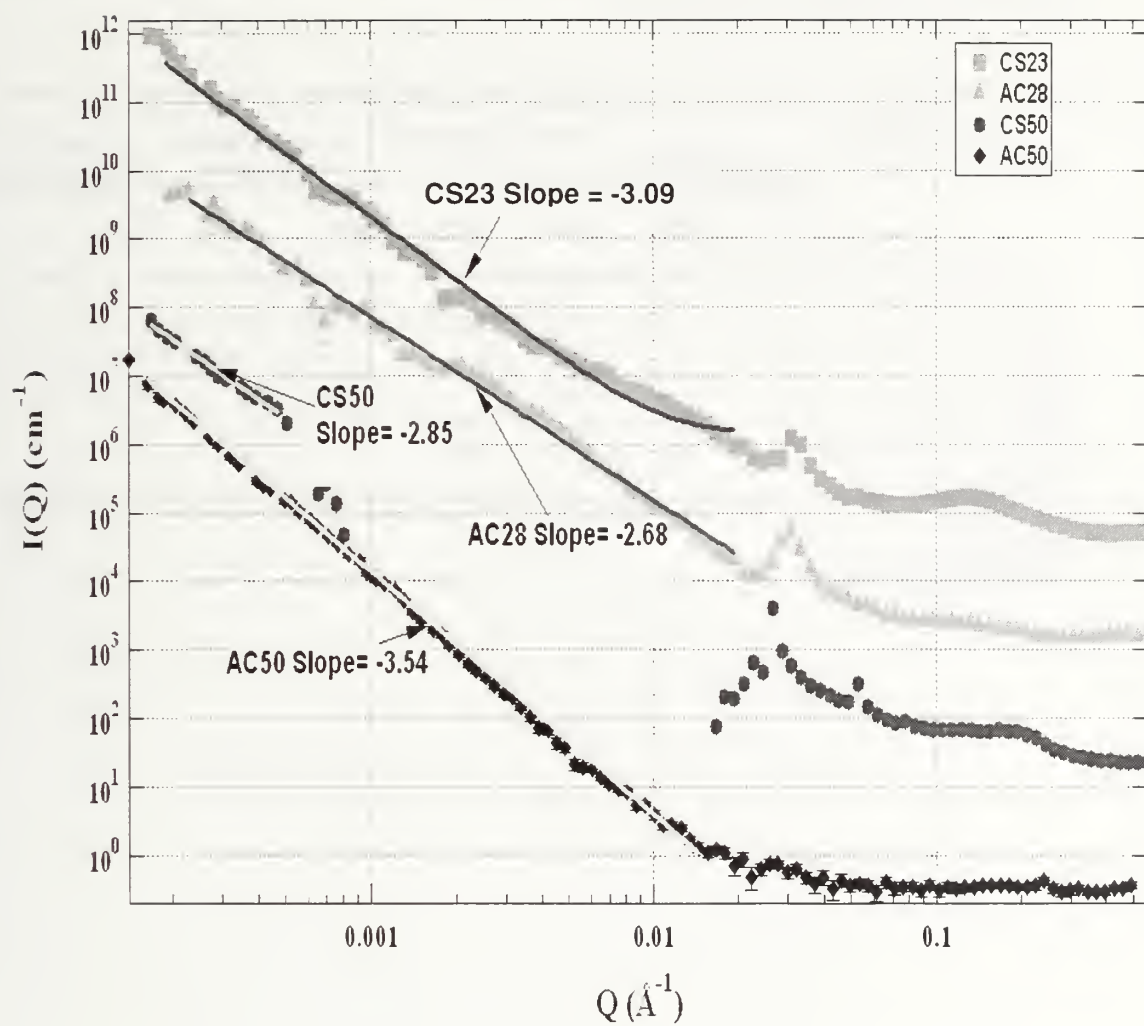


Figure 2.4 Ultra Small Angle Scattering Profiles for the FISS samples.

Table 2.1 Thickness, Water uptake, methanol permeability and ionic conductivity of materials investigated in this work.

Polymer	Dry Thickness (µm)	Water Uptake (%)		Methanol Permeability (cm ² /s)		In Plane Conductivity (S/cm)		Across Plane Conductivity (S/cm)	
		20°C ^b	60°C ^b	20°C	60°C	20°C ^b	60°C ^b	20°C ^b	60°C ^b
Nafion 112	50			2.6×10^{-7}	25.4×10^{-7}	1.82×10^{-2}	6.45×10^{-2}	8.47×10^{-5}	3.51×10^{-4}
AC50	81	17	595	2.0×10^{-8}	a	1.06×10^{-3}	1.33×10^{-3}	5.38×10^{-6}	1.57×10^{-4}
CS50	91	5	a	2.4×10^{-7}	a	1.26×10^{-3}	a	4.24×10^{-6}	a
AC28	69	5.4	257	0	2.0×10^{-8}	a	a	a	a
CS23	74	2.4	129	0	2.0×10^{-8}	a	a	a	a

^aNot Measurable

^bProcessing Temperature

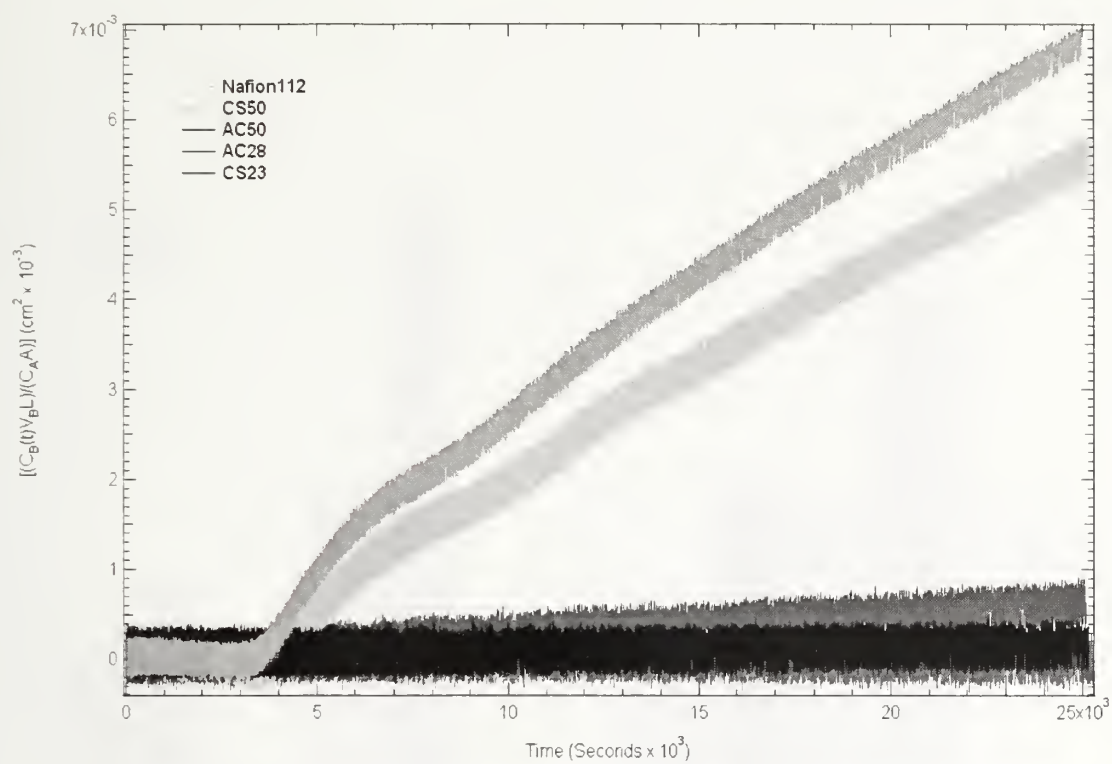


Figure 2.5 Specific concentration of permeated methanol versus Time measured at 20°C.

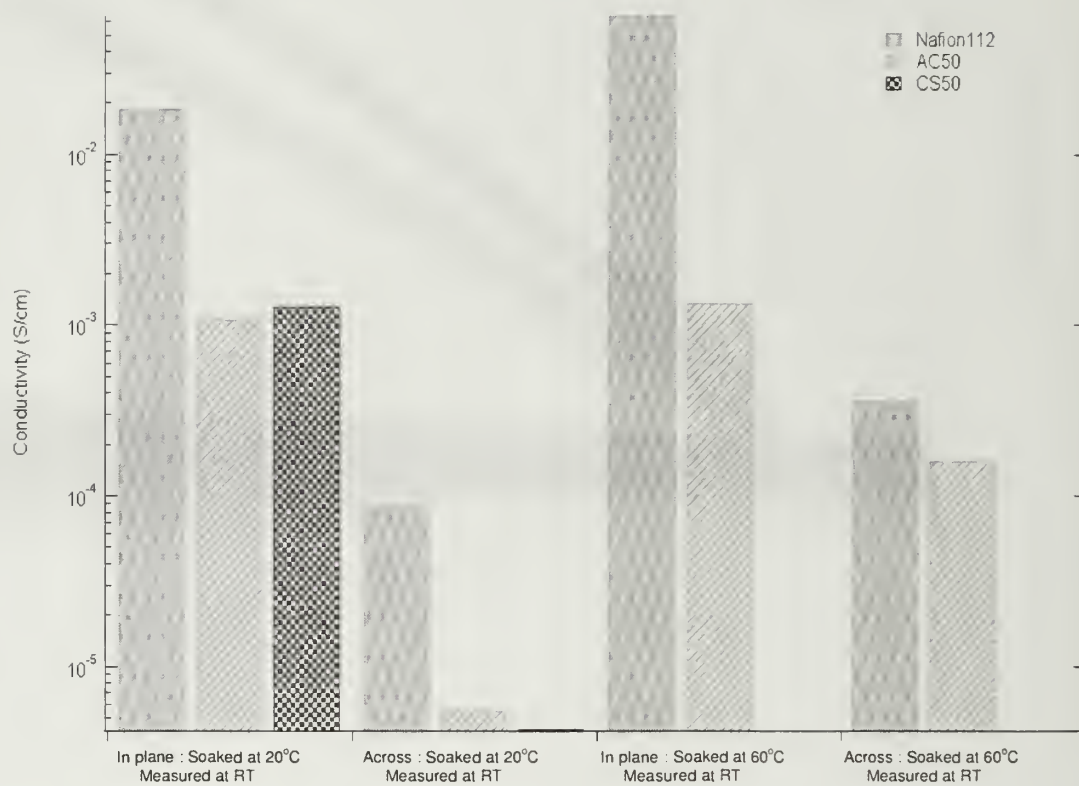


Figure 2.6 Ionic Conductivity of measurable samples.

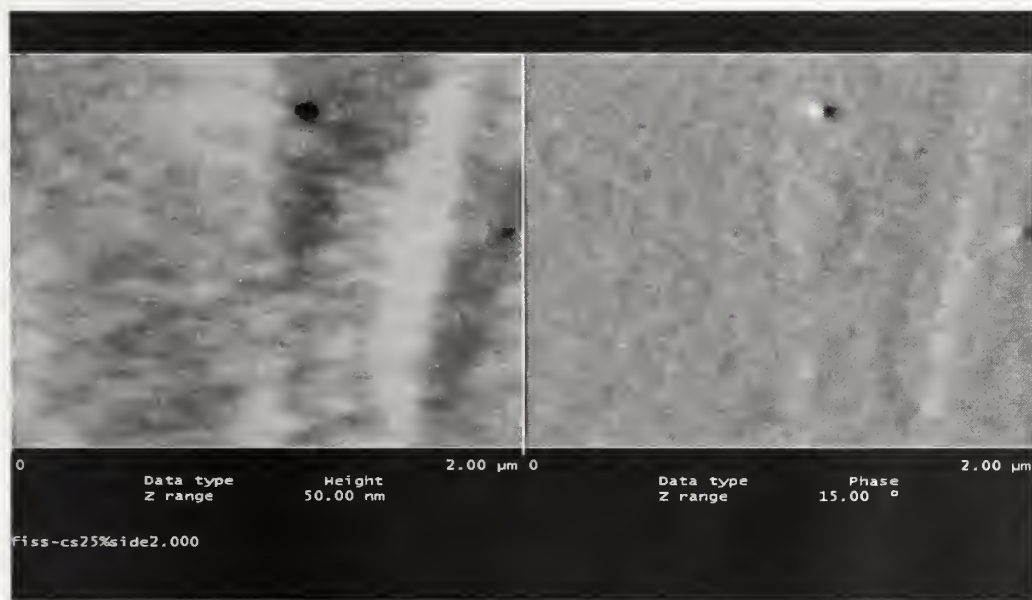
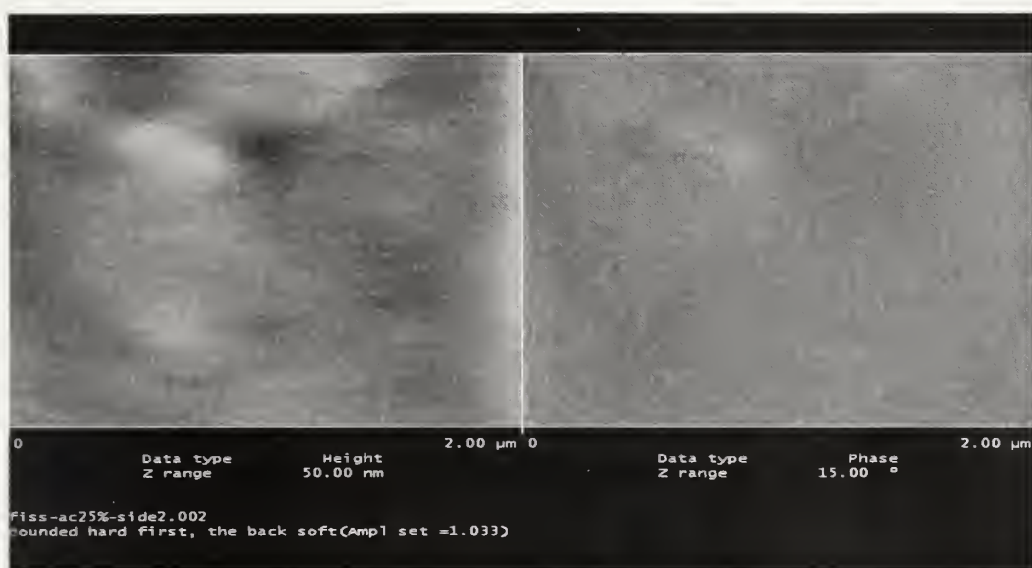
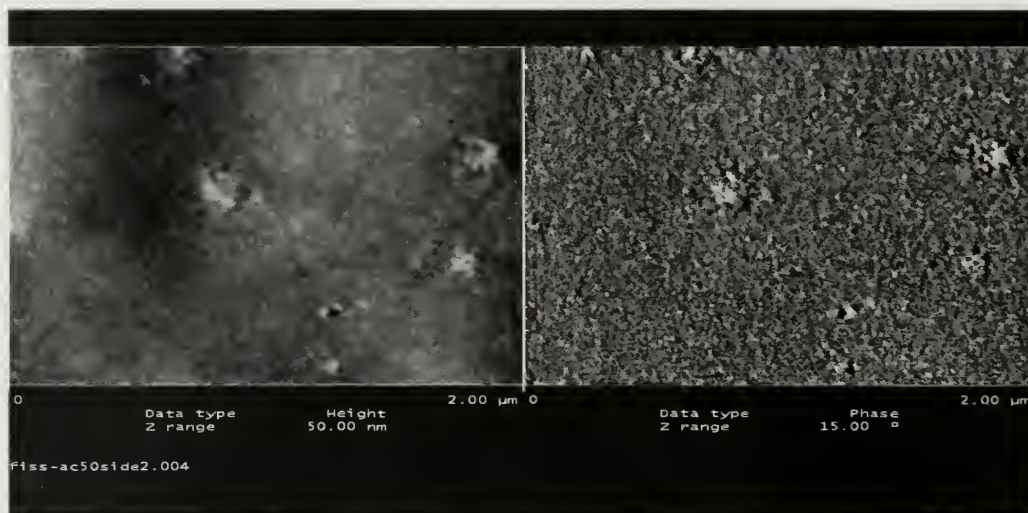


Figure 2.7 AFM images of membrane surface adjacent to casting glass plane. (Continued)



AC50



CS50

Figure 2.7 (Continued)

CHAPTER 3

POLYMER ELECTROLYTE MEMBRANES FROM FLUORINATED POLY(ISOPRENE)-BLOCK-SULFONATED POLY(STYRENE): STRUCTURAL EVOLUTION WITH HYDRATION AND HEATING

3.1 Abstract

SANS and USAXS have been used to study the structural evolution of FISS materials as they have evolved from the dry state to the water swollen state. A dilation of the nanometer-scale hydrophilic domains has been observed as hydration increased, with greater dilation occurring in the higher sulfonated sample or upon hydration at higher temperatures. Furthermore a decrease in the order in these phase separated structures is reduced upon swelling. The glass transition temperature of the fluorinated blocks have been seen to decrease upon hydration of these materials, and at the highest hydration levels, DSC has shown the presence of tightly bound water. A precipitous drop in the mechanical integrity of the AC50 materials is also observed upon exceeding the T_g as measured by DMTA. Finally, highly sulfonated CS97 samples have shown the formation of spherical micelles, even at concentrations as low as 0.05 mg/ml. This is related to the great dissimilarity of the blocks (fluoropolymer versus ionic) in these ionomers. The sizes of these micelles range from 13-13.5 nm, with the higher concentration solutions having smaller radius of gyration, possibly due to crowding effects.

3.2 Introduction

The study of the structure of ionomers under conditions at which they will be used can shed light on the observed properties of such materials. Ionomers have increasing

utility in various areas of research and industry such as batteries, fuel cells, electrolysis cells, ion exchange membranes, sensors, electrochemical capacitors, modified electrodes and even golf balls¹.

Ionomers typically are comprised of a hydrophilic acid bearing phase embedded in a hydrophobic phase. The hydrophilic phases are known to form due to aggregates of the acid groups into multiplets or larger clusters²⁻⁴. NafionTM which is the most used ionomer material in PEM applications, is composed of a hydrophobic fluoropolymer backbone and hydrophilic fluorosulfonic acid bearing side chains⁵. Other materials range from fluoropolymer to aromatic to hydrocarbon backboned materials, bearing pendant acid groups in one configuration or another⁶.

The clusters formed by the acid groups at the end of the side chains are essential in facilitating ionic conductivity by absorbing water which dissociates the proton counter ions, forming a hydronium ions which in turn hop from one acid site to the next during transport⁷. Thus the quantity, shape, size, and connectivity of these ionic aggregates dictate the observed transport properties of such materials.

When block copolymers of these ionomers are made, typically in the diblock, triblock or graft copolymer architectures⁸, an extra level of morphological complexity is introduced which yields a hierarchical structure. As in normal block copolymers, nanometer scale phase separation occurs between the blocks, creating separate hydrophobic and hydrophilic domains with morphologies similar to neutral block

copolymers. The acid groups in the hydrophilic domains further form clusters at a smaller length scale^{9,10}.

Swelling or dilation of ionomers upon increasing water or methanol content, and at service temperatures is also an important factor affecting conductivity and mechanical integrity. Block copolymer ionomers with one block being a fluoropolymer have been shown to exhibit enhanced network formation and mechanical integrity especially when hydrated¹¹. Backbone stiffness and counterions attached to the acid sites are known to affect the degree of water uptake and hence, swelling^{6,12}. The structure of NafionTM has been shown to undergo evolution and phase inversion in order to conserve specific surface as water content increases¹³.

With a view to understanding of the swelling induced structural evolution of our fluorinated poly(Isoprene)-*block*-sulfonated poly(Styrene) ionomers from the dry membrane to solution, we have investigated its structure using USAXS and SANS under conditions mimicking fuel cell usage. Furthermore we have looked at the state of water in these systems, and the effect of swelling on thermal transitions using differential scanning calorimetry (DSC). Finally the thermal and mechanical transitions were studied using dynamic mechanical thermal analysis (DMTA).

3.3 Experimental Section

3.3.1 Materials

The synthetic procedures and characterization for fluorinated poly(Isoprene)-*block*-sulfonated poly(Styrene) (FISS) materials have been described in detail

elsewhere¹⁴. The precursor poly(styrene)-block- poly(Isoprene) (PS-PI) diblock copolymer used in this work was anionically polymerized, having reported characteristics: $M_w = 31,200$, $PDI = 1.05$, 27mol% PS. The fluorinated samples cast into membranes were sulfonated to 23,28 and 50 mol%, as determined by 1H NMR. Some of these samples were neutralized to the cesium salt form, and the balance left in the acid form. The cesium form facilitates contrast in the X-ray scattering experiments, besides exhibiting different transport properties. NafionTM 112 was generously donated by Atofina Chemicals Inc., and was pretreated to the acid form according to the procedure reported elsewhere¹⁵. Another PS-PI diblock copolymer having $M_w = 32,700$, $PDI = 1.01$, 52mol% PS; was fluorinated and sulfonation to 97mol% for use in micellization studies in aqueous media. A sample coded FISS-AC50 would refer to the acid form of the material, sulfonated to 50mol% of the styrene units in the PS block.

3.3.2 Preparation of Membranes

Freeze dried FISS samples were dissolved in a mixture of toluene/N-methylformamide(THF/NMF:85/15 (w/w)) with a concentration ranging from 12-15 wt%. The NMF was used as a polar cosolvent. These solutions were then cast onto glass plates for a day in the fume hood at room temperature for rapid casting of kinetically trapped disordered morphology. Subsequently they were placed in an oven for 1 day at 60°C, and finally in the oven at 60°C under vacuum for a day to remove most of the residual solvent. The acid-form samples were further reactivated by soaking overnight in a 2M aqueous HCL solution containing methanol (20v/v) to enhance swelling and acid permeation. They were thereafter rinsed repeatedly in deionized water till PH was

neutralized and then dried at 60°C in a vacuum oven for a day, and again in vacuum plus 60°C for one day. Cast membranes were subsequently removed and stored in airtight bags for further usage. Dry membrane thicknesses were measured using a digital micrometer and range from 60-90 μm . The Nafion 112 samples were also rinsed until PH was neutral, then dried at 60°C in a vacuum oven for a day and stored in the same way.

3.3.3 Structural Characterization

Small angle x-ray scattering(SAXS) was performed at the Advanced Photon Source(APS) in Argonne National Laboratory on beamline 32-ID, fitted with a Bonse-Hart camera typically used for ultra small angle x-ray scattering (USAXS), which has been described elsewhere. The x-ray energies range from 7 to 18 keV, yielding a q range from 0.0001 to 1.0 \AA^{-1} (where q , the scattering vector is equal to $4\pi \sin(\theta) / \lambda$, where 2θ is the scattering angle and λ is the wavelength of the incident radiation). The beam size was 1mm x 2mm, and a 1-dimensional photodiode detector was used. Air-blanks were subtracted and slit desmearing of the resulting data was carried out using the lake method. All SAXS data were collected with the samples in the transmission position, with membrane normal in the direction of the beam.

Small angle neutron scattering (SANS) experiments were also carried out on both dry and hydrated samples, at the Intense pulsed Neutron Source (IPNS) at the Argonne National Laboratory. The Small Angle Scattering Instrument (SASI) , having a q range of 0.007 to 1.45 \AA^{-1} was used having a q resolution of 0.3 to 0.036. This instrument used an area detector, with area of 50 x 50 cm^2 and 3 - 5 mm (FWHM) detector resolution. The

samples were sealed in quartz cells and empty cells were also run for background subtraction.

Samples were hydrated by soaking in D₂O or D₂O vapor for at least 16 hours each at both room temperature (23°C) and 60°C. The humidity of the D₂O vapor was controlled by placing jars of appropriate saturated salt solutions of D₂O, having known equilibrium relative humidities¹⁶ into sealed plastic containers, with the membrane samples also placed within the sealed chamber but separate from the solution. A relative humidity and temperature meter was also placed in this chamber before sealing. At the end of the immersion period the hydrated samples were rapidly placed in the quartz cells after blotting of surface D₂O, with the edges sealed using TeflonTM tape to prevent evaporation. These as well as blank cells were placed in the beamline and experimental runs were carried out at room temperature for hydrated membrane samples.

In order to study the self-assembled structure of these ionomers in solution, aqueous solutions of the highly sulfonated samples were made. These samples were dissolved in D₂O with concentration ranging from 0.05 to 10 mg/ml. For the SANS experiments, the solutions were poured into 1 mm thick quartz liquid cells. The lids of these cells were wrapped with teflon tape to prevent evaporation or spillage. These sealed cells as well as cells containing pure D₂O were placed in the neutron beamline at room temperature.

3.3.4 Thermal Characterization

As-received FISS samples were placed in a desiccator over Phosphorus pentoxide for a week in order to dry any absorbed water. They were subsequently placed in an oven at 105°C overnight under Nitrogen flow. DSC analysis was performed on these dry materials, using a TA Instruments Q200 calorimeter. 4-7mg for samples was placed in aluminum pans, which were sealed in the press. Heating and cooling rate was set to 10°C min⁻¹. Hydrated membrane samples prepared using water, with the same procedure as described above for SANS measurements, were also sealed in aluminum pans and analyzed.

Dynamic mechanical analyses of the cast FISS membranes were performed with a TA Instruments' DMA 2980, using tensile fixtures. The samples had thicknesses as given in Table 3.3 below, with length and width of 10mm and 5mm respectively. Heating rate was 3°C/min, in a temperature range from 25°C - 140°C, Strain of 15 μ m amplitude and frequency of 1 Hz. The tensile storage modulus and loss modulus were measured.

3.4 Results and Discussions

3.4.1 Structural Evolution with hydration

The structural evolution of PEM membranes under conditions mimicking use environment is essential to understand the true structure, from which their properties emanate. Specifically the changes in domain sizes as well as the hierarchical structure of the block copolymer ionomers, under varying degrees of hydration and at different temperatures, shed light on the changing transport properties that have been recorded.

In order to determine the center-to-center distance (d spacing) of block copolymer domains and the acid clusters of the FISS samples USAXS experiments were done. The results are summarized below in Table 3.1. Both the AC28 and CS23 samples have the same block d spacing of 20.3nm and cluster d spacing of 4.7nm. The AC50 and CS50 samples on the other hand have differing d spacing of 22.7nm and 23.7nm respectively. The difference is related to the fact that, though they have the same sulfonation level, they however have different morphologies (see chapter 2) , and hence will have different packing of the chains resulting in different d spacings. The cluster d spacing for the CS50 sample is also less than that for the CS23 sample because of the higher number of clustered acid sites which are more closely packed.

Scattering profiles from these dry FISS samples were also obtained using SANS for comparison and are shown in figure 3.1 below. There is a difference in the neutron scattering length density (SLD) between the fluorinated poly(Isoprene) (FI) and the sulfonated poly(Styrene) (SS) blocks. The values for the neutron SLD for both FI and SS block as well as for D₂O are tabulated in Table 3.2. The contrast between two scattering units is defined as their difference in neutron SLD squared¹⁷. Using this approach the contrast between D₂O and the FI block gives $0.2423 \times 10^{22} \text{ cm}^{-4}$, while between 50mol % Sulfonated Poly(styrene) and an adjacent FI block gives $0.00065 \times 10^{22} \text{ cm}^{-4}$. The latter contrast though not as great as the former, is sufficient to reveal visible block phase separation peaks, as for some of the other samples.

As can be seen in figure 3.1 the CS50 samples have a d spacing of 22.2 nm as compared to 23.7 nm obtained by USAXS. Also the AC28 and CS23 samples have d spacings of 20.2 nm and 19.2 nm, respectively, compared to 20.3 nm measured by USAXS. There is no distinguishable peak for the AC50 sample, which may be due to a diffuse boundary between phases. Only block phase separation peaks can be seen in these SANS spectra, since there is no deuterated water (D_2O) in the clusters. The spectra have been shifted on the intensity axis for clarity.

Upon hydration of these same materials with D_2O as described above, at room temperature ($23^\circ C$) and at $60^\circ C$, new d spacings were recorded at the block and cluster peaks emerged for some of the samples, showing the hierarchical structure. Figure 3.2 shows the SANS data obtained from FISS samples hydrated at these temperatures.

Since the contrast for these SANS experiments is from the D_2O absorbed into the hydrophilic domain, several trends may be observed as more of it is absorbed. It is expected that the contrast with the rest of the polystyrene in that domain should become sharper and the peak position may shift to lower q values. Also, since the D_2O is absorbed essentially in the hydrophilic domain, there will emerge a clear peak due to the block phase separation and a shift in the peak position as more D_2O is absorbed. This is observed clearly for the AC50 samples, where the block separation peak moved from a q value of $0.023710 \text{ \AA}^{-1}$ to $0.017699 \text{ \AA}^{-1}$ when hydrated at $23^\circ C$ and at $60^\circ C$ respectively. This corresponds to d spacings of 26.5 nm and 35.5 nm respectively. Compared to the d spacing of 22.7 nm from the same sample in the dry state obtained by USAXS, these new

d spacings represent an increase of 16.7% and 36.0% in center to center distance of this sample. This indicates a clear trend of domain dilation with increased hydration.

A similar trend can be seen for the CS50 sample. In the dry state the block d spacing was 23.7nm from USAXS, whereas after soaking in D₂O at 23°C, it increases to 27.8 nm representing a 17.3% increase. Upon soaking this sample at 60°C it disintegrates and forms a swollen gel which shows a micelle-like scattering profile. Both the AC50 and CS50 curves lose their distinct hierarchical features when soaked at 60°C, confirming their change in structure. The AC28 and CS23 samples show essentially the same block phase separation peak position as they absorb relatively smaller amounts of D₂O (See Chapter 2).

On the cluster length scale the same trend can be seen. The CS50 sample which had a cluster d spacing of 3.2 nm in the dry state indicated by the broad peak at higher q^{18} , has a center shifted to approximately 5.8 nm upon soaking at 23°C. The AC50 sample which had no cluster peak in the dry state SANS, shows a 3.2nm spacing peak when soaked at 23°C, which becomes vague after soaking at 60°C. This is an indication of a coalescence process of the D₂O containing cluster pools, which blurs out individual cluster entities. This leads to a three dimensional network of hydrated channels, resulting in a jump of ionic conductivity. A similar structural evolution has been shown for NafionTM upon increased hydration¹³, which results in a percolation threshold in its ionic conductivity.

The change in domain spacing of AC28 and AC50 immersed in D₂O liquid and its vapor at different relative humidity values are shown in Figure 3.3. The same trend of domain dilation, as indicated by first order peak maximum shift to low q , is seen as humidity is increased up till immersion in liquid. This domain dilation can be also more prominent for the higher sulfonated AC50 sample than for the AC28 sample as expected. The lower temperature and lower humidity (35% RH) spectra, show little or no change from the dry state.

The Half-width at half-maximum (HWHM) of the scattering peak gives a clear indication of the degree of order in a phase separated block copolymer system. Broader peaks indicate a more disordered liquid-like systems.^{19,20} As seen in figure 3.2(a) the peak for AC50 samples are much broader than the CS50 samples, indicating a more disordered morphology, as seen also from TEM (See chapter 2). The broadness also indicated the presence of more deuterated water D₂O in this sample. Upon soaking in D₂O at 60°C the block domain peak further broadens out into a shoulder, confirming extensive loss of order and liquid-like structure. This can also be seen by the disappearance of a distinct cluster peak, supporting the suggestion that a three-dimensional network structure of hydrated channels has evolved. The domain dilation and coalescence of cluster pools to form conducting channels as described above, has been modeled in figure 3.4 below. It must be borne in mind that the uptake of hydrophilic molecules in ionomers is closely related to temperature, and there is sometimes a precipitous change in swelling accompanying thermal transitions²¹.

3.4.2 Thermal and Mechanical Transitions.

The transition from a glassy to a rubbery state in an amorphous polymer or polymer segment can be detected through a change in heat capacity of the polymer, which is measurable by DSC. The DSC thermograms of some of the dried as-received FISS materials are shown in figure 3.5 for the second heating scan of a heat-cool-heat cycle. The AC28 and AC50 samples have similar glass transition (T_g) temperature at 45.3°C and 45.5°C, in good agreement with literature²². However the CS50 sample has a T_g of 32.6 °C for the FI block.. The difference between the cesium and the acid (proton) material transitions is likely due to the relatively more bulky cesium ions and the way it effects the whole chain mobility. The T_g of the sulfonated PS block was undetectable even when probed up to 170 °C, and may have been elevated beyond this temperature due to sulfonation as seen in other ionomers^{23,24}.

Upon a transition from the glassy state to the rubbery state in the fluorinated poly(Isoprene) block, which is the bulk phase of the polymer, the mechanical integrity of the whole PEM made from this material is compromised. This is shown in figure 3.6 below in which the Storage modulus of the AC50 sample drops by more than 90% between 45°C and 60°C (at 1hz frequency). Since the storage modulus in viscoelastic solids measure the stored energy or the solid-like characteristic of a viscoelastic material²⁵, it means that this material will flow under desirable fuel cell membrane application temperatures (60°C-100°C), even without considering the softening effects swelling. On the other hand the NafionTM, though not as stiff at room temperature, maintains appreciable mechanical integrity under desirable use temperatures.

Membrane samples from the same batch used for the SANS experiments were soaked in the same manner in deionized water for 16 hours, at room temperature and at 60°C and the DSC thermograms obtained thereafter are shown in figure 3.7. After soaking 20 °C a depression in the glass transition of all the samples that were measured in the dry state was recorded. The data are summarized in Tables 3.3, and show that the highest Tg reduction of 6.2 °C was observed for AC50, which has the highest water uptake value for membranes soaked at 20 °C. This indicated that the absorbed water serves as a plasticizer even in the hydrophobic FI domain. Similar glass transition reduction effects observed in other ionomer systems have been attributed to the presence of non-freezing water²⁷.

The state of water in the hydrophilic domains of an ionomer can be deduced from the characteristics of the melting endotherm, upon the melting of frozen absorbed water, via differential scanning calorimetry²⁶. The occurrence of a broad melting endotherm between -20 °C and 20 °C, has been attributed to the melting of freezable water that is loosely bound to the polymer chains²⁸. The same kind of features have been observed for the FISS samples soaked at 60°C and seen in figure 3.7(b). The broadest peaks are observed for the samples with correspondingly large water uptake values, as can be seen in table 3.3. The peak area gives a measure of the crystallization enthalpy (effectively how much water is bound to the acid sites of the ionomer), and shows that AC50 has the largest crystallization enthalpy and also the largest water uptake at this pre-soak temperature. No sharp spike can be seen in the thermograms suggesting the absence of free- water in the system. Nafion 112 membranes on the other hand show much less

loosely bound water under the same conditions, than AC50. They were also much less visibly swollen after soaking at 60°C but had better transport properties, suggesting that they use the water they do absorb much more efficiently than the FISS-AC50 material. Also there is no glass transition observable in the FISS samples because they are, to varying degrees, essentially in the gel state upon soaking at 60°C.

3.4.3 Micelle Formation

Amphiphilic polymers and oligomers (surfactants) are well known to self assemble into various kinds of micelles in a liquid medium. In an aqueous medium, the hydrophilic part of the polymer would face the water, while shielding the hydrophobic portions of the chains in the micelle core, thus preventing unfavorable interactions with the water. Many types of micellar structures are known and well studied including spherical, ellipsoidal, cylindrical, bilayer (vesicles), however for the most part they can be approximated as being spherical.

Small angle scattering is widely used as a tool for characterizing the size, shape, and other features of these micellar aggregates. In our SANS experiments with FISS-CS97 materials, the contrast which leads to scattering is due to the difference in neutron SLD between D₂O and both the FI and SS block of this highly sulfonated water soluble sample. Calculations using SLD figures from table 3.2, show that the ratio SLD for D₂O versus FI block is 4.7, while for sPS (Cs⁺) versus FI block is 1.3, therefore the strongest contrast is between the D₂O or aqueous surrounding medium and the FI chains in the core of the micelles. In this scenario the structure of the hydrophilic polymer

chains in the micelle corona can also be determined as, they are an intermediate region between the core, and the D₂O only regions, this is known as shell contrast..

The SANS profiles for solutions of the CS97 samples with concentrations of 0.05, 1, and 10 mg/ml in D₂O are shown in figure 3.8(a). The curves for 1, and 10 mg/ml solutions have essentially the same shape, with a form factor peak in the mid q range around the same position indicating they have similar shapes and sizes. In the high q region, where the smallest features can be seen, the slopes of the curve indicate the conformation of the hydrophilic chains dangling in the D₂O. A $I(q)$ dependence of q^{-2} , indicates gaussian chains whereas, a q^{-1} dependence indicates 1-dimensions objects, or stretched out chains²⁹. The Power law fits to the data show, that the 1mg/ml solution have approximately q^{-1} dependence, whereas the 10mg/ml solution has q^{-2} dependence. This can be explained by the fact that the latter have less space for each micelle due to the higher concentration than the former, and so the chains have less room to stretch. The low concentration, 0.05 mg/ml solution has too little scattering to discern this slope due to very few scattering objects being present and hence low counting statistics.

The shape of micelles can be determined by the use of a kratky plot³⁰. The kratky, $I(q) \times q^2$ versus q plot for a spherical object exhibits a clear peak, with its position dependent on the objects radius of gyration. This is because the Gaussian coil (low q or guinier) portion of the curve is multiplied by relatively small q^2 value³¹. At higher angles, where the guinier approximation no longer holds, the curve should obey the porod approximation ($I(q) \propto q^{-4}$) and the intensity should sharply decrease when

multiplied by q^2 , forming a peak. As can be seen for the Kratky plots in figure 3.8(b), all the plots show a distinct peaks(the peak for the 0.05 mg/ml is visible at a smaller scale), confirming the micelles are essentially spherical. The peak for the 10mg/ml sample is positioned at slightly higher q value, indicating a smaller radius of gyration.

The size of a micelle can be determined from the net scattering intensity $I(q)$ based on the Guinier approximation (at low q values) as expressed in the equation below:

$$I(q) = I(0) \exp (-R_g^2 q^2/3) \quad (1)$$

Where $I(0)$ denotes the scattering intensity extrapolated to zero angle and R_g is the radius of gyration. The initial slope in the logarithm plot of equation (1) gives the radius of gyration of the micelle³⁰. The Guinier plots and analysis of the micelle data studied are shown in figure 3.8(c). The radius of gyration values for the 0.05, 1, and 10 mg/ml solution micelles are 13.3, 13.5 and 130 nm respectively. The results for the 0.05 and 1 mg/ml solutions are almost the same, with the largest size of 13.5nm for the 1mg/ml sample. The size for the 10mg/ml sample is slightly smaller, further confirming the suggestion that the 1mg/ml has stretched out chains which may increase its radius of gyration, whereas the 10mg/ml samples may experience some crowding effects and so show a smaller radius of gyration with Gaussian, random coils.

3.5 Conclusions

SANS and USAXS have been used to study the structural evolution of FISS materials as they have evolved from the dry state to the water soluble state. A dilation of

the nanometer-scale hydrophilic domains has been observed as hydration was increased, with higher swelling for the higher sulfonated samples or upon hydrating at higher temperatures. Furthermore a decrease in the order in these microphase separated structures is reduced upon dilation. The glass transition temperature of the fluorinated blocks, have been seen to decrease upon hydration of these materials; and at the highest hydration levels DSC has shown the presence of tightly bound water. A precipitous drop in the mechanical integrity of the AC50 materials is also observed upon exceeding its T_g . These results explain the bursting of the membranes during methanol permeability testing at 60°C, and the sharp increase in methanol permeability with increased temperature. To further develop these materials, new approaches must be found to limit the domain dilation, and increase the glass transitions way beyond the operating temperature.

Finally highly sulfonated CS97 samples have shown self-assembly into spherical micelles in aqueous media, even at concentrations as low as 0.05 mg/ml. This is related to the highly dissimilar blocks (fluoropolymer versus ionic) in these ionomer. The sizes of these micelles range from 13-13.5 nm, with the higher concentration solutions having smaller radius of gyration, possibly due to crowding effects.

3.6 References

- (1) <http://www.freepatentsonline.com/6140436.html>
- (2) Longworth, R.; Vaughan, D.J. Polym. Prepr. (Am. Chem. Soc. , Div. Polym. Chem.) **1968**, 9, 525.
- (3) Eisenberg, A. *Macromolecules* **1970**, 3, 147.
- (4) Semonov, A. N.; Nyrkova, I.A.; Kholkhov, A. R. *Macromolecules* **1995**, 28, 7491.
- (5) Gierke, T.D.; Munn, G.E.; Wilson, F.C. *J. Polymer Sci: Polym. Phys. Ed.* **1981**, 19, 1687.
- (6) Hickner, M. A.; Ghassemi, H.; Kim, Y. S.; Einsla, B.R.; McGrath, J. E. *Chemical Reviews* ,**2004**, 104,,4587.
- (7) O'Hayre, R. P.; Cha, S.; Cololla, W.; Prinz, F.B. In *Fuel Cell Fundamentals* ; 1 ed.; John Wiley& Sons, Inc: New York ,**2006**; p 15.
- (8) Yang, Y.; Holdcroft, S. *Fuel Cells* **2005**, 5,171.
- (9) Lu, X.; Steckle, W.P. Weiss, R.A. *Macromolecules* **1993** 26, 5876.
- (10) Williams, C.E.; Russell, T.P.; Jerome, R.; Horrión, J. *Macromolecules* **1986**, 18, 2877.
- (11) Bishop, M.T.; Karasz, F.E.; Russo, P.S.; Langley, K.H. *Macromolecules*. **1985** ,18, 86.
- (12) Tricoli, V. *J. Electrochem. Soc.* **1998**, 145, 3798.
- (13) Gebel, G. *Polymer* **2000**, 41, 5829.
- (14) Huang ,T.; Gido, S.P.; Mays, J.W. *Synthesis and Characterization of Fluorinated and Sulfonated Block Copolymers for Fuel Cell Proton Exchange Membrane*, Unpublished manuscript.
- (15) Miyake, N.; Wainright, J.S.; Savinell, R.F. *J. Eletrochem. Soc.* **2001**, 148, A898.
- (16) The OMEGA® Temperature Handbook and Encyclopedia, Vol. MMV™ 5th Edition®
- (17) <http://www.isis.rl.ac.uk/largescale/loq/documents/sans.htm>

- (18) Peiffer, D.G.; Weiss, R.A.; Lundberg, R.D. *J. Polym. Sci., Polym. Phys.* **1982**, 20, 1563.
- (19) Ryu, D.Y.; Jeong, U.; Kim, J.K.; Russell, T.P. *Nature Materials* **2002**, 1, 114.
- (20) Rodriguez-Abreu, C.; Lazzari, M.; Varade, D. ; Kaneko, M ; Aramaki, K. ; Quintela, M.A.L. *Colloid Polym. Sci.* **2007**, 285, 673.
- (21) Kreuer, K.D. *Solid State Ionics* **1997**, 97, 1.
- (22) Ren, Y.; Lodge, T.P; Hillmyer, M.A. *J. Am. Chem. Soc.* **1998**, 120, 6830.
- (23) Weiss, R.A.; Sen, A.; Pottick, L.A.; Willis, C.L. *Polymer* 1991, 32, 2785.
- (24) Rigdahl, M.; Eisenberg, A. *J. Polym. Sci., Polym. Phys. Edn.* **1981**, 19, 1641.
- (25) Meyers, M.A.; Chawla, K.K. *Mechanical Behaviour of Materials*, Prentice Hall, 1999, 98.
- (26) Hickner et al. *Fuel Cells* **2005**, 5, 213.
- (27) Kim, Y.S.; Dong, L.; Hickner, M.A.; Glass, T.E.; Webb, V.; McGrath, J. E. *Macromolecules* **2003**, 36 6281.
- (28) Nakamura, K.; Hatakeyama, T.; Hatakeyama, H. *Polymer* **1983**, 24, 871.
- (29) Kataoka, M.; Hagihara, Y.; Mihara, K.; Goto, Y. *J. Mol. Biol.* **1993**, 229, 591.
- (30) Sugiura, S. et al. *J. Coll. Interf. Sci.* 2001, 240, 566.
- (31) Flanagan, J.M.; Kataoka, M.; Fujisawa, T. Engelman, D.M. *Biochemistry* 1993, 32, 10359.

Table 3.1 Dry sample center-to-center distances for fluorinated poly(Isoprene)-*block*-sulfonated poly(Styrene) (FISS) obtained by USAXS.

Sample	D spacing of Block, nm	D spacing of Cluster, nm
FISS-AC28	20.3	4.7
FISS-CS23	20.3	4.7
FISS-AC50	22.7	
FISS-CS50	23.7	3.2

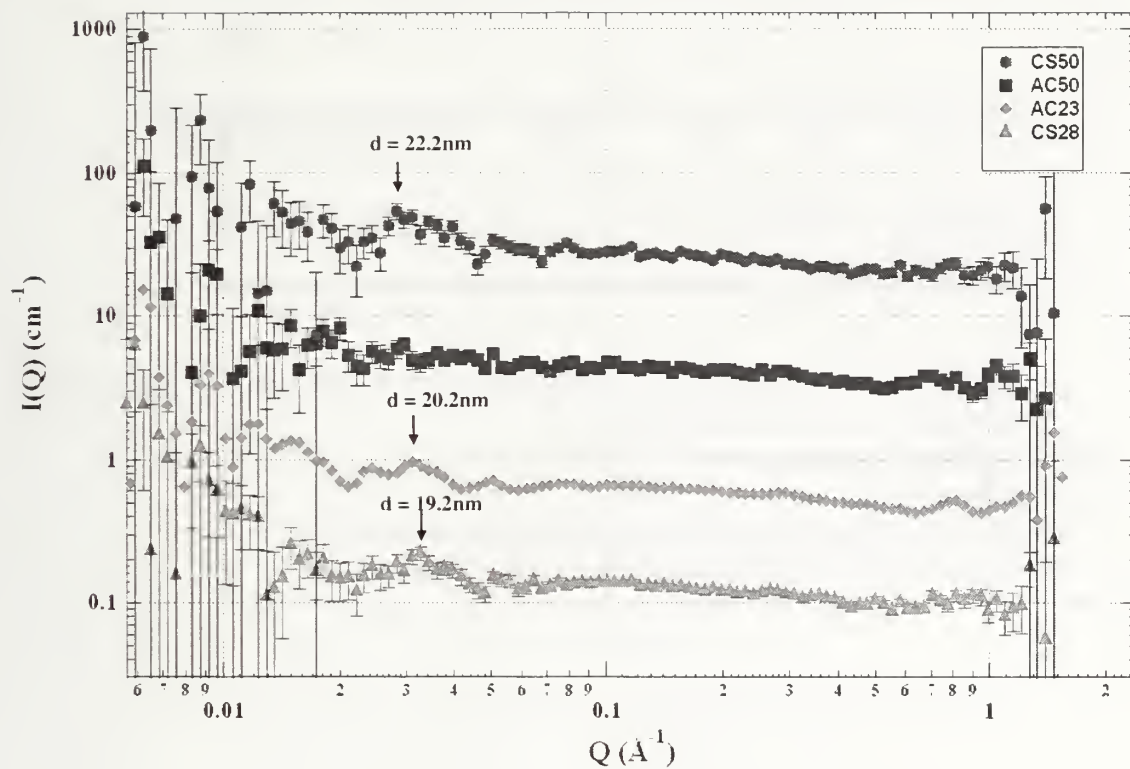


Figure 3.1 SANS profiles from fluorinated poly(Isoprene)-*block*-sulfonated poly(Styrene) dry at 23°C.

Table 3.2 Neutron Scattering length densities calculated for different parts of fluorinated poly(Isoprene)-*block*-sulfonated poly(Styrene) and D₂O.

Scattering Unit	D ₂ O	FI	PS	sPS (H ⁺)	sPS (Cs ⁺)
Neutron SLD* (cm ⁻² x 10 ⁻¹¹)	0.6236	0.1313	0.1374	0.2519	0.1764

* Calculated using scattering cross section data from T. P Russell's, Polymer Physical Chemistry lecture notes and Reference 16.

FI: fluorinated poly(Isoprene)

PS: poly(Styrene)

sPS (H⁺): sulfonated poly(Styrene) with proton counterion

sPS (H⁺): sulfonated poly(Styrene) with cesium counterion

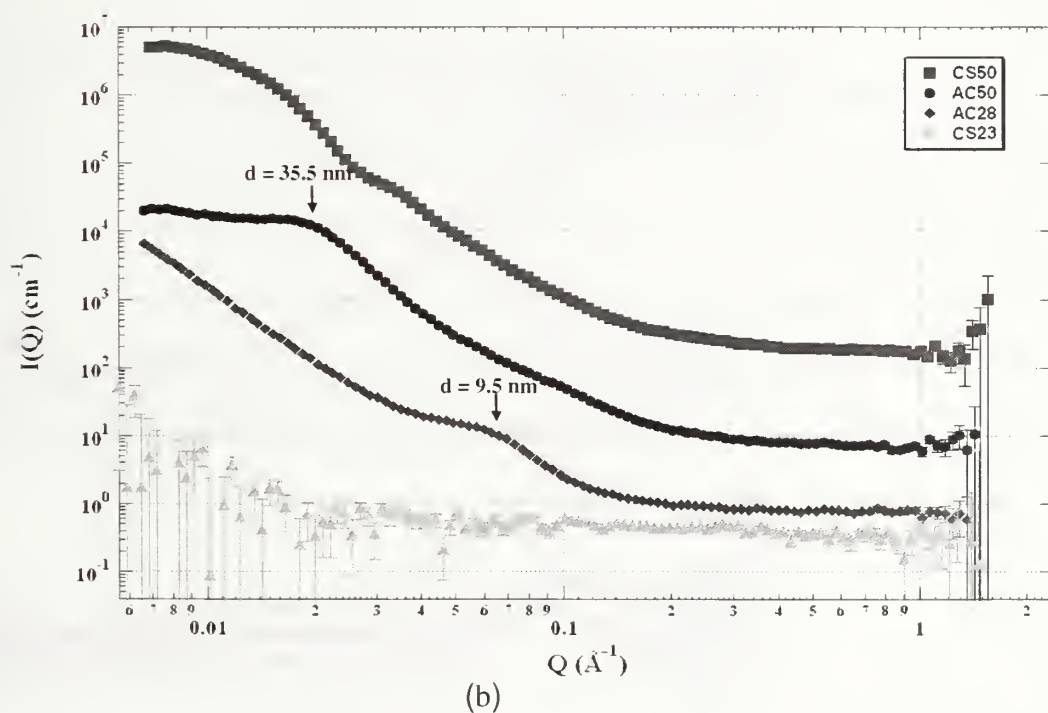
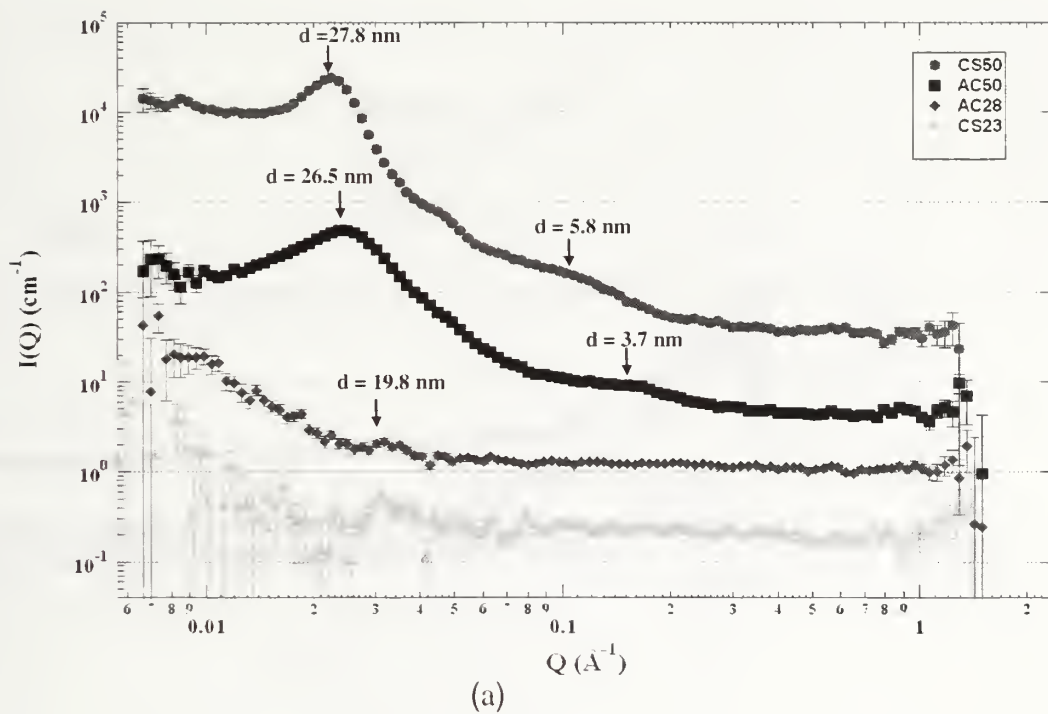
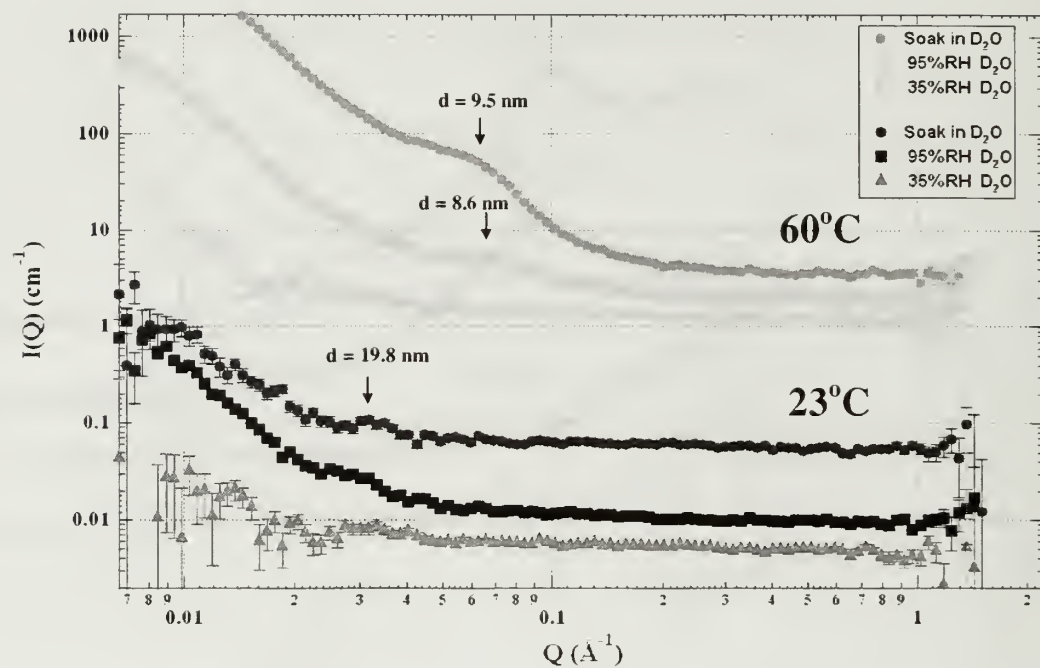
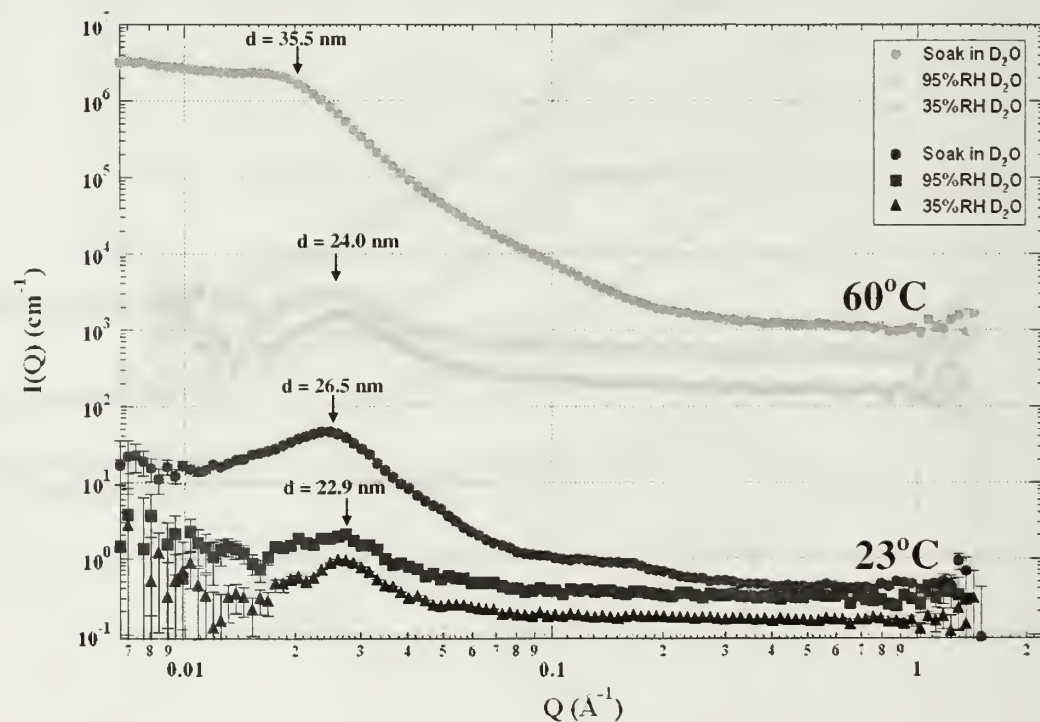


Figure 3.2 SANS profiles from fluorinated poly(Isoprene)-*block*-sulfonated poly(Styrene) soaked for 16 hours in D_2O at (a) 23°C and (b) 60°C .



(a)



(b)

Figure 3.3 SANS profiles from fluorinated poly(Isoprene)-*block*-sulfonated poly(Styrene) soaked for 16 hours in D_2O and its vapor for (a) AC28 and (b) AC50.

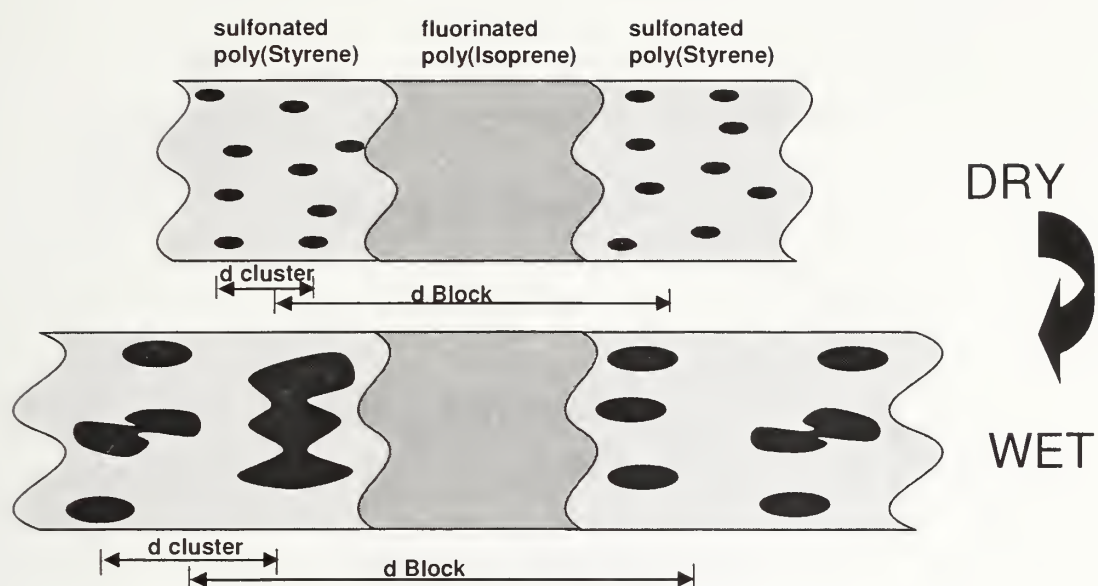


Figure 3.4 Schematic of structural evolution with increased hydration.

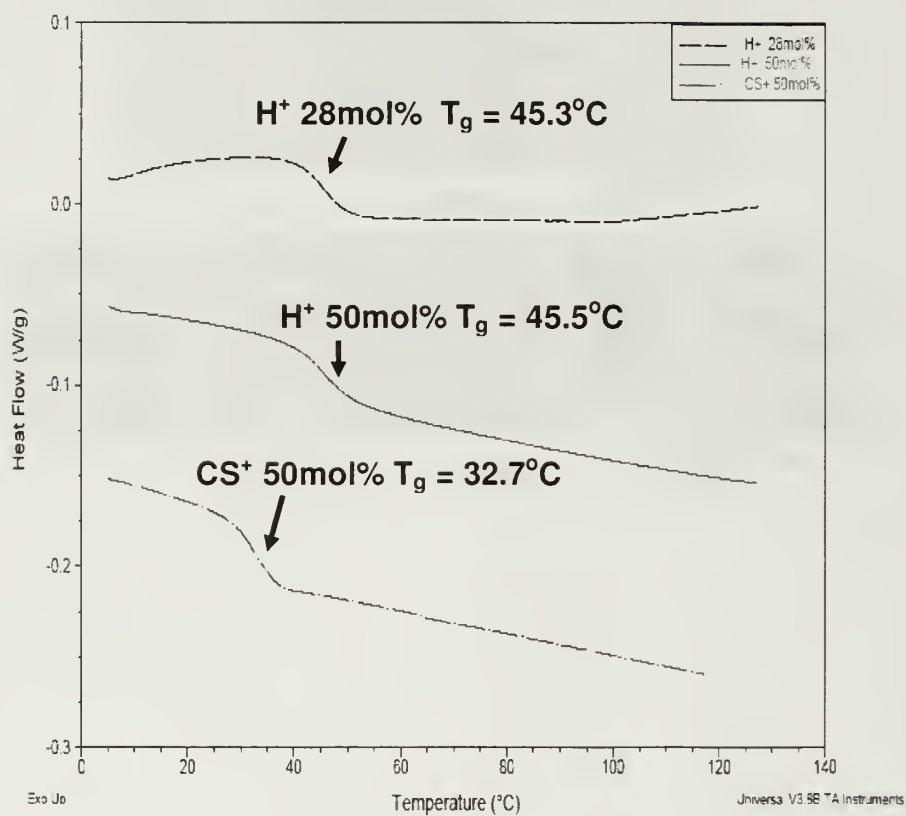


Figure 3.5 DSC thermogram from fluorinated poly(Isoprene)-*block*-sulfonated poly(Styrene) as received samples dried under nitrogen flow overnight at 105°C.

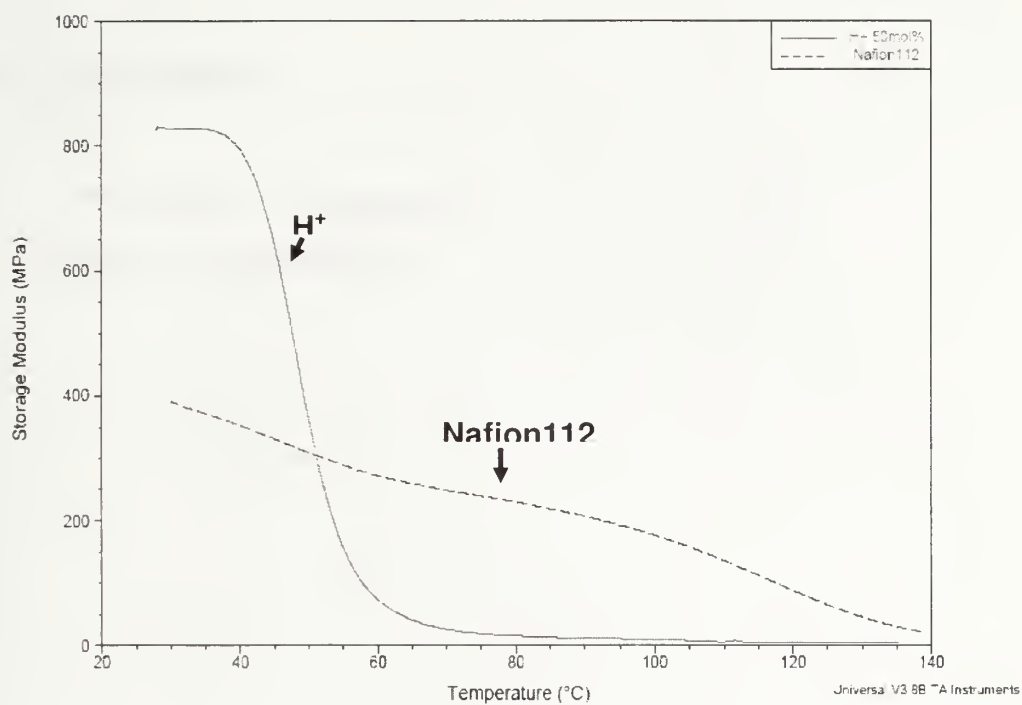
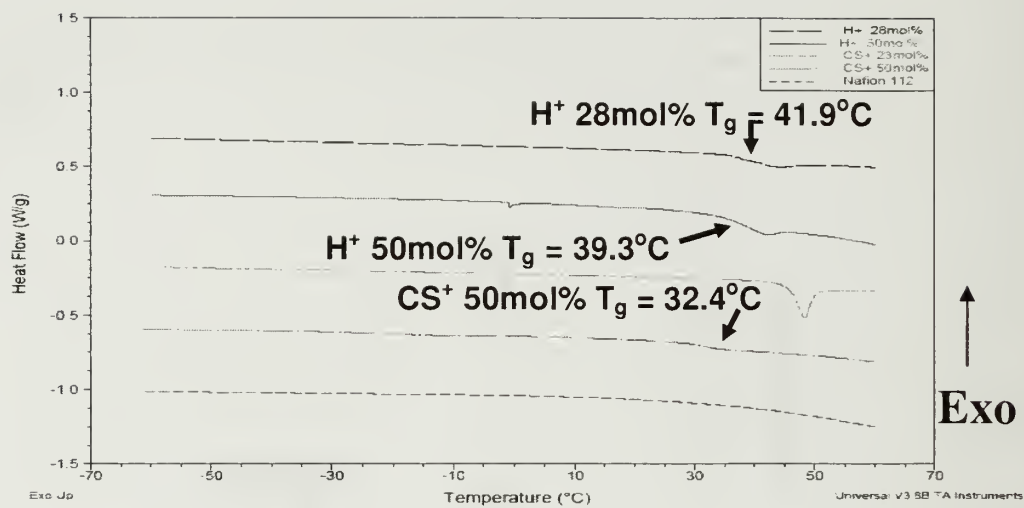
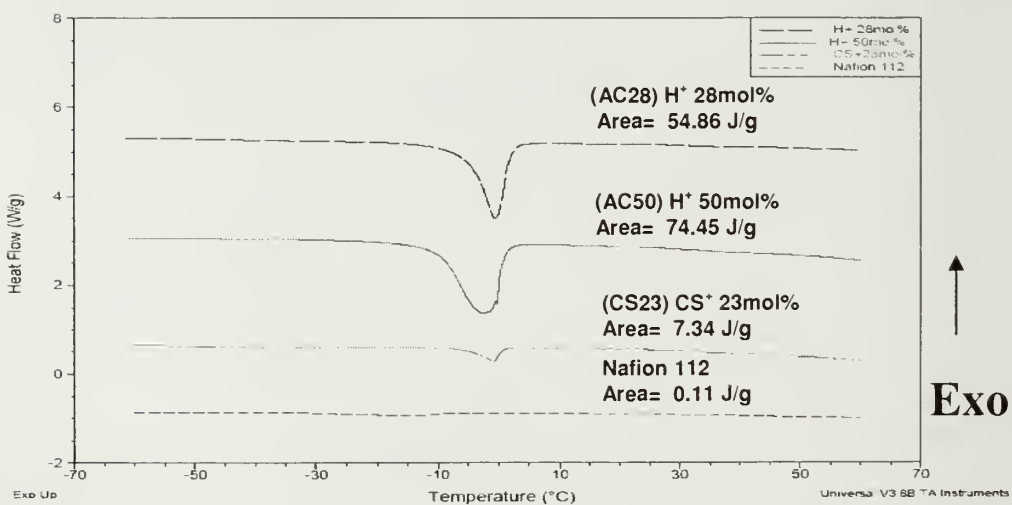


Figure 3.6 DMTA curves for fluorinated poly(Isoprene)-*block*-sulfonated poly(Styrene) and Nafion™ samples pre-dried under nitrogen flow overnight at 105°C. Tension Mode.



(a)



(b)

Figure 3.7 DSC thermograms from fluorinated poly(Isoprene)-*block*-sulfonated poly(Styrene) soaked for 16 hours in H₂O at (a) 23°C and (b) 60°C.

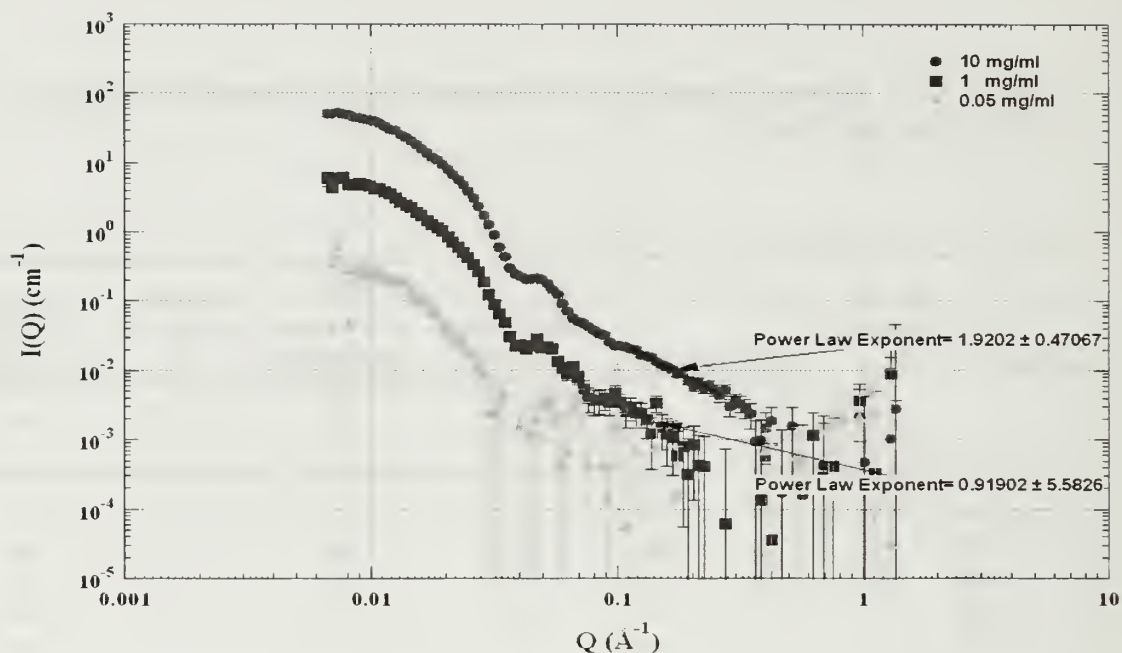
Table 3.3 Thermal properties of fluorinated poly(Isoprene)-*block*-sulfonated poly(Styrene) and NafionTM.

Polymer	Dry Thickness (μm)	Water Uptake (%)		Glass Transition Dried($^{\circ}\text{C}$)	Glass Transition after soaking ($^{\circ}\text{C}$)	Tg Reduction after soaking ($^{\circ}\text{C}$)	Area/Water absorbed after soaking (J/g)
		20 $^{\circ}\text{C}^{\text{b}}$	60 $^{\circ}\text{C}^{\text{b}}$	105 $^{\circ}\text{C}^{\text{c}}$	20 $^{\circ}\text{C}^{\text{b}}$	20 $^{\circ}\text{C}^{\text{b}}$	60 $^{\circ}\text{C}^{\text{b}}$
Nafion 112	50						0.11
FISS-AC50	81	17	595	45.5	39.3	6.2	74.45
FISS-CS50	91	5	a	32.6	32.4	0.2	a
FISS-AC28	69	5.4	257	45.3	41.9	3.4	54.86
FISS-CS23	74	2.4	129				7.34

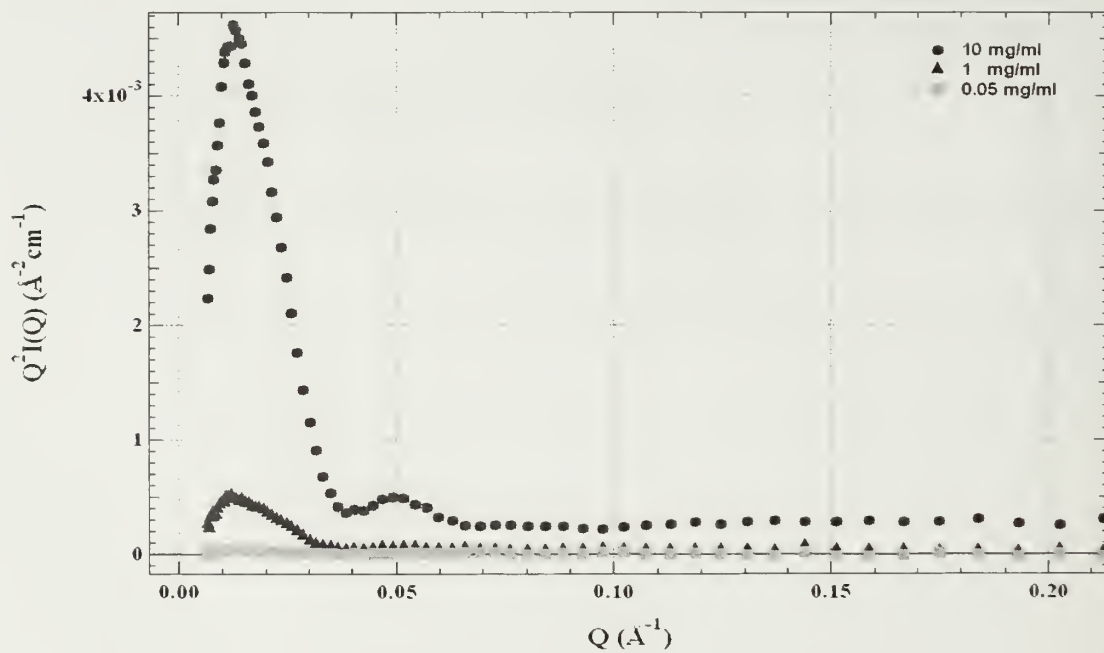
^aNot Measurable

^bPre-soak Temperature in Deionized water

^cPre-Dry Temperature under N₂ flow



(a)



(b)

Figure 3.8 SANS profiles from fluorinated poly(Isoprene)-*block*-sulfonated poly(Styrene) micelles formed in D_2O (a) profiles with Power law fits (b) Kratky plots (c) Guinier plots and analysis. (Continued)

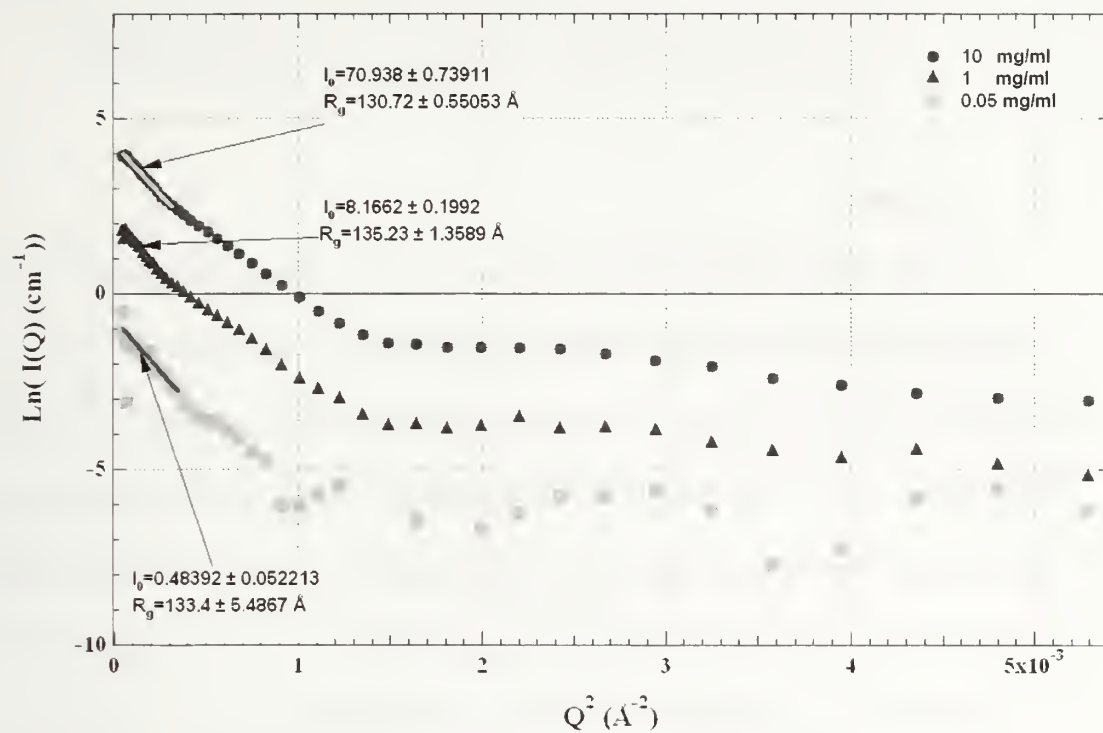


Figure 3.8 (Continued)

CHAPTER 4

POLYMER ELECTROLYTE MEMBRANES FROM FLUORINATED POLY(ISOPRENE)-BLOCK-SULFONATED POLY(STYRENE): MICRODOMAIN ORIENTATION BY EXTERNAL FIELD.

4.1 Abstract

In this study, block copolymer ionomers of the cesium salt (20 mol %) of fluorinated poly(Isoprene)-block-sulfonated poly(Styrene) have been spun cast into membranes and annealed under an electric field of ~ 40 V/ μm at 130°C for 24 hours. This resulted in the transformation of the morphology from a random phase separated state to one preferentially oriented in the direction of the electric field but with smaller domain sizes. The effect of this change in morphology was a 2.5 times increase in the ionic conductivity as measured by electrochemical impedance spectroscopy, at all humidity conditions measured. This can be attributed to the increased connectivity of the ionic domains. This technique may find application in the fabrication of nanostructured polyelectrolytes with enhanced charge transport capacity.

4.2 Introduction

The use of external fields to orient the different components of a polymeric system has gained significant interest over the last decade. It involves the application of an external field to induce structural rearrangement of a material to achieve preferential texture in a desired direction. Different kinds of external field have been employed including shear^{1,2}, electric fields³⁻⁵, solvent evaporation^{6,7}, and mechanical constraints^{8,9} and magnetic fields¹⁰. These techniques commonly employ the interaction of the field with the anisotropic portions of the materials having different components that

are not phase mixed such as blends, block copolymers, or polymer- nanoparticle mixtures.

The purpose of such microdomain orientation is typically to enhance orientation dependent properties, and has found application in the fabrication of templating nanowire arrays^{11,12}, photonic crystals^{13,14}, and improved gaseous permeability¹⁵. The effective diffusion of small molecules through polymeric microdomains has been shown to vary inversely to the square of tortuosity¹⁶, where tortuosity is a measure of the degree of twisting of the domains. In essence a block copolymer with oriented domains has been shown to have much higher transport of the penetrant small molecules in the direction of orientation.

This same approach has been applied to the improvement of ionic conductivity. A study by Weiss and Coworkers et al.^{17,18} showed that blend of sulfonated Poly (Ether Ketone Ketone) ionomer and neutral Poly (Ether Imide) cast under an electric field(E-field), yielded a morphology with the ionic component oriented in the direction of this E-field (Perpendicular to plane of membrane) and resulted in orders of magnitude increase in ionic conductivity. Also LiI:PEO based solid Polymer electrolyte for batteries showed one- order of magnitude increase in Li ion conductivity upon orientation of the PEO crystalline chains, by incorporation of magnetic particles and application of a magnetic field¹⁹. Furthermore it has been predicted that an orientation of block copolymer ionomer domains in the direction of desired ionic conductivity would enhance their utility as Polymer electrolyte fuel Cell membranes²⁰.

Block copolymers are particularly suited for microdomain orientation by external fields, due to their predictable formation of microstructures with anisotropic domains, such as lamellae or hexagonally packed cylinders. Much work has been done on the orientation of block copolymers using E-Fields. Most of the work has centered on poly(Styrene)-poly(Methyl Methacrylate) (PS-*b*-PMMA) block copolymers^{3,5,21,22}, and their complexes with Lithium salts²³. Some work has also been done on rubbery di- and tri-block copolymers of poly(Styrene)-poly(Isoprene), as well as poly(Styrene)-poly(Ethylene-co-butylene)- poly(Styrene) (sSEBS) as shown in figure 4.1.

The driving force for the alignment of block microdomains is due to the dielectric constant difference between the dissimilar blocks. Recent experimental studies in the melt have suggested that disordering of the original lamellar morphology is followed by rotation of the smaller grains formed in the direction of the applied E-field^{24,25}, whereas studies from solution suggest the latter step is preceded by defect translation²⁶. These suggested pathways have also been corroborated by simulation^{27,28}.

Few studies have been reported on the orientation of ionomers by any external field^{29,30}. This was found to be a nontrivial task as the ionic aggregation of the acid sites severely limited chain mobility, in nematic liquid crystal domains. Alternatively track-etched membranes with pores oriented normal to the plane of the membrane, have been filled with ionomers, yielding significant increase in ionic conductivity compared to isotropic membranes^{31,32}. This work is focused on the orientation of block copolymer

ionomer domains normal to the plane of membranes formed from them and investigation of the resultant effects on proton conductivity.

4.3 Experimental Section

4.3.1 Materials

The synthetic procedure and characterization for fluorinated poly(Isoprene)-block- sulfonated poly(styrene) (FISS) materials have been described in detail elsewhere³³. The precursor poly(styrene)-block- poly(Isoprene) (PS-PI) diblock copolymer used in this work was anionically polymerized, having reported characteristics: $M_w = 27,000$, $PDI = 1.05$, 50mol% PS. The fluorinated samples had the PS block sulfonated to 20 mol%, as determined by 1H NMR, and subsequently neutralized to the cesium salt form. This sample will be referred to as FISS-CS20 hereafter.

4.3.2 Preparation of Membrane

Membranes from the FISS-CS20 samples were prepared by spin coating a 5 wt % solution in Tetrahydrofuran (THF) onto a silicon substrate on which gold had been deposited, as shown in figure 4.2 below. Spin speed was at 1000 rpm and was left to spin for 5mins. The resultant film was ~ 500nm in thickness as determined by a Dektak³ profilometer. A piece of this membrane coated wafer was reserved as the As-cast sample.

4.3.3 E-field Alignment Experiments.

An aluminized Kapton film was used as an upper electrode, having ~ 25 μm layer of crosslinked poly(Dimethylsiloxane) (PDMS) (Slygard) cured on the kapton side. This

was necessary to have an intimate contact between the top electrode and the copolymer film, thus eliminating insulating air gaps. The sandwiched capacitor, was placed in an oven with a nitrogen flow blanket, and annealed at 130°C for 24 hours under an E-field strength of $\sim 40\text{V}/\mu\text{m}$ as shown in figure 4.3. The E-field was typically applied before the oven got heated. The whole setup was quenched to room temperature before the applied E-field was removed.

4.3.4 Transmission Electron Microscopy(TEM).

TEM samples were prepared from both the As-Cast and E-Field samples. A thin layer of gold, and then carbon was sputtered unto the surface of the membrane still in the gold coated wafer. The gold serves as a membrane edge marker, while the carbon serves as an epoxy diffusion barrier. Both samples were then embedded and cured in room temperature cure Epoxy for 24 hours. The membrane was then separated from the substrate by immersing in liquid nitrogen, and subsequently 50 nm thin sections of the sample were cut across the thickness of the membrane (E-field direction) using a Leica Ultracut UCT cryomicrotome at -120°C. These were then collected on copper grids and stained with RuO_4 vapor for 1 hour. It is assumed that only the unsulfonated polystyrene domains were stained. TEM images were obtained using a JEOL-2010 microscope operating at an accelerating voltage of 200KV in the bright field mode.

4.3.5 Ionic Conductivity.

Ionic (cesium) conductivity of the membranes were measured by means of two probe complex impedance spectroscopy techniques, which measure conductivity normal

to the plane of the membrane respectively. Pieces of both the As-cast and E-field samples still on the gold plated substrates were immersed in a chamber with 50% relative humidity (RH) for 24 hours, and then rapidly sandwiched between another piece of gold coated silicon wafer (gold face touching membrane). A solartron 1252A frequency response analyzer linked to a an SI 1287 electrochemical interface was used within a frequency range of 0.1 and 300KHz, and the value of the real intercept in the imaginary vs. real impedance plot (Bode plot) in the high frequency range is taken as the bulk resistance of the membrane to ionic conductivity, as described in elsewhere³⁴. The same test was repeated for the same samples after soaking in a 100% RH chamber for 7 hours.

4.4 Results and discussions

The value of orientation of ion conducting domains in the direction of the desired ion transport has been demonstrated for batteries and for fuel cell polymer electrolytes. However facile direct methods to orient block copolymer ionomers, which have increasing appeal as fuel cell membrane materials due to their fast and predictable self-assembly into nanometer lengthscale structures, are still lacking. The above described experiments were carried out to investigate the viability of electric field induced alignment in this regard.

Cross sectional TEM micrographs of FISS-CS20 samples, which were spun coated, and subsequently annealed under an electric field are shown in figure 4.4 below. The as-cast samples show a randomly (mixed) oriented morphology, with the dark portion being the sulfonated Poly(styrene) domains. This is the typical cylindrical

morphology expected from a elastomer-styrene block copolymer with a PS minor component of around 25-27mol % as shown in figure 4.1(a). The rapid spin coating and solvent evaporation results in a kinetically trapped morphology.

Upon annealing of an uncharged block copolymer under an electric field, an orientation of the domains in the direction of the electric field is achieved, by one of the mechanisms discussed earlier, as seen in figure 4.1(b). It is observed that the orientation of the domains does not visibly affect the domain size. However, upon application of a similar treatment to the sulfonated FISS-CS20 samples, there is a visible reduction in the domain size as seen in figure 4.4(b). This results in a much finer grained morphology, and essentially a greater degree of connectivity in the hydrophilic domains.

Also it has been shown that the order in self assembled morphologies observed in cast block copolymers ionomers is reduced upon annealing³⁵. This observed change is related to the fact that the electrostatic interactions leading to the formation of ionic clusters are much stronger than the weak non-covalent interactions that lead to block copolymer phase separation. These behave as physical cross links, hence reducing the mobility of the chains and hindering their self assembly into equilibrium structures³⁶. So upon annealing the polymer chains gain energy for increased mobility, and this allows the ionic groups to come in the vicinity of one another more often and interact, locking in a structure at a shorter length scale (see chapter 3) than for block phase separation, in a random fashion. This then templates the self-assembly of the block copolymer dissimilar chains which are chemically connected together, in an equally random fashion, at a

lengthscale limited by the molecular dimensions. This process may play a significant part in the smaller, grainy morphology observed upon annealing of the FISS-CS20 samples.

On the other hand, a slight preferential orientation of these grainy domains can be observed in the direction of the applied E-field (indicated by the arrow). This orientation is by no means complete or exclusive, as it is the result of competition between electrostatically induced random orientation; and polarization of the anisotropic microphase structure by the electric field inducing alignment in its direction. The dominant effect will depend on field strength, temperature of annealing, duration of annealing, and ionic content to varying degrees. A more extensive and systematic study will be required to decouple and quantify the influence of each.

The ionic (cesium) conductivity of As-Cast and E-field annealed FISS-CS20 samples from different pieces of the same spin-coated silicon substrate, has been measured across the plane of the membrane, and results are shown in figure 4.5. The data clearly indicates an increase in conductivity of ~ 2.5 times upon annealing under an electric field over the as-cast samples. The low absolute figures are either due to the low relative mobility of the heavy cesium ion being measured, or the low humidity or hydration condition, however the increase in conductivity is consistent for both humidity conditions measured.

This increase in conductivity may be attributed to the high domain connectivity, in the grainy random morphology of the Efield annealed sample or due to the induced

preferential orientation in the electric field direction, which is also the direction in which ionic conductivity was measured. An increase in conductivity can however be the result of either of these morphological attributed or both. A more exhaustive study of this approach to increasing conductivity in block ionomers will be required, however this approach shows significant promise as a facile means of creating nanostructured ionomer membranes with controlled orientation.

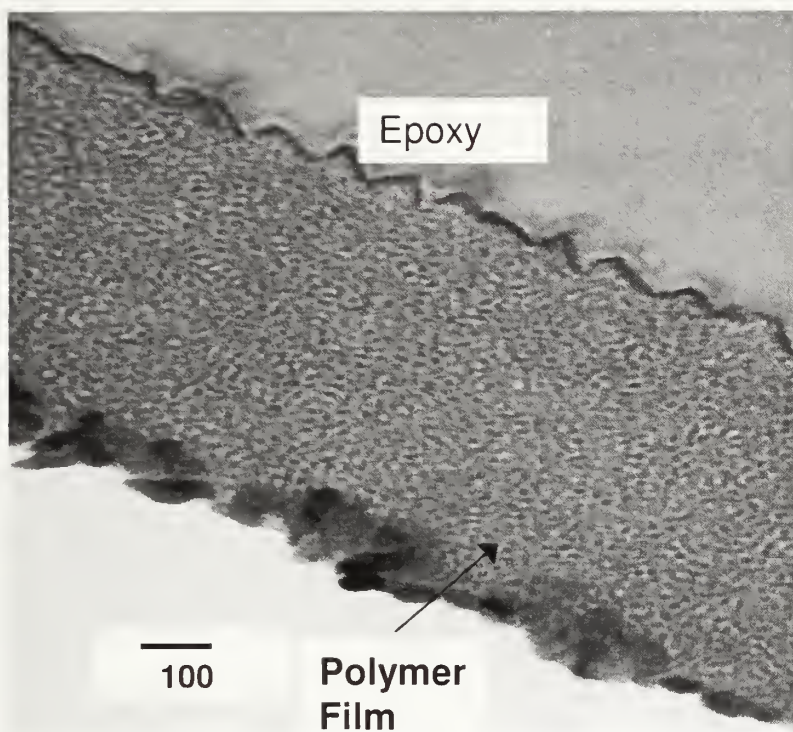
4.5 Conclusions

Annealing of cesium salt (20 mol %) of fluorinated Poly(Isoprene)-block-sulfonated poly(Styrene) transforms its morphology from a random phase separated state to one preferentially oriented in the direction of the electric field but with smaller domain sizes. This morphological change can be tentatively attributed to a competition between templating intermolecular electrostatic interactions of the ionic groups on the sulfonated blocks and the polarization of the dissimilar block domains in the electric field. The effect of this change in morphology is a 2.5 time increase in the ionic conductivity as measured by electrochemical impedance spectroscopy, at all the humidity conditions measured. This can be attributed to the increased connectivity of the ionic domains.

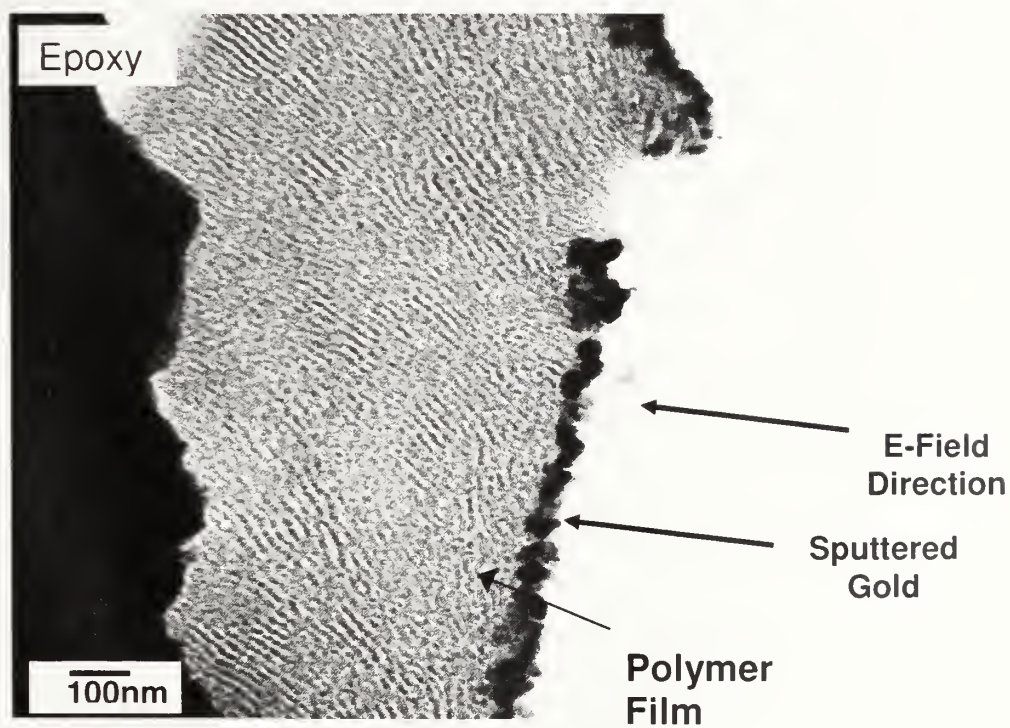
4.6 References

- (1) Schmidt, G.; Richtering, W.; Lindner, P.; Alexandridis, P. *Macromolecules* **1998**, 31, 2293.
- (2) Zipfel, J.; Berghausen, J.; Schmidt, G.; Lindner, P.; Alexandridis, P.; Tsianou, M.; Richtering, W. *Phys. Chem., Chem. Phys.* **1999**, 1, 3905.
- (3) Amundson, K. et al. *Macromolecules* **1991**, 24, 6546.
- (4) Amundson, K.; Helfand, E.; Quan, X.; Smith, S.D.; *Macromolecules* **1993**, 26, 2698.
- (5) Morkved, T.L.; Lu, M.; Urbas, A.M.; Ehrichs, E.E.; Jaeger, H.M.; Mansky, P.; Russell, T.P. *Science* **1996**, 273, 931.
- (6) Kim, G.; Libera, M. *Macromolecules* **1998**, 31, 2569.
- (7) Kim, S.H.; Misner, M.J.; Xu, T.; Kimura, M.; Russell, T.P.; *Adv. Mater.* **2004** 16, 226.
- (8) Kofinas, P.; Cohen, R.E. *Macromolecules* **1994**, 24, 3002.
- (9) Zhao, Y.; Roche, P.; Yuan, G. *Macromolecules* **1996**, 29, 4619.
- (10) Grigorova, T.; Pispas, S.; Hadjicristidis, N.; Thurn-Albrecht, T. *Macromolecules*, **2005**, 38, 7430.
- (11) Thurn-Albrecht, T. et al. *Science* **2000**, 290, 2126.
- (12) Lopes, W.A.; Jaeger, H.M. *Nature* **2001**, 414, 735.
- (13) Van Blaaderen, A.; Wiltzius, P. *Adv. Mater.* **1997**, 9, 833.
- (14) Zhong, Y.; Wu, L.; Su, H.; Wong, K.S.; Wang, H. *Optics Express* **2006**, 14, 6837.
- (15) Drzal, P.L.; Halasa, A.F.; Kofinas, P. *Polymer* **2000**, 41, 4671.
- (16) Faridi, N.; Duda, J.L.; Hadj-Romdhane, I. *Ind. Eng. Chem. Res.* **1995**, 34, 3556.
- (17) Weiss, R.A. et al. DOE Hydrogen Program FY **2004** Progress Report.
- (18) Bellows, R. et al. DOE Hydrogen Program FY **2004** Progress Report.
- (19) Golodnitsky, D.; Livshits, E.; Kovarsky, R.; Peled, E.; Chung, S.H.; Suarez, S.; Greenbaum, S.G. *Electrochem. and Solid State Letters* **2004**, 7, A412.

- (20) Elabd, Y.A.; Walker, C. W.; Beyer, F. L. J. Membr. Sci. **2004**, 231, 181.
- (21) Thurn-Albbrecht, T. ; DeRouchey, J. Russell,T.P. ; Jaeger, H.M. Macromolecules **2000**, 33, 3250.
- (22) Xu, T. et al. Macromolecules **2005**, 38, 10788.
- (23) Wang, J. ; Leiston-Belanger, J.M. ; Sievert, J.D. ; Russell, T.P Macromolecules **2006**, 39, 8487.
- (24) Xu, T. ; Zhu, Y. ; Gido, S.P. ; Russell, T.P. Macromolecules **2004**, 37, 2625.
- (25) DeRouchey, J. ; Thurn-Albrecht, T. ; Russell, T.P.; Kolb, R. Macromolecules **2004** 37 2538.
- (26) Boker, A.; Knoll, A.; Elbs, H.; Abetz, V.; Muller, A.H.E.; Krausch, G. Macromolecules **2002**, 35, 1319.
- (27) Tsori, Y.; Andelman, D. Macromolecules **2002**, 35, 5161.
- (28) Zvelindovsky, A.V.; Sevink, G.J.A. Phys. Rev. Lett. **2003**, 90, 049601.
- (29) Yuan, G.; Zhao, Y. Polymer **1995**, 36, 2725.
- (30) Roche, P.; Zhao, Y. Macromolecules **1995**, 28, 2819.
- (31) Chen, H.; Palmese, G.R.; Elabd, Y.A. Chem. Mater. **2006**, 18, 4875.
- (32) Fang, Y.; Leddy, J. J. Phys. Chem.. **1995**, 99, 6064.
- (33) Huang ,T.; Gido, S.P.; Mays, J.W. *Synthesis and Characterization of Fluorinated and Sulfonated Block Copolymers for Fuel Cell Proton Exchange Membrane*, Unpublished manuscript.
- (34) See Chapter 2: Experimental Section.
- (35) Mani, S.; Weiss, R.A.; Williams, C.E.; Hahn, S.F. Macromolecules **1999** 32, 3663.
- (36) Blackwell, R.I.; Mauritz, K.A. Polymer **2004**, 45, 3457.



(a)



(b)

Figure 4.1 TEM micrographs showing sSEBS samples (a) As-Cast , (b) After Electric field of $\sim 45\text{V}/\mu\text{m}$ applied at 208°C , for 24 hours.

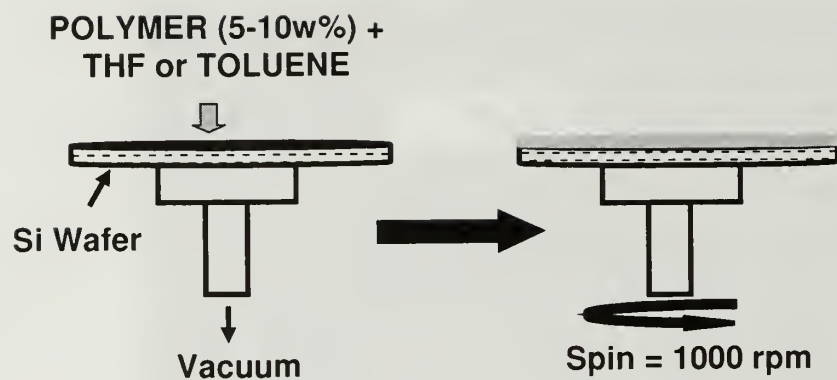


Figure 4.2 Schematic of spin casting operation.

Electric Field Apparatus

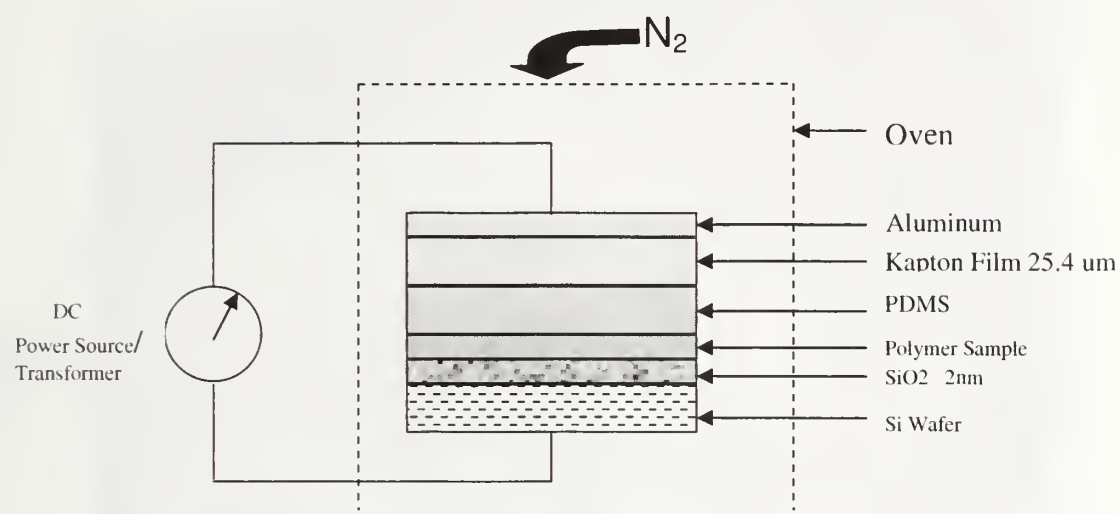
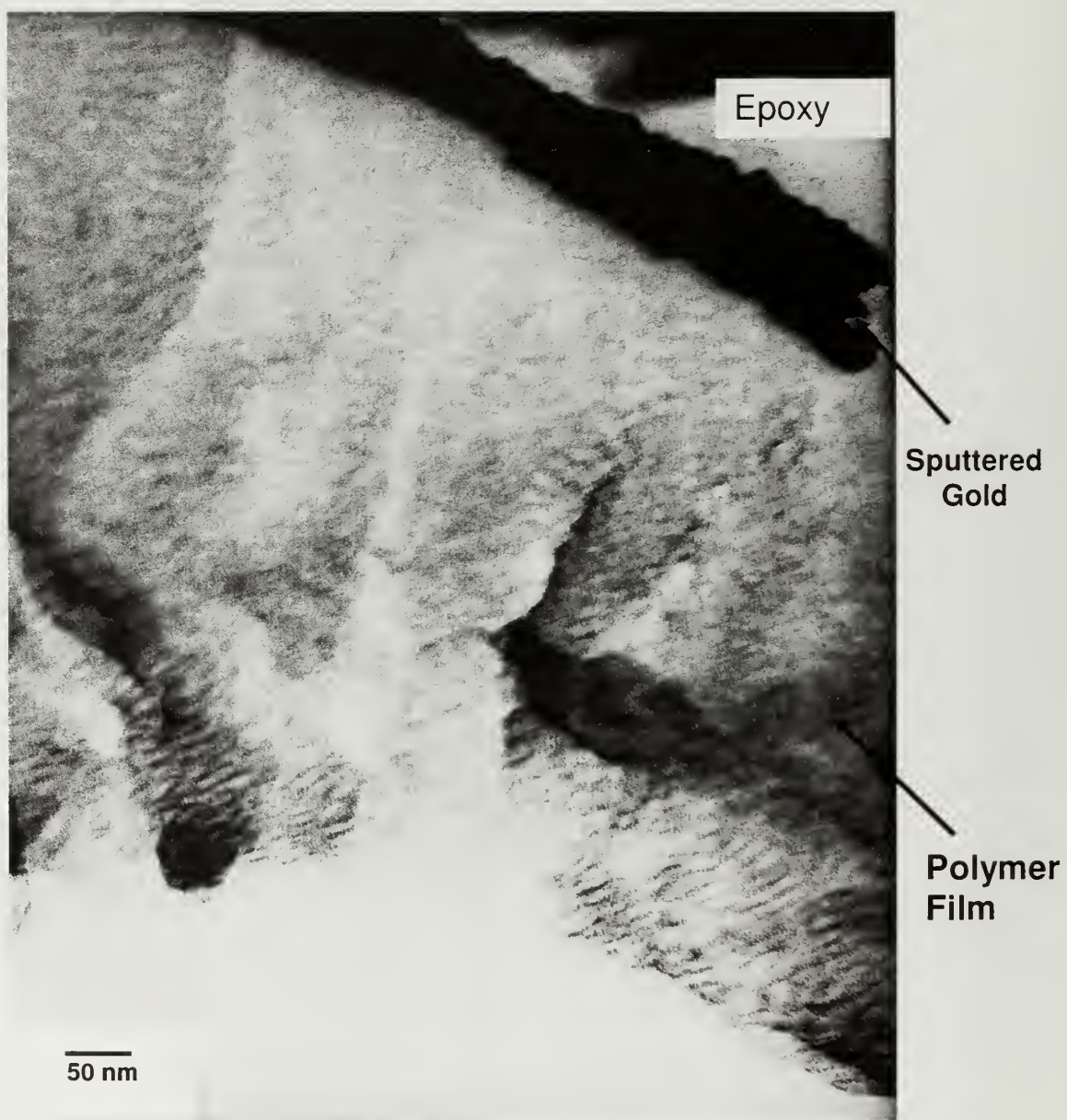
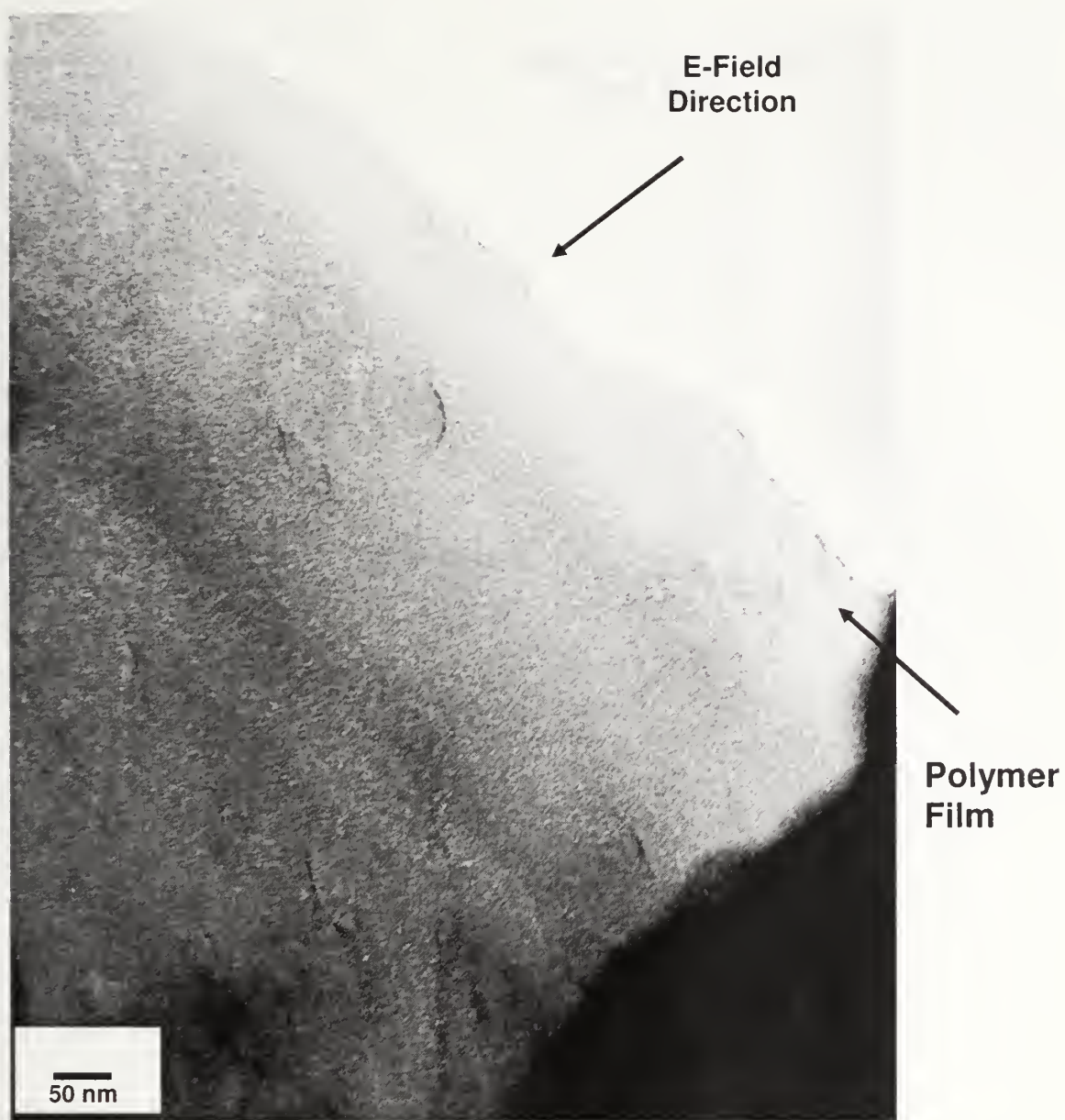


Figure 4.3 Schematic of Electric Field Alignment Experimental Setup.



(a)

Figure 4.4 TEM micrographs showing FISS-CS20 samples (a) As-Cast , (b) After annealing under Electric field of $\sim 40\text{V}/\mu\text{m}$ applied at 130°C , for 24 hours. (Continued).



(b)

Figure 4.4 Continued.

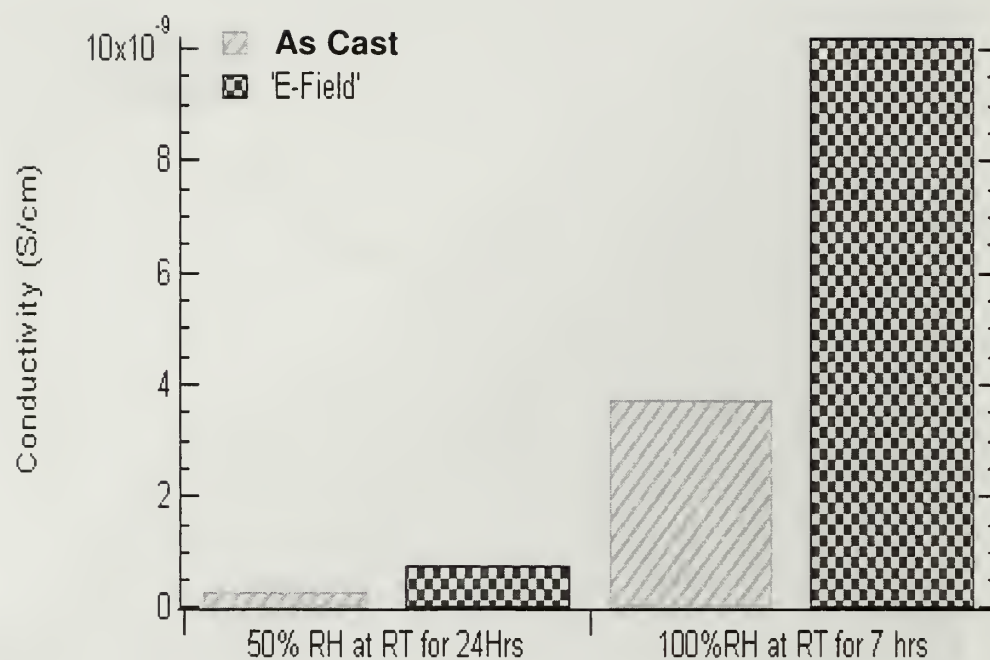


Figure 4.5 Ionic (cesium) conductivity results for As-Cast and Efield annealed FISS-CS20 samples.

CHAPTER 5

POLYMER ELECTROLYTE MEMBRANES FROM ELECTROSPUN SULFONATED POLY(ARYL ETHER KETONE) NANOFIBER MATS.

5.1 Abstract

Sulfonated poly(ether ether ketone) has been electrospun and electrosprayed by varying concentration in DMF, yielding isotropic fibrous mats and beads. The glass transition temperatures of these materials have been shown to be higher than those of the unsulfonated precursors and they increase with increasing sulfonation, due to hydrogen bonding induced rigidity. The presence of sulfonic acid groups on the surface has been confirmed by means of x-ray photoelectron spectroscopy, with sulfur representing 3% of the surface elemental composition. These acid groups on the surface of internal fibers, help to form a 3 dimensional network of conducting channels in the voids of the fibrous mats upon hydration. This in turn has led to an improvement of conductivity from 0.033 S/cm for void-less solution cast membranes to 0.040 S/cm for the electrospun fibrous mats.

5.2 Introduction

A lot of emphasis has been placed of late in the research and development community on the unique properties materials exhibit at the nanometer lengthscale. Besides other intriguing physical phenomena that occur at this lengthscale, the basic increases in surface –to-volume ratio and aspect ratio confer on nanoscale materials a lot of advantages that have been harnessed in technological areas such as catalysis, composites, and purification.

One facile means of fabricating such, nanostructures with high surface-to-volume and aspect ratio is through Electrostatic spinning or Electrospinning. Electrospinning (or similarly electrospraying) is an old technique that has been used for centuries in the materials science field to fabrication articles with small features, based on the interaction between the molten material or a solution containing it, and electricity. The technique was first applied in general to distort a drop of fluid with an electric charged object¹, and more specifically with regard to polymeric systems, they were first mentioned in a 1934 patent by Formhals².

This process basically involves the pumping of the polymer solution or melt, through a metallic spinneret (or syringe) with a small hole, forming a droplet at the tip. Upon application of a high voltage between this spinneret and a grounded metallic target of opposite polarity, a uniformly distributed electrostatic charge is induced on the droplet. When this charge exceeds the surface tension on the droplet surface, charge repulsion leads to what is known as a Taylor cone formation, and then a jet of fluid is ejected towards the grounded target. This fluid jet experiences instabilities; elongation and evaporation while in flight and eventually deposited as a continuous filament of the polymer typically in a random manner onto the grounded metallic target.³.

Many variations of this basic method have been developed including the application of high speed rotating wheel collectors to effect alignment of nanofibers^{4,5}. Fiber dimensions reported, have varied from microns to less than 100nm^{6,3}. The

dimension and other morphological features of these nanofibers, have been shown to depend on a lot of parameters including Polymer Properties (type, molecular weight, architecture); Solution properties (viscosity, elasticity, ionic salt content, surface tension); Process Parameters (Electrical Potential, gap distance, flow rate to spinneret, target motion); and Ambient conditions (temperature , humidity, Air circulation velocity). For instance it has been shown that increasing the polymer concentration, reducing the applied electrical potential or reducing the surface tension of the solution would lead to smoother fibers without beads⁷⁻⁹.

The applications for this fabrication technique continue to be developed and expanded with reported applications including composite reinforcement¹⁰, filtration¹¹, Medical Prostheses¹², Wound Dressing¹³, drug delivery¹⁴, protective and breathable clothing¹⁵, batteries¹⁶, optical shutters¹⁷, biochemical and optical sensors^{18,19}, nanotubule templates²⁰. The electrospinning technique has also been successfully applied to more than 40 different types of polymers, as reported in literature³.

Partially charged polymers, Ionomers, are typically polymers that possess acid groups on some of the monomer units. Sulfonic or carboxylic acids are most commonly used, with the stronger perfluorosulfonic acid bearing ionomers such as NafionTM finding widespread commercial application in the PEM fuel cell and ion exchange industries. These ionomers are typically cast as pin-hole free membranes, by controlled processing which results in specific morphologies that reflect on their transport properties. Several differing models have been put forth for the morphology of NafionTM with little

consensus, which would properly explain their good ion transport properties. However, there is a strong evidence that its morphology transforms from a cluster-channel model to a rod-like model²¹ as the membrane is hydrated. This in effect means that the basis for the good ionic transport properties are cylindrical ionic channels running in three dimensions through out the hydrated membrane. It is our aim in this work to create similar 3-dimensional ionic channels in the voids of random mats of electrospun sulfonated Poly(Aryl ether ketone)s.

A combination of hydrophilic and hydrophobic components of NafionTM chemical structure (See chapter 1), confer on it mechanical, thermal and oxidative stability even under harsh environments. In light of this there has been increasing interest in the development of ionomers based on polymers having good thermal and mechanical properties²². One such class of polymers are poly(Aryl Ether ketone)s, which are commercially available as high performance polymers having good thermal, mechanical and oxidative stability. The sulfonation of these polymers is relatively well developed, and has been applied to the preparation and study of PEMs²³⁻²⁵.

In this work, the electrospinning of sulfonated Poly(Aryl ether ketone)s, namely sulfonated poly(ether ether ketone) (sPEEK) will be studied. The electrospinning characteristics, nanofiber mat morphology, as well as their applicability as PEMs will be investigated. There are few mentions in literature of electrospun nanofibers for electrochemical applications. Choi et al. have reported the use of electrospun poly(vinylidene fluoride) (PVDF) mats for battery polyelectrolyte membranes, using

$\text{LiN}(\text{CF}_3\text{SO}_2)_2$ liquid electrolyte trapped in the voids of the mats as the source of ions for conductivity²⁶. More specifically only one reference reports the use of electrospun and electrosprayed sulfonated poly(ether ether ketone ketone) (sPEEKK) mats for PEM membranes, with high proton conductivity recorded being attributed to ionic channels in the interstices of nanofibers or nanospheres²⁷.

5.3 Experimental Section

5.3.1 Materials

The synthetic procedure and characterization for the sulfonated poly(ether ether ketone) (sPEEK) sample used in this study have been described in detail elsewhere²⁸. The samples having an ion exchange capacity of 0.66 meq/g and 1.97 mEq.g and a precursor poly(ether ether ketone) (PEEK) molecular weight (95,000 Da) have been studied. Solutions of the sPEEK(1.97 meq/g) sample in N,N-dimethylformamide (DMF), with concentrations ranging from 5- 22 wt%, were prepared for electrospinning and stirred for several hours before electrospinning.

5.3.2 Preparation of Membranes

Membranes from isotropic mats of electrospun nanofibers were prepared by electrospinning using 5-10ml normjectTM syringes, fitted with aluminum needles as shown in figure 5.1 below. The tip of the needle on the syringe was clamped by an alligator clip electrode connected to the voltage source and the solution was pumped with a KD Scientific syringe pump out of the needle, forcing its flight to a grounded aluminum foil or aluminum coated kapton foil. The kapton film coated with aluminum on the back

was used so as to prevent contamination of the sulfonate counterions. The sPEEK web was therefore deposited on the kapton side, with the aluminum back coating serving as an attractive pseudo-target. The flowrate through the syringe was varied from 10 $\mu\text{L}/\text{min}$ - 100 $\mu\text{L}/\text{min}$, the applied voltage from a Matsusada Precision Inc. power source was varied from 9 - 22 kilo Volts, and the distance from the syringe tip to the grounded target was similarly varied from 7cm -15cm.

For comparison, a membrane of sPEEK was cast from 9wt% solution of sPEEK 1.97 meq/g in DMF, onto a neutralized glass plate. This drop cast solution was then put in the fume hood for 9 hours to dry slowly, then in the oven for 9 hours at 105°C, then with vacuum and at 105°C in the oven for 12 hours. The collected web of sPEEK nanofibers were also dried under a nitrogen flow at 120°C for 12 hours. The samples for the ionic conductivity were subsequently reactivated by soaking overnight in a 2M aqueous HCL solution. They were thereafter rinsed repeatedly in deionized water till PH was neutralized and redried. Dry membrane thicknesses were measured using a digital micrometer and range from 220-300 μm .

5.3.3 Thermal Characterization

Electrospun membrane samples were subsequently placed in an oven at 105°C overnight under Nitrogen flow. Differential Scanning Calorimetry(DSC) analysis was performed on these dry materials, using a TA Instruments Q200 calorimeter. 4-7mg for samples was placed in aluminum pans, which were sealed in the press. Heating and cooling rate was set to 10°C min^{-1} . Virgin sPEEK and PEEK samples were also placed in

TA Instruments ThermoGravimetric Analyzer(TGA 2950) , and percent weight loss was measured as the samples were heated from room temperature till 1000°C under nitrogen flow.

5.3.4 Scanning Electron Microscopy(SEM)

The morphology of the electrospun fiber mats were studied by means of a Field Emission Scanning electron microscope (FESEM, JEOL 6320 FXV) operating at an accelerating voltage of 5 or 10 Kilovolts. All samples were sputter coated with gold, and mounted with carbon tape unto an aluminum stub prior to the performance of SEM.

5.3.5 X-Ray Photoelectron Spectroscopy(XPS)

The surface elemental composition of the sPEEK electrospun nanofibers were determined by x-ray photoelectron spectroscopy (XPS). XPS spectra are obtained by irradiating a material with a beam of x-rays while simultaneously measuring the kinetic energy and number of electrons that escape from the top 1 to 10 nm of the material being analyzed²⁹. A Physical Electronics Quantum 2000 Scanning ESCA Microprobe was used on predried samples, with an Aluminum x-ray source at a take-off angle of 15 degrees.

5.3.6 Ionic Conductivity.

Proton conductivity of the membranes were measured by means of two probe complex impedance spectroscopy techniques, which measure conductivity normal to the plane of the membrane. Pieces of both the electrospun and solution cast samples were

immersed in deionized water for several hours, and then rapidly sandwiched between pieces of graphite paper, held together by slight spring tension between two aluminum studs which had copper wire electrode connections to the Electrochemical impedance setup. This comprised of a solartron 1252A frequency response analyzer linked to an SI 1287 electrochemical interface was used within a frequency range of 0.1 and 300KHz, and the value of the real intercept in the Imaginary vs. real impedance plot (Bode plot) in the high frequency range is taken as the bulk resistance of the membrane to ionic conductivity, as described in elsewhere³⁰.

5.4 Results and discussions

Thermal stability is a prerequisite for any candidate material for PEM application. This property must therefore be determined to screen out membrane materials that decompose or soften below or close to the use temperature. In view of this, the degradation temperature as well as the glass transition temperature of the as-received sPEEK materials have been measured by TGA and DSC respectively.

Figure 5.2(a) shows the TGA data for PEEK, sPEEK (0.66 meq/g) and sPEEK (1.97 meq/g) (Listed in increasing order sulfonation). The samples had been predried under nitrogen flow overnight at 105°C, however the sulfonated samples still show some residual water increasing in order of sulfonation. The initial weight loss prior to 100°C indicates a 2 % water content for the sPEEK (0.66 meq/g) sample, and an 8wt% water content for the sPEEK (1.97 meq/g) sample which is as expected with increasing sulfonation which means larger number of acid sites to absorb and hold water molecules.

The second set of weight loss points (between 300-330°C) are as a result of the disintegration of the sulfonic acid clusters³¹, and as expected the sPEEK (1.97meq/g) sample shows a greater drop in weight due to the higher sulfonation. Finally we see a precipitous drop in weight due to the decomposition of the aromatic PEEK chain between 480-555°C. These thermal transitions are high enough to ensure the suitability sPEEK materials far beyond a 100°C temperature range.

The DSC thermograms for the second heating scans of materials studied are shown in figure 5.2(b). The thermograms show the glass transitions (T_g) of the PEEK and sPEEK samples studied. The samples show an increase in glass transition temperature in increasing order of sulfonation with PEEK $T_g = 149.6^\circ\text{C}$, sPEEK0.66 $T_g = 174.5^\circ\text{C}$, and sPEEK1.97 $T_g = 183.8^\circ\text{C}$. This trend is similar to that shown by other styrene sulfonic acid based ionomers³² and also observed in other sPEEK studies, and has been attributed to the formation of a stiffer polymer due to inter and intra molecular bridges formed by hydrogen bonding with other ionic groups^{31,33}. The T_g therefore increases with increasing sulfonation due to increased hydrogen bonding sites. These materials are therefore suitable for water-based conductivity at 100°C or less in PEM applications.

The morphology of nanostructures formed by electrospinning or electrospraying can also be looked at by means of SEM. The structures produced by varying concentration of the sPEEK1.97meq/g in solution from 10wt% to 20 wt% have been shown in figure 5.3. The other spinning parameters were kept constant at flow rate of 100ul/min, voltage of 18,000 V, and distance of 13 cm to the target. These results show

the profound effect of solution properties on the microstructure. The formation of beaded or spherical morphology is observed at lower concentration as shown in figure 5.3 (c),(d). Higher concentration solutions are known to produce smoother beadless fibers, because they have faster drying times in flight and more chain entanglement to rapidly form a continuous fiber skin^{27,34}. Also as you increase the ionomer concentration in solution the charge density of free ions in the solution increases, and as seen when salt concentration in spinning solution is increased³⁵, there is an increase in the elongation force experienced by the solution jet flying in the electric field thus resulting in more continuous fibers being formed, as seen in figure 5.3 (a),(b).

Spinning conditions for making fibrous mats for PEM applications were optimized at 22wt% sPEEK1.97meq/g in DMF, 12, 000 volts, 10 -12.5 ul/min flowrate, 5 -7 cm. An example of the fiber mats thus obtained is shown in figure 5.4. In order to determine if the sulfonic acid groups are on the surface of the fibers, XPS studies of the surface elements were carried out as described above, and spectra are shown in figure 5.5 below. The spectra show a distinct 2p orbital peak for sulfur which can only be present due to the sulfonic acid groups on the surface of the fiber mat. Analyses of the peak areas give the relative atomic ratios of each atom present; and shows that 3% of the electrons knocked off the surface of the fibers were from sulfur. This data confirms that there are sulfonic acid sites on the fiber surfaces in the 3 dimensional network formed by the interstices of the fibers. This basically provides proton(H^+) counterions that can be dissociated upon hydration to affect ionic conductivity.

The conductivity values measured for the solution cast and electrospun membranes, have been summarized in table 5.1. The conductivity values are normalized by the thicknesses which are similar. There is an improvement in the conductivity measure for the fibrous mats over the solution cast membranes from 0.033 to 0.040 S/cm. This can be attributed to the increased surface area with exposed sulfonic acid groups, in contact with water. This water serves as the medium of dissociation and transport of the exposed protons resulting in conductivity. This value of 0.040 S/cm reached by the fibrous mats may actually not be the ultimate attainable conductivity, as some of the water is pulled out by capillary effects of the blotting paper used, during wiping off of surface water from the membranes while transferring from water to EIS setup. However this is standard practice, and the electrospun mat conductivity measured is the same as that measured for the electrospun SPEKK (2.01 meq/g) of similar ion exchange capacity²⁷. As in that work a great increase in the conductivity of the mats can be achieved by using the spherical morphology electrosprayed samples, as this has a higher internal surface area.

5.5 Conclusions

Sulfonated poly(ether ether ketone) has been electrospun and electrosprayed yielding isotropic fibrous mats and beads by varying concentration. The glass transition of this material has been shown to be higher than the unsulfonated precursors, due to hydrogen-bonding induced rigidity. The T_g increases with increasing sulfonation. The presence of sulfonic acid groups on the surface has been confirmed by means of XPS, with sulfur representing 3% of the surface elemental composition. This acid groups on

the surface of internal fibers, helps to form a 3 dimensional network of conducting channels in the voids of the fibrous mats upon hydration. This leads to improvement of conductivity from 0.033 S/cm for void-less solution cast membranes, to 0.040 S/cm for the electrospun mats. The utility of this technique for PEM applications can be enhanced by spraying of dense mats of spherical beads. The capillary effect upon blotting surface water can be mitigated by pressing the fibrous mats above the T_g to seal the surface pores. This will also stop the permeation of H_2 or methanol in a PEM fuel cell.

5.6 References

- (1) Gilbert, W. In "On Loadstone and Magnetic bodies and on the Great magnet of Earth" **1600**.
- (2) Formhals, A. US Patent 1,975,504, **1934**.
- (3) Huang, Z.; Zhang, Y.Z.; Kotaki, M.; Ramakrishna, S. Composites Science and Technology **2003**, 63, 2223.
- (4) Boland, E.D.; Wnek, G.E.; Simpson, D.G.; Palowski, K.J.; Bowlin, G.L. J. Macromol. Sci. Pur. Appl. Chem. **2001**, A38, 1231.
- (5) Fennessey, S.F.; Pedicini, A.; Farris, R.J. In ACS Symposium Series: Polymeric Nanofibers **2006**, 918, 300.
- (6) Baumgarten, P.K. J. Colloid and Interf. Sci. **1971**, 36, 71.
- (7) Fong, H.; Reneker, D.H. J. Polym. Sci.: Part B Polym. Phys. **1999**, 37, 3488.
- (8) Doshi, J.; Reneker, D.H. J. electrostatics, **1995**, 35, 151.
- (9) Deitzel, J.M.; Kleinmeyer, J. Harris, D.; Tan, N.C.B. Polymer **2001**, 42, 261.
- (10) Kim, J.S.; Reneker, D.H. Polymer Composites **1999**, 20, 124.
- (11) Groitzsch, D.; Fahrbach, E. US Patent 4,618,524, **1986**.
- (12) Berry, J.P US Patent 4,965,110, **1990**.
- (13) Coffee, R.A. PCT/GB97/01968, **1998**.
- (14) Kenawy, E.R. et al. J. Controlled Release **2002** 81, 57.
- (15) Schreuder-Gibson, H.L. et al. J. Advanced Materials **2002**, 34, 44.
- (16) Norris, I.D.; Shaker, M.M.; Ko, F.K.; Macdiarmid, A.G. Synthetic Metals **2000**, 114, 109.
- (17) Waters, C.M.; noakes, T.J.; Pavery, I.; Hitomi, C. US Patent 5,088,807, **1992**.
- (18) Kwoun, S.J.; Lec, R.M.; Han, B.; ko, F.K. In Proceedings of the IEEE/EIA: International Frequency Control symposium 2000, p. 57.
- (19) Lee, S.H.; Ku, B.C.; wang, X.; Samuelson, L.A.; Kumar, J. Mat. Res. Soc. Symp. Proc. **2002**, 708, 403.

- (20) Bognitzki, M. et al. *Advanced Materials* **2000**, 12, 637.
- (21) Mauritz, K.A.; Moore, R.B. *Chemical Reviews* **2004**, 104, 4535.
- (22) Hickner, M.A.; Ghassemi, H.; Kim, Y.S.; Einsla, B.R.; McGrath, J.E. *Chemical Reviews* **2004**, 104, 4587.
- (23) Swier, S.; Chun, Y.S.; Gasa, J.; Shaw, M.T.; Weiss, R.A. *Polymer Eng. Sci.* **2005**, 45, 1081.
- (24) Reyna-Valencia, A.; Kaliaguine, S.; Bousmina, M. J. *Appld. Polym. Sci.* **2006**, 99, 756.
- (25) Carbone, A. et al. *J. Power Sources* **2006**, 163, 18.
- (26) Choi, S.W.; Jo, S.M.; Lee, W.S.; Kim, Y. *Advanced Materials* **2003**, 15, 2027.
- (27) Li, X.; Hao, X.; Xu, D.; Zhang, G.; Zhong, S.; Na, H.; Wang, D. J. *Membr. Sci.* **2006**, 281, 1.
- (28) Shurui, S.; and Weiss, R.A. Private communication.
- (29) http://en.wikipedia.org/wiki/X-ray_photoelectron_spectroscopy
- (30) See Chapter 2, Section 2.3.4.
- (31) Carbone, A. et. al. *J. Power Sources* **2006**, 163, 18.
- (32) Weiss, R.A.; Sen, A.; Pottick, L.A.; Willis, C.L. *Polymer* **1991**, 32, 2785.
- (33) Zaidi, S.M.J. et al. *J. Membr. Sci.* **2000**, 173, 17.
- (34) Fong, H.; Chun, I.; Reneker, D.H. *Polymer* **1999**, 40, 4585.
- (35) Zong, X. et al. *Polymer*, **2002**, 43, 4403.

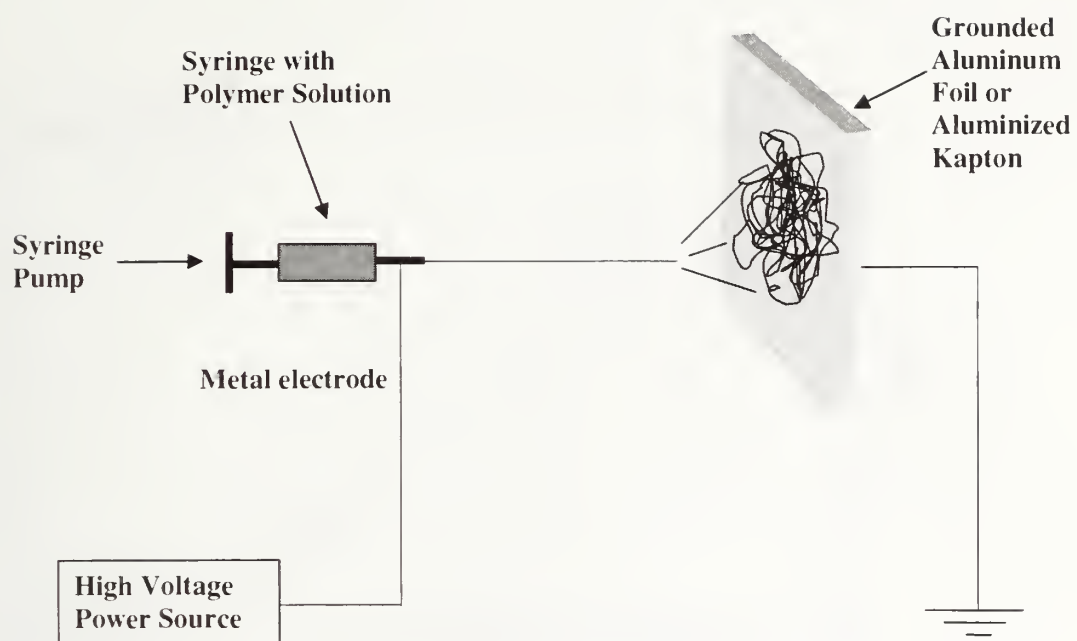
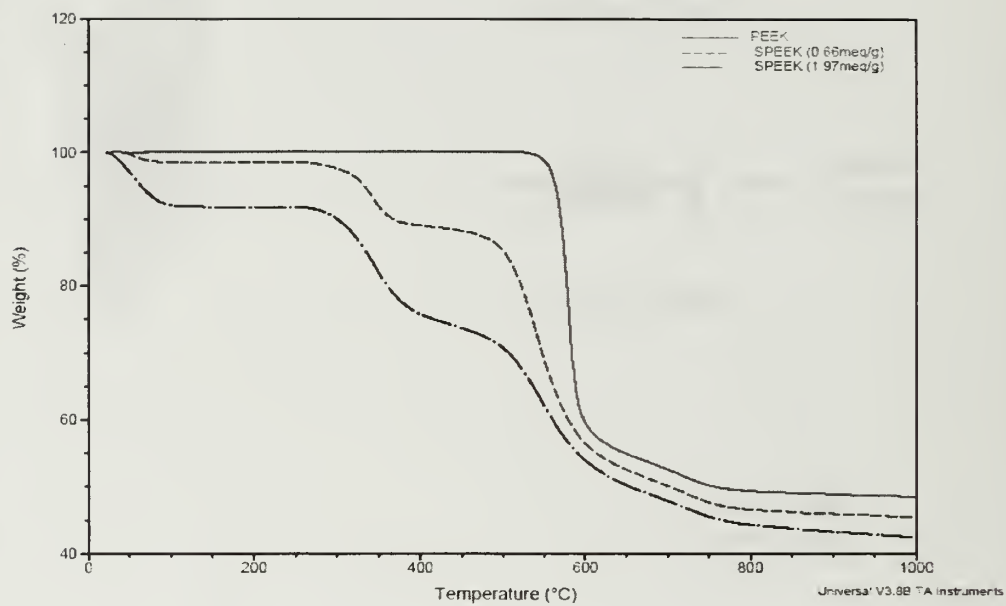
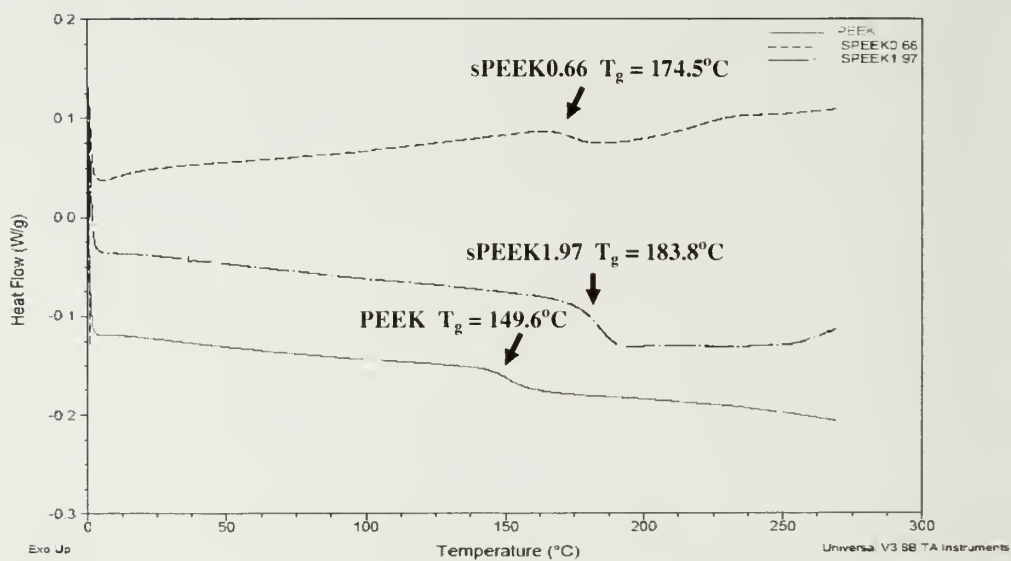


Figure 5.1 Schematic of Electrospinning Experimental Setup.

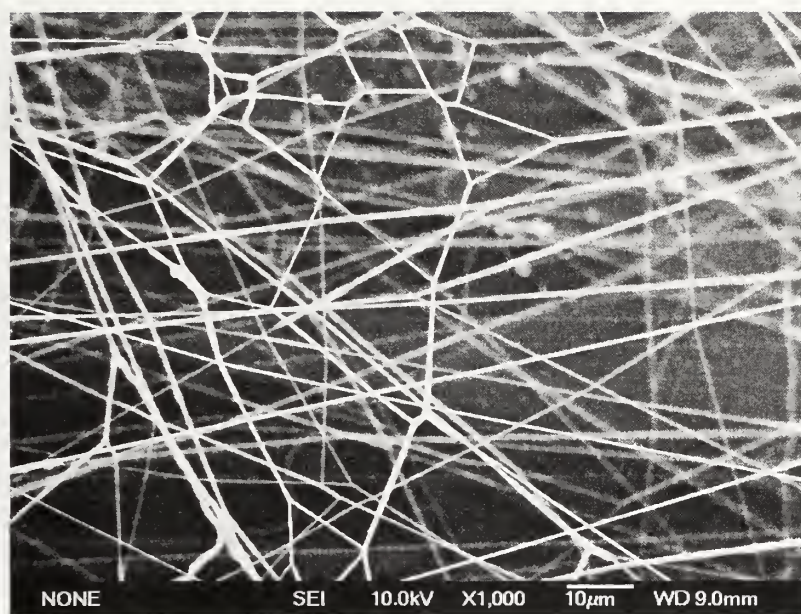


(a)

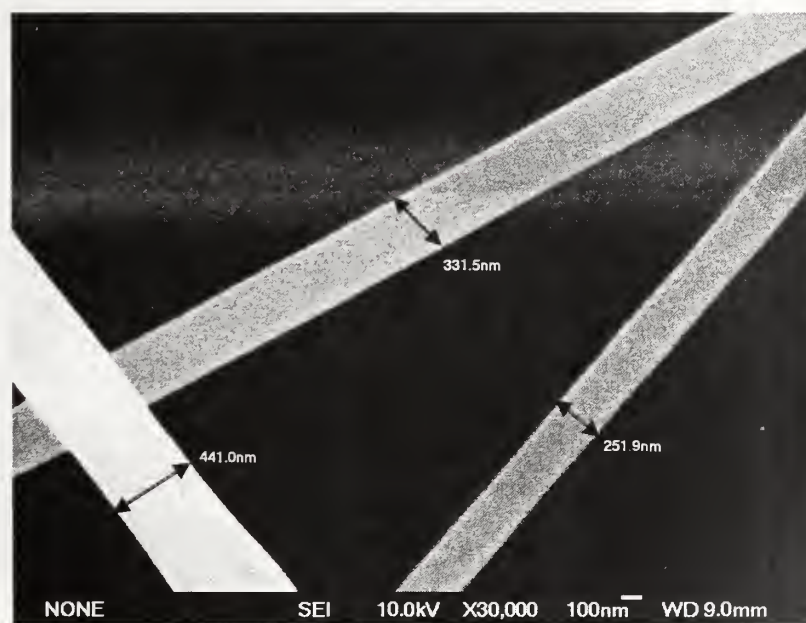


(b)

Figure 5.2 Thermograms for PEEK, sPEEK0.66, sPEEK1.97 from (a) TGA (b) DSC measurements.

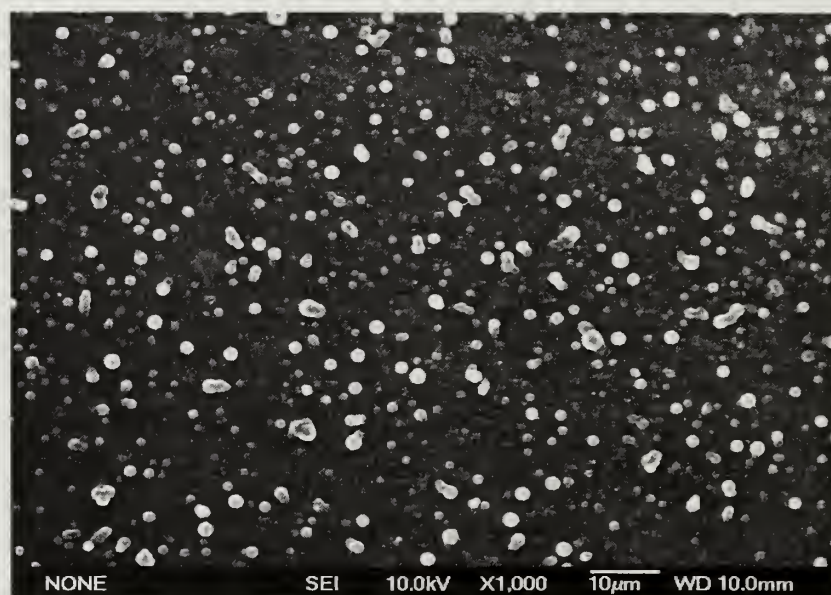


(a)



(b)

Figure 5.3 SEM images for sPEEK1.97 from (a),(b) electrospun from 20wt% solution in DMF (c),(d) electrosprayed from 10wt% solution in DMF, at 18kV, 100ul/min and 13cm distance from target. (continued)



(c)



(d)

Figure 5.3 (continued)

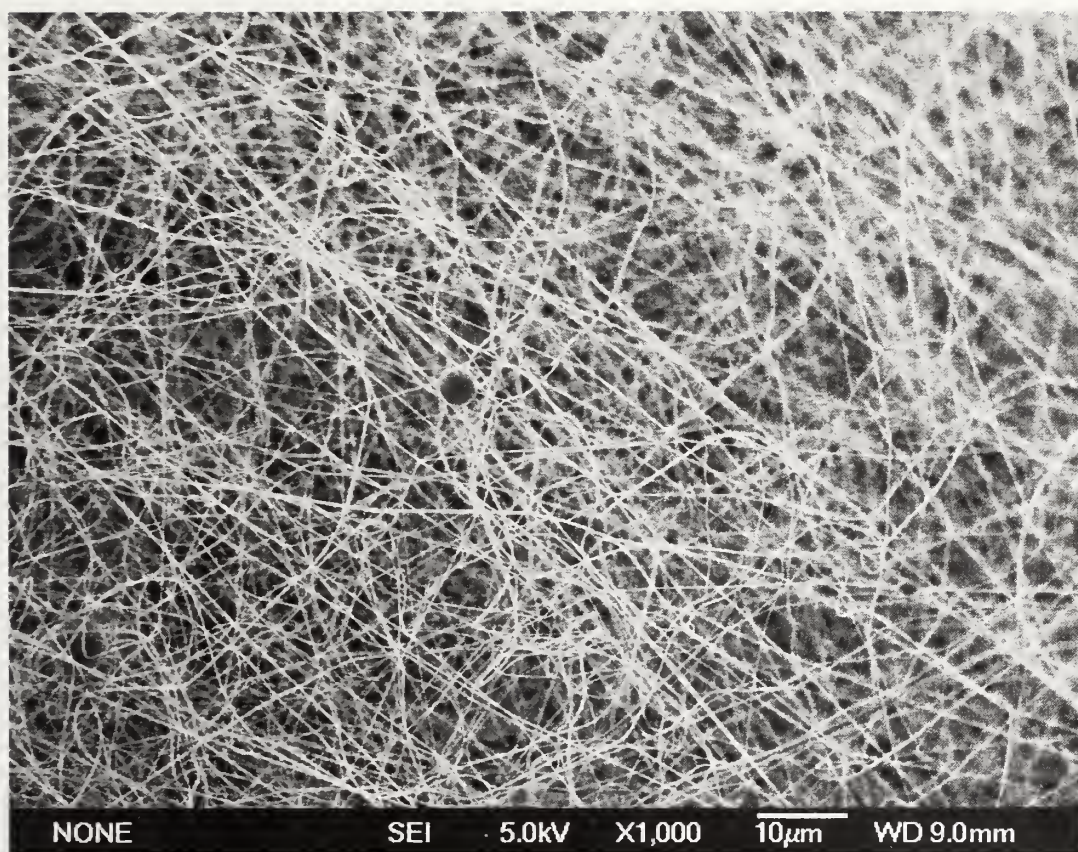


Figure 5.4 SEM images for sPEEK1.97 from electrospun from 22wt% solution in DMF at 12kV, 12.5 ul/min and 7 cm distance from target.

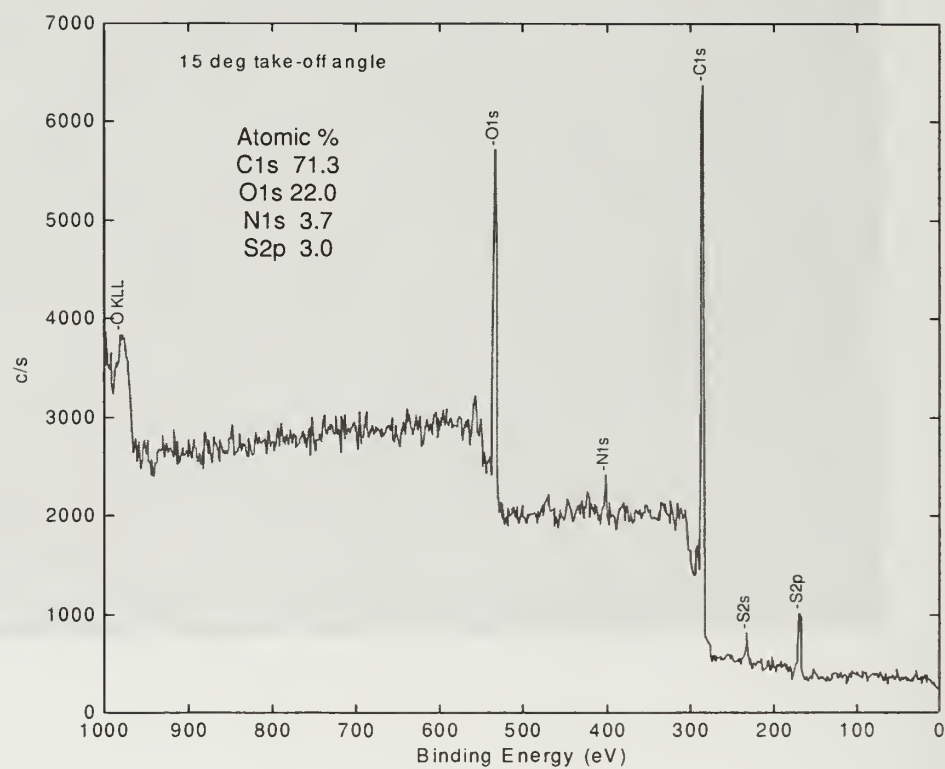


Figure 5.5 XPS images for sPEEK1.97 from electrospun from 22wt% solution in DMF at 12kV, 10 - 12.5 $\mu\text{l}/\text{min}$ and 5-7 cm distance from target.

Table 5.1 Conductivity, and membrane thickness for sulfonated Poly(Ether Ether Ketone) (1.97 meq/g) obtained by EIS, and micrometer.

Sample	sPEEK 1.97meq/g Electrospun mat	sPEEK 1.97 meq/g solution Cast
Membrane Thickness (um)	294	223
Conductivity (S/cm)	0.040	0.033

CHAPTER 6

SUMMARY AND POSSIBLE FUTURE DIRECTIONS.

Time will tell whether the dream of fuel cell technology application as a commercially successful alternative source of energy will be realized, however their continues to be a great deal of scientific research and development being done in this regard. In the time since this work began their have been announcements of imminent commercialization of Direct Methanol Fuel Cells for portable iPod like devices by Toshiba and other electronics manufacturer, however years have passed since without fruition. Honda announced late last year that they would have fuel cell vehicles available for sale this summer of 2008.

The main technical hurdles still remain the development of suitable alternative catalyst, inexpensive membranes that can work with less water dependence, portable storage and delivery of hydrogen fuel, and the systems engineering of the whole fuel cell. On the polymer electrolyte membrane front, there is a strong thrust towards making membranes that are conducive to higher temperature (120-150°C) and that can work with little or no hydration. This trend I believe will continue into the future.

Block copolymers, or hybrids of organic and inorganic materials will eventually prove useful in commercial PEMs. Different components of the membrane will have to deliver different properties, with the synergy being required to fulfill the often competing demands of an operating fuel cell environment.

In this work we have been able to create randomly microphase separated polymer electrolyte membranes from fluorinated poly(Isoprene)-block-sulfonated poly(Styrene). These membranes exhibit low methanol permeability at room temperature, but they swell greatly upon hydration at 60°C due to the low glass transition temperature of the fluorinated block leading to domain dilation. This leads to mechanical failure of the membranes under osmotic stress as seen in the methanol permeability data and the great drop in storage modulus beyond T_g .

To circumvent this I believe the unsulfonated poly(Styrene) units can be crosslinked by UV/Ozone application (or chemical means), to lock in the microstructure. Better still a fluorinated block with a higher T_g , such as fluorinated poly(Cyclohexadiene) or a fluorinated aromatic polymer, could help preserve mechanical integrity. Otherwise the PS block could be fluorinated instead, and the elastomeric poly(Isoprene) sulfonated as has been done for commercially available *kraton*TM materials.

Some improvement in the conductivity of the membrane was achieved by application of electric field as expected, however a more detailed and systematic study can be done with more promising polymer samples. Studying the effect of parameters such as the applied field strength, temperature, presence of solvent may yield some interesting findings. However this is not a trivial pursuit as the electrostatic effects must first be screened or somehow quenched before or during electric field annealing.

Sulfonated poly (ether ether ketone) was electrospun and electrosprayed into isotropic nanofiber mats or droplets showing surface functionality. This exercise was much more difficult than for the uncharged polymers as there was random electrostatic attraction to any metallic or sharp object in the spinning chamber making it very difficult to collect samples. The mats showed improved proton conductivity over the solution cast membranes, but will fail in a PEM application. As suggested by Prof. Tom Russell, they could be melt-pressed to seal the surface voids. On the other hand I feel a hydrophobic polymer such as poly(vinylidene fluoride) could be cast from a different solvent into the interstices of the mats to block the pores, or be electrospun with sPEEK to form blend fibers and then melt pressed. This will help avoid gross swelling and maintain mechanical integrity of the membranes upon hydration. Selah.

BIBLIOGRAPHY

- (1) O'Hayre, R.P.; Cha, S.; Cololla, W.; Prinz, F.B. *Fuel Cell Fundamentals* ; 1 ed.; John Wiley & Sons, Inc. NY, **2006**.
- (2) <http://www.sae.org/technology/fuelcells-history.htm>.
- (3) Carrette, L.; Friedrich, K.A.; Stimming, U. *Fuel Cells* **2001**, 1, 5.
- (4) Hickner, M.A.; Ghassemi, H.; Kim, Y.S.; Einsla, B.R.; McGrath, J.E. *Chemical Reviews* ,**2004**, 104, 4587.
- (5) Arico, A.S.; Srinivasan, S.; Antonucci, V. *Fuel Cells* **2001**, 1, 133.
- (6) Yang, Y.; Holdcroft, S. *Fuel Cells* **2005**, 5, 171.
- (7) Bishop, M.T.; Karasz, F.E.; Russo, P.S.; Langley, K.H. *Macromolecules* **1985** ,18, 86.
- (8) Wainright, J.S.; Wang, J.T.; Weng, D.; Savinell, R.F.; Litt, M.J. *J. Electrochem. Soc.* **1995**, 142, L121.
- (9) Miyatake, K.; Hay, A.S.; *J. Polym. Sci., Part A: Polym. Chem* **2001**, 39, 3770.
- (10) Savett, S.C.; Atkins, J.R.; Sides, C.R.; Harris, J.L.; Thomas, B.H.; Creager, S.E.; Pennington, W.T.; DesMarteau, D.D. *J. Electrochem. Soc.* **2002**, 149, A 1527.
- (11) Kim, Y.S.; Wang, F.; Hickner, M.; Zawodzinski, T.A.; McGrath, J.E. *J. Membr. Sci.*, **2003**, 212, 263.
- (12) Herz, H.G.; Kreuer, K.D.; Maier, J.; Scharfenberger, G.; Schuster, M.F.; Meyer, W.H. *Electrochim. Acta* **2003**, 48, 2165.
- (13) Hickner, M.A.; Pivovar, B.S. *Fuel Cells* **2005**, 5, 213.
- (14) Khandpur, A.K.; forster, S.; Bates, F.S.; Hamley, I.M.; Ryan, A.J.; Bras, W.; Almdal, K.; Mortensen, K. *Macromolecules* **1995**, 28, 8796.
- (15) Rubatat, L.; Rollet, A.L.; Gebel, G.; Diat, O. *Macromolecules* **2002**, 35, 4050.
- (16) Yang, Y.; Shi, Z.; Holdcroft, S. *Macromolecules* **2004**, 37, 1678.

- (17) Kim, J.; Kim, B.; Jung, B.; Kang, Y.S.; Ha, H.Y.; Oh, I.H.; Ihn, K.J. *Macromol. Rapid. Commun.* **2002**, 23, 753.
- (18) Won, J.; Park, H.H.; Kim, Y.J.; Choi, S.W.; Ha, H.Y.; Oh, I.H.; Kim, H.S.; Kang, Y.S.; Ihn, K.J. *Macromolecules* **2003**, 36, 3226.
- (19) Huang, T.; Gido, S.P.; Mays, J.W. in *Synthesis and characterization of Fluorinated and sulfonated Block copolymers for Fuel Cell Proton Exchange Membranes*. Unpublished Manual.
- (20) Swier, S.; Chun, Y.S.; Gasa, J.; Shaw, M.T.; Weiss, R.A. *Polymer Eng. & Sci.* **2005**, 1081.
- (21) Weiss, R.A.; Shaw, M.T. *DOE Hydrogen Program FY 2004 Progress Report*.
- (22) Golodnitsky, D.; Livshits, E.; Kovarsky, R.; Peled, E.; Chung, S.H.; Suarez, S.; Greenbaum, S. *Electrochem. & Solid State Lett.* **2004**, 7, A412.
- (23) Huang et al. *Composites Sci. and Tech.* **2003**, 63, 2223.
- (24) Choi, S.W.; Jo, S. M.; Lee, W.S.; Kim, Y. *Adv. Mater.* **2003**, 15, 2027.
- (25) Gierke, T.D.; Munn, G.E.; Wilson, F.C. *J. Polymer Sci: Polym. Phys. Ed.* **1981**, 19, 1687.
- (26) Gido, S.P. In *ACS Symposium series: New Polymeric Materials* **2005**, 916, 309.
- (27) Kim, B.; Kim, J.; Jung, B. *J. of Membrane Science* **2005**, 250, 175.
- (28) Tricoli, V. *J. Electrochem. Soc.* **1998**, 145, 3798.
- (29) Miyake, N.; Wainright, J.S.; Savinell, R.F. *J. Electrochem. Soc.* **2001**, 148, A898.
- (30) Long, G.G.; Allen, A.J.; Ilavsky, J.; Jemian, P.R.; Zschack, P. In *Synchrotron Radiation Instrumentation: Eleventh US National Conference*, CP521, Pianetta, P.; Winick, H. Eds.; , American Institute of Physics, College Park, **2000**, pp. 183–187.
- (31) Elabd, Y. A.; Napadensky, E.; Sloan, J. M.; Crawford, D.M.; Walker, C.W. *J. Membr. Sci.* **2003**, 217, 227.
- (32) Crank, J. *The Mathematics of Diffusion*; Oxford University Press: Oxford, **1975**.
- (33) Cahan, B.D.; Wainright, J.S. *J. Electrochem. Soc.* **1993**, 140, L185.

- (34) Drzal, P.L.; Halasa, A.F.; Kofinas, P. *Polymer* **2000**, 41, 4671.
- (35) Elabd, Y. A.; Napadensky, E.; Walker, C. W.; Winey, K. I. *Macromolecules* **2006**, 39, 399.
- (36) Bates, F. S. *Science* **1991**, 251, 898.
- (37) Bucknall, D.G.; Anderson, H.L. *Science* **2003**, 302, 1904.
- (38) Storey, R.F.; Baugh III, D.W. *Polymer* **2000**, 41, 3205.
- (39) Serpico, J.M.; Ehrenberg, S.G.; Fontanella, J.J.; Jiao, X.; Perahia, D.; McGrady, K.A.; Sanders, E.H.; Kellogg, G. E.; Wnek, G. E. *Macromolecules* **2002**, 35, 5916.
- (40) Isaacs-Sodeye A. I.; Huang T.; Mays J.; Gido S. P. "Block copolymer ionomers from Fluorinated Poly(Isoprene)-*block*-Sulfonated Poly(Styrene) 2: Structural evolution with swelling and in solution" *Manuscript in Preparation*.
- (41) Williams, C.E.; Russell, T.P.; Jerome, R.; Horrion, J. *Macromolecules* **1986**, 18, 2877.
- (42) Lu, X.; Steckle, W.P. Weiss, R.A. *Macromolecules* **1993**, 26, 5876.
- (43) Sakurai, S.; Momii, T.; Taie, K.; Shibayama, M.; Nomura, S.; Hashimoto, T. *Macromolecules* **1993**, 26, 485.
- (44) Yarusso, D.J.; Cooper, S. L. *Macromolecules* **1983**, 16, 1871.
- (45) Roe, R. *Methods of X-Ray and Neutron Scattering in Polymer Science*; Oxford University Press: New York, **2000**; p189.
- (46) Cotton, F.A.; Wilkinson, G. *Advanced Inorganic Chemistry*, John Wiley: New York, **1972**, p 645.
- (47) Carretta, N.; Tricoli, V.; Picchioni, F. J. *J. Membr. Sci.* **2000**, 166, 189.
- (48) Deluca, N. W.; Elabd, Y. A. J. *Polym. Sci., Part B: Polym. Phys.* **2006**, 44, 2201.
- (49) Swier, S.; Chun, Y.S.; Gasa, J.; Shaw, M.T.; Weiss, R.A. *Polymer Eng. Sci.* **2005**, 45, 1081.
- (50) Pivovar, B.S.; Wang, Y.; Cussler, E.L. *J. Membr. Sci.* **1999**, 154, 155.
- (51) Alberti, G.; Constantino, U.; Casciola, M.; Ferroni, S.; Massinelli, L.; Staiti, P. *Solid State Ionics* **2001**, 145, 249.

- (52) <http://www.freepatentsonline.com/6140436.html>
- (53) Longworth, R.; Vaughan, D.J. Polym. Prepr. (Am. Chem. Soc. , Div. Polym. Chem.) **1968**, 9, 525.
- (54) Eisenberg, A. *Macromolecules* **1970**, 3, 147.
- (55) Semonov, A. N.; Nyrkova, I.A.; Kholkhov, A. R. *Macromolecules* **1995**, 28, 7491.
- (56) Gebel, G. *Polymer* **2000**, 41, 5829.
- (57) The OMEGA® Temperature Handbook and Encyclopedia, Vol. MMV™ 5th Edition®
- (58) <http://www.isis.rl.ac.uk/largescale/loq/documents/sans.htm>
- (59) Peiffer, D.G.; Weiss, R.A.; Lundberg, R.D. J. Polym. Sci., Polym. Phys. **1982**, 20, 1563.
- (60) Ryu, D.Y.; Jeong, U.; Kim, J.K.; Russell, T.P. *Nature Materials* **2002**, 1, 114.
- (61) Rodriguez-Abreu, C.; Lazzari, M.; Varade, D. ; Kaneko, M ; Aramaki, K. ; Quintela, M.A.L. *Colloid Polym. Sci.* **2007**, 285, 673.
- (62) Kreuer, K.D. *Solid State Ionics* **1997**, 97, 1.
- (63) Ren, Y.; Lodge, T.P; Hillmyer, M.A. J. Am. Chem. Soc. **1998**, 120, 6830.
- (64) Weiss, R.A.; Sen, A.; Pottick, L.A.; Willis, C.L. *Polymer* **1991**, 32, 2785.
- (65) Rigdahl, M.; Eisenberg, A. J. Polym. Sci., Polym. Phys. Edn. **1981**, 19, 1641.
- (66) Meyers, M.A.; Chawla, K.K. *Mechanical Behaviour of Materials*, Prentice Hall, **1999**, 98.
- (67) Kim, Y.S.; Dong, L.; Hickner, M.A.; Glass, T.E.; Webb, V.; McGrath, J. E. *Macromolecules* **2003**, 36 6281.
- (68) Nakamura, K.; Hatakeyama, T.; Hatakeyama, H. *Polymer* **1983**, 24, 871.
- (69) Kataoka, M.; Hagihara, Y.; Mihara, K.; Goto, Y J. Mol. Biol. **1993**, 229, 591.
- (70) Sugiura, S. et al. J. Coll. Interf. Sci. **2001**, 240, 566.

- (71) Flanagan, J.M.; Kataoka, M.; Fujisawa, T. Engelman, D.M. *Biochemistry* **1993**, 32, 10359.
- (72) Schmidt, G.; Richtering, W.; Lindner, P.; Alexandridis, P. *Macromolecules* **1998**, 31, 2293.
- (73) Zipfel, J.; Berghausen, J.; Schmidt, G.; Lindner, P.; Alexandridis, P. Tsianou, M.; Richtering, W. *Phys. Chem.. Chem. Phys.* **1999**, 1, 3905.
- (74) Amundson, K. et al. *Macromolecules* **1991**, 24, 6546.
- (75) Amundson, K. ; Helfand, E. ; Quan, X. ; Smith, S.D.; *Macromolecules* **1993**, 26, 2698.
- (76) Morkved, T.L.; Lu, M.; Urbas, A.M.; Ehrichs, E.E.; Jaeger, H.M.; Mansky, P.; Russell, T.P. *Science* **1996**, 273, 931.
- (77) Kim, G.; Libera, M. *Macromolecules* **1998**, 31, 2569.
- (78) Kim, S.H.; Misner, M.J.; Xu, T.; Kimura, M.; Russell, T.P.; *Adv. Mater.* **2004** 16, 226.
- (79) Kofinas, P.; Cohen, R.E. *Macromolecules* **1994**, 24, 3002.
- (80) Zhao, Y.; Roche, P.; Yuan, G. *Macromolecules* **1996**, 29, 4619.
- (81) Grigorova, T.; Pispas, S.; Hadjicristidis, N., Thurn-Albrecht, T. *Macromolecules*, **2005**, 38, 7430.
- (82) Thurn-Albrecht, T. et al. *Science* **2000**, 290, 2126.
- (83) Lopes, W.A. ; Jaeger, H.M. *Nature* **2001**, 414, 735.
- (84) Van Blaaderen, A.; Wiltzius, P. *Adv. Mater.* **1997**, 9 833.
- (85) Zhong, Y.; Wu, L.; Su, H.; Wong, K.S.; Wang, H. *Optics Express* **2006**, 14, 6837.
- (86) Drzal, P.L.; Halasa, A.F.; Kofinas, P. *Polymer* **2000**, 41, 4671.
- (87) Faridi, N.; Duda, J.L.; Hadj-Romdhane, I. *Ind. Eng. Chem. Res.* **1995**, 34, 3556.
- (88) Bellows, R. et al. DOE Hydrogen Program FY **2004** Progress Report.
- (89) Golodnitsky, D.; Livshits, E.; Kovarsky, R.; Peled, E.; Chung, S.H.; Suarez, S.; Greenbaum, S.G. *Electrochem. and Solid State Letters* **2004**, 7, A412.

- (90) Elabd, Y.A.; Walker, C. W.; Beyer, F. L. J. Membr. Sci. **2004**, 231, 181.
- (91) Thurn-Albbrecht, T. ; DeRouchey, J. Russell,T.P. ; Jaeger, H.M. Macromolecules **2000**, 33, 3250.
- (92) Xu, T. et al. Macromolecules **2005**, 38, 10788.
- (93) Wang, J. ; Leiston-Belanger, J.M. ; Sievert, J.D. ; Russell, T.P Macromolecules **2006**, 39, 8487.
- (94) Xu, T. ; Zhu, Y. ; Gido, S.P. ; Russell, T.P. Macromolecules **2004**, 37, 2625.
- (95) DeRouchey, J. ; Thurn-Albrecht, T. ; Russell, T.P.; Kolb, R. Macromolecules **2004**, 37 2538.
- (96) Boker, A.; Knoll, A.; Elbs, H.; Abetz, V.; Muller, A.H.E.; Krausch, G. Macromolecules **2002**, 35, 1319.
- (97) Tsori, Y.; Andelman, D. Macromolecules **2002**, 35, 5161.
- (98) Zvelindovsky, A.V.; Sevink, G.J.A. Phys. Rev. Lett. **2003**, 90, 049601.
- (99) Yuan, G.; Zhao, Y. Polymer **1995**, 36, 2725.
- (100) Roche, P.; Zhao, Y. Macromolecules **1995**, 28, 2819.
- (101) Chen, H.; Palmese, G.R.; Elabd, Y.A. Chem. Mater. **2006**, 18, 4875.
- (102) Fang, Y.; Leddy, J. J. Phys. Chem.. **1995**, 99, 6064.
- (103) Mani, S.; Weiss, R.A.; Williams, C.E.; Hahn, S.F. Macromolecules **1999**, 32, 3663.
- (104) Blackwell, R.I.; Mauritz, K.A. Polymer **2004**, 45, 3457.
- (105) Gilbert, W. In “ On Loadstone and Magnetic bodies and on the Great magnet of Earth” **1600**.
- (106) Formhals, A. US Patent 1,975,504, **1934**.
- (107) Huang, Z.; Zhang, Y.Z.; Kotaki, M.; Ramakrishna, S. Composites Science and Technology **2003**, 63, 2223.
- (108) Boland, E.D.; Wnek, G.E.; Simpson, D.G.; Palowski, K.J.; Bowlin, G.L. J. Macromol. Sci. Pur. Appl. Chem. **2001**, A38, 1231.

- (109) Fennessey, S.F.; Pedicini, A.; Farris, R.J. In ACS Symposium Series: Polymeric Nanofibers **2006**, 918, 300.
- (110) Baumgarten, P.K. J. Colloid and Interf. Sci. **1971**, 36, 71.
- (111) Fong, H.; Reneker, D.H. J. Polym. Sci.: Part B Polym. Phys. **1999**, 37, 3488.
- (112) Doshi, J.; Reneker, D.H. J. electrostatics, **1995**, 35, 151.
- (113) Deitzel, J.M.; Kleinmeyer, J. Harris, D.; Tan, N.C.B. Polymer **2001**, 42, 261.
- (114) Kim, J.S.; Reneker, D.H. Polymer Composites **1999**, 20, 124.
- (115) Groitzsch, D.; Fahrback, E. US Patent 4,618,524, **1986**.
- (116) Berry, J.P US Patent 4,965,110, **1990**.
- (117) Coffee, R.A. PCT/GB97/01968, **1998**.
- (118) Kenawy, E.R. et al. J. Controlled Release **2002** 81, 57.
- (119) Schreuder-Gibson, H.L. et al. J. Advanced Materials **2002**, 34, 44.
- (120) Norris, I.D.; Shaker, M.M.; Ko, F.K.; Macdiarmid, A.G. Synthetic Metals **2000**, 114, 109.
- (121) Waters, C.M.; noakes, T.J.; Paverty, I.; Hitomi, C. US Patent 5,088,807, **1992**.
- (122) Kwoun, S.J.; Lec, R.M.; Han, B.; ko, F.K. In Proceedings of the IEEE/EIA: International Frequency Control symposium 2000, p. 57.
- (123) Lee, S.H.; Ku, B.C.; wang, X.; Samuelson, L.A.; Kumar, J. Mat. Res. Soc. Symp. Proc. **2002**, 708, 403.
- (124) Bognitzki, M. et al. Advanced Materials **2000**, 12, 637.
- (125) Mauritz, K.A.; Moore, R.B. Chemical Reviews **2004**, 104, 4535.
- (126) Reyna-Valencia, A.; Kaliaguine, S.; Bousmina, M. J. Appld. Polym. Sci. **2006**, 99, 756.
- (127) Carbone, A. et al. J. Power Sources **2006**, 163, 18.
- (128) Choi, S.W.; Jo, S.M.; Lee, W.S.; Kim, Y. Advanced Materials **2003**, 15, 2027.

- (129) Li, X.; Hao, X.; Xu, D.; Zhang, G.; Zhong, S.; Na, H.; Wang, D. J. Membr. Sci. **2006**, 281, 1.
- (130) Shurui, S.; and Weiss, R.A. Private communication.
- (131) http://en.wikipedia.org/wiki/X-ray_photoelectron_spectroscopy
- (132) Zaidi, S.M.J. et al. J. Membr. Sci. **2000**, 173, 17.
- (133) Fong, H.; Chun, I.; Reneker, D.H. Polymer **1999**, 40, 4585.
- (134) Zong, X. et al. Polymer, **2002**, 43, 4403.

5528-17
5125-7

